Mathematical Modelling of the Dynamic Role of the HPA Axis in the Immune System

Elisabeth Ottesen Bangsgaard

Kongens Lyngby 2015

Technical University of Denmark
Department of Applied Mathematics and Computer Science
Richard Petersens Plads, building 324,
2800 Kongens Lyngby, Denmark
Phone +45 4525 3031
compute@compute.dtu.dk
www.compute.dtu.dk

Summary (English)

The aim of the thesis is to formulate a model describing the dynamic role of the Hypothalamic-Pituitary-Adrenal (HPA) axis in the immune system. The two subsidiary goals of the thesis are the formulation of two models describing the acute inflammatory response and the dynamics of the hormones of the HPA axis, respectively. All three models are compared to available data.

In the first part of the thesis, information of existent models in the literature, describing the acute inflammatory response is collected after which a minimal, mathematical model is formulated. The model is a reduced and modified version of a model proposed by Roy et al. (2009). The model is compared to the model proposed by Roy et al. (2009) and data measured in rats. Existence and uniqueness of the solutions to the system together with the existence of an attracting trapping region is proved. The model is simulated for rats exposed to three different doses of the endotoxin (lipopolysaccharides, LPS).

The second part of the thesis deals with the formulation of a mathematical model describing the interactions of the hormones in the HPA axis. The model is formulated on the basis of a model proposed by Ottesen (2011) and the work accomplished by Rasmussen et al. (2015). Existence and uniqueness of the solutions to the system together with the existence of an attracting trapping region is proved. A good approximation of the model is fitted convincingly to ACTH and cortisol concentration data from eight individuals.

In the last part of the thesis, biological reasoning and mathematical modelling is used to formulate a model describing the dynamical role of the HPA axis in the immune system, by coupling the two studied models. The parameters are

estimated using concentration data of TNF-α, ACTH and cortisol after injection of endotoxin. Finally, the model is compared to a model recently proposed by Malek et al. (2015) and simulated for different dosing and timing scenarios.

Summary (Danish)

Formålet med dette kandidatspeciale er at formulere en model, der beskriver den dynamiske rolle af hypothalamus-hypofyse-binyre-aksen (HPA-aksen) i immunsystemt. Delmålene for dette kandidatspeciale er at formulere to modeller, som beskriver det akutte inflammatoriske respons og dynamikken af hormonerne i HPA aksen. Alle tre modeller er sammenlignet med tilgængeligt data.

I den første del af specialet indsamles information om eksisterende modeller i litteraturen, der beskriver det akutte inflammatoriske respons, hvorefter en minimal, matematisk model er formuleret. Modellen er en reduceret og modificeret udgave af en model foreslået af Roy et al. (2009). Modellen sammenholdes med modellen foreslået af Roy et al. (2009) og data fra rotter. Eksistens og entydighed af løsningen til systemet samt eksistensen af et tiltrækkende, fangende område er bevist. Modellen bruges til at simulere rotter udsat for tre forskellige doser af endotoxin (lipopolysakkarider, LPS).

Den anden del af specialet omhandler formuleringen af en matematisk model, der beskriver interaktionerne mellem hormonerne i HPA-aksen. Modellen er formuleret på baggrund af en model foreslået af Ottesen (2011) og arbejdet udført af Rasmussen et al. (2015). Eksistens og entydig-hed af løsningen til systemet samt eksistensen af et tiltrækkende, fangende område er bevist. En god approksimation til modellen er fittet overbevisende til data for koncentrationerne af ACTH og kortisol fra otte individer.

I den sidste del af specialet er biologisk ræsonnement og matematisk modellering udnyttet til at formulere en model, som beskriver HPA-aksens dynamiske rolle i immunsystemet, ved at koble de to studerede modeller. Parametrene er bestemt

ved at fitte modellen til TNF-α, ACTH og kortisol koncentrationer, målt efter injektion af endotoxin. Endelig er modellen sammenlignet med en model foreslået fornylig af Malek et al. (2015) og simuleret for forskellige doserings og tidsmæssige scenarier.

Preface

This thesis was prepared at the Department of Applied Mathematics and Computer Science at the Technological University of Denmark (DTU Compute) in fulfilment of the requirements for acquiring a Master of Science in Engineering (Mathematical Modelling and Computing).

The thesis was completed from August 24, 2015 to January 23, 2016 under supervision of Poul G. Hjorth, Associate Professor at DTU Compute and Jesper Mehlsen, Chief Physician at Frederiksberg Hospital.

Lyngby, 23-January-2015

Elisabeth Ottesen Bangsgaard

Acknowledgements

I would like to thank my supervisor, Poul Hjorth, for his susceptibility to my project ideas, his belief in me and his valuable guidance.

I would like to thank Jesper Mehlsen, for providing essential knowledge of the medical world and useful biological and physical understanding of the immune system.

I would also like to thank Johnny Ottesen, Professor at Roskilde University, for suggesting this exciting project.

Finally, I would like to thank my friends and family for supporting me during the project.

Contents

Chapter 1

Introduction

The purpose of this thesis is to combine biological knowledge and mathematical modelling to develop a model describing the interactions between two subsystems. The two subsystems are the acute inflammatory response and the Hypothalamic-Pituitary-Adrenal axis (HPA axis). These systems are commonly believed to interact with each other, to maintain homeostasis (the steady and healthy state) in the body under the influence of stress. Both mental stress and physically stress, such as exposure to endotoxin, can disturb the homeostasis of the body.[4,32] Insight into the immune system can be gained by formulating a mathematical model of the dynamic influence of the HPA axis in the immune system. Especially, it can lead to insight into the effect of the observed ultradian and circadian rhythms of the hormones of the HPA axis (ACTH and cortisol).

The thesis is divided into three parts. The first part focuses on developing a minimal, adequate model describing the acute inflammatory response. The second part concentrates on the formulation of a model describing the interaction between the hormones of the HPA axis. The content of the last part is the formulation of a new coupled model describing the interactions between the two subsystems studied in the two first parts.

As a last part of the introduction, a motivation for using mathematical modelling is provided, followed by a project plan for the thesis.

1.1 Mathematical Modelling

Recently, the interplay between the acute inflammatory response and the HPA axis has gained interest. Modelling the coupled system, can help understanding the interactions in relation to illness and diseases. Understanding the connection between the systems can be very useful, when investigating how to avoid diseases, and in drug development, for instance. It may help refining diagnoses and improve treatment planing. The model can also be used for preparing or suggesting targeted studies which may reduce animal testing as well.

Unlike purely statistical modelling, the mathematical modelling may provide information of potential mechanisms rather than correlation between factors. Combining mathematical and statistical modelling and data fitting makes it possible to describe and simulate the interactions between the acute inflammatory system and the HPA axis. Additionally, data may make it possible to validate the model and evaluate its predictability.

The balance between describing the biological system as simple as possible and maintaining the complexity is essential. An overly simplistic model leaves out potentially important interactions and mechanisms, while a too complex model can lead to over-parametrisation. Over-parametrisation may lead to wrong conclusions and interpretations. Thus, keeping the model as simple as possible, while maintaining sufficient details to capture the essential biological mechanisms is used as a guiding principle in this thesis.

1.2 Project Plan

The project plan outlines the objectives of the thesis. The focus in the thesis is to use applied mathematics, in the form of systems of ordinary differential equations (ODEs), on real-world systems and to use simulation tools, such as `MATLAB` (R2015) and `Maple` (2015), to study them. The plan is divided into three parts, covering the three phases of the project:

- Formulate a model describing the acute inflammatory response
  - Collect information of existing models in the literature
  - Choose an adequate mathematical model
  - Use model reduction to formulate a minimal, adequate mathematical model
  - Compare model predictions to data
- Formulate a model describing the hormones of the Hypothalamic-Pituitary-Adrenal axis (HPA axis)
  - Collect information of existing models in the literature
  - Choose an adequate mathematical model
  - Compare model predictions to data
  - Estimate parameters for individual subjects
- Formulate a model describing the role of the HPA axis in the immune system
  - Collect information of existing models in the literature
  - Propose various coupling mechanisms between the two models
  - Compare model predictions to data
  - Simulate the model for different dosing and timing scenarios

Chapter 2

Acute Inflammatory Response

Local acute inflammatory response is activated, when an attack or injury to the body is recognised. The innate immune system may initiates the response in an attempt to eliminate invading pathogens. Inflammation is most often identified initially by the symptoms of redness, pain, heat and swelling[32]. When the immune system detects a pathogenic threat (such as bacteria, parasites or viruses), it activates macrophages to engulf or eliminate the difficulties[19]. Actually, the engulfing cells are called monocytes when they are in the blood and evolves to macrophages in tissue. In this thesis, however, these types of cells will be refereed to as phagocytic cells. Additionally, the phagocytic cells stimulates an increase of the release of cytokines, which are messenger cells of the immune system[19,33]. Generally cytokines can be classified into two groups, those which promote and stimulate the inflammation (pro-inflammatory cytokines) and those which inhibit and dampen the inflammation (anti-inflammatory cytokines). The pro-inflammatory cytokines activate more phagocytic cells and up-regulate other cytokines contemporary, while the anti-inflammatory cytokines inhibit the activation of the phagocytic cells and down-regulate pro-inflammatory cytokines[33]. The most generally acknowledged pro-inflammatory cytokines are tumor necrosis factor-α (TNF-α), interleukin 6 (IL-6) and interleukin 1 (IL-1), while interleukin 10 (IL-10) is considered as one very important

group of anti-inflammatory cytokines[19,32,33].

After the clearance of the targeted pathogenic treat, it is crucial to inhibit the inflammation and return to homeostasis, which is considered as the healthy stable state of the body. Thus the magnitude of the inflammatory response is of highest importance. Deficient response leaves surviving pathogens, which can lead to serious infections of the body such as sepsis, while excessive response can lead to tissue damage and diseases like rheumatoid arthritis, Crohn's disease, atherosclerosis, diabetes, and Alzheimer's disease.[32,33]

In this chapter, an initially eight dimensional model of the acute inflammatory response in rats is presented and reduced, leading to a five dimensional model. The reduced model is partly validated by comparison to data and residual plots, and the existence of a positive trapping region is shown. Finally a discussion of using a rat model for studying the response in humans is carried out.

2.1 Modelling Approaches

In this section, several model approaches are reviewed while their advantages and limitations are discussed. In literature, a number of different approaches to modelling the acute immune response can be found. Over time, both rather complex models and quite simple models have been develop aiming to study and understand the systemic as well as detailed mechanisms in immune defence.

One of the simplest models has been proposed by Baker et al. (2013), only considering pro- and anti-inflammatory cytokines in an attempt to mathematically investigate the system and the involvement of the cytokines in the disease rheumatoid arthritis. Due to the simplicity of the model (only two variables), it can be investigated analytically. Even though the conceptual model output cannot be compared to real data, the behaviour of the system can be studied by bifurcation theory, for instance[3].

In 2006, Reynolds et al. published a four dimensional model describing the interactions between pathogens, phagocytes (eating-cells), tissue damage and anti-inflammatory mediators (representing cortisol and interleukin-10). The aim of this work was to investigate the importance of the dynamic anti-inflammation for restoring homeostasis and defeat infection. Once again, the model is conceptual and not compared to experimental data, however the authors claims that the model is developed from subsystems with biologically plausible dynamics[28].

In contrast to these oversimplified models of the acute inflammatory systems,

is the model proposed by Chow et al. (2005). The system is described by a model consisting of 15 variables and no less than 98 parameters. The overall goal was to find a model, balancing biological realism and simplicity, which could qualitatively describe many known scenarios of inflammation for a fixed set of parameters. The model output is matched to data for mice, receiving LPS (endotoxin) at different doses. Even though the model is very complex, it only mimics some of the dynamics in the data, however the fit of the model to the data is in many of the cases poor. In addition, the system is not identifiable with respect to the data, since the model is overparametrised.[6]

A model which is not too complicated nor oversimplified is proposed by Roy et al. (2009). The model consists of eight differential equations which captures the behaviour of the cytokines IL-6, IL-10 and TNF-α in rats. The model is validated by comparison to data collected from an experiment, where rats received LPS. Although the model fits the data very well, the article was never published. Even though the model is not too complicated compared to others, it still features eight variables and 46 parameters[29]. The model features eight variables representing LPS, phagocytic cells, tissue-damage, pro-inflammatory cytokines (TNF-α and IL6), fast acting anti-inflammatory cytokine (IL10) and slow acting anti-inflammatory mediators, describing the acute inflammatory response in rats receiving different doses of endotoxin.

In his Ph.D., Dennis O. Frank simplifies the eight dimensional model proposed by Roy et al. to a seven dimensional model[12]. Arguing that the variable representing the slow acting anti-inflammatory mediators, such as cortisol, is not measurable while it appears to have least interactions in the system, this variable is removed from the system. The simplified model, with only 6 less parameters, is calibrated to the same data as the eight dimensional model, resulting in equally accuracy of predictions. However, since the connection between the acute inflammatory response and the slow acting anti-inflammatory hormone cortisol is of interest in the thesis, this simplification will not be studied further.

Finding a balance between biological realism and simplicity, is crucial when modelling a biological phenomena. Various modelling approaches of the acute inflammatory response have been proposed over the years, but still, there is no commonly used model. The model proposed by Roy et al. (2009) captures many of the components of the response (in rats) to some detail, however in a simplified way, which makes it a basis model for investigating the system.

In the following section, the eight dimensional model of the acute inflammatory response proposed by Roy et al. (2009) is presented.

2.2 Rat Model of Acute Inflammatory Response

The model proposed by Roy et al. (2009) seem to describe the dynamic between the anti-inflammatory cytokine IL-10 and the pro-inflammatory cytokines IL-6 and TNF-α convincingly. Thus, this model approach is an opportunity for studying the acute inflammatory system. However the model equations are complicated and contains a great number of parameters to be determined.

The model consists of eight ordinary differential equations representing the states of endotoxin concentration (P), total number of activated phagocytic cells (N), tissue-damage marker (D), concentrations of pro-inflammatory cytokines ($IL6$ and TNF), concentration of anti-inflammatory cytokine ($IL10$), a (non specified) tissue-damage driven IL-10 promoter (Y_{IL10}) and a state representing slow acting anti-inflammatory mediators, such as TGF-β1 and cortisol (C_A). Three of the eight variables in the model are measured in a rat experiment, where rats where exposed to three different doses of endotoxin (3, 6 or 12 mg/kg). The measured variables are $IL6$, TNF and $IL10$ obtained from blood samples taken at time 0, 1, 2, 4, 8, 12 and 24 hours after the injection of endotoxin. Four rats were sacrificed at each time point and the data is expressed as mean and standard deviation.

The main objective of the model is to capture the dynamics and reproduce the blood concentrations of IL-6, TNF-α, IL-10 and the slow acting anti-inflammatory mediators, but since the variable C_A represents various substances, it is not measured in the experiment and therefore not accessible. The parameters are estimated using the data for two of the endotoxin doses (3 and 12 mg/kg), while the data for endotoxin dose 6 mg/kg is used for evaluating the performance and prediction of the model.

The model equations describe a number of interactions between the dependent variables, which is summarised in the following bullets:

- The concentration of endotoxin (P) initiates the response by up-regulating and activating the total number of activated phagocytic cells (N).
- Activated phagocytic cells (N) up-regulate the pro-inflammatory cytokines (TNF and $IL6$), the anti-inflammatory mediators ($IL10$ and C_A) and the marker for tissue-damage (D).
- The non-accessible tissue damage marker (D) up-regulates the activated phagocytic cells (N) while contributing to an up-regulation of IL-10 through the IL-10 promoter (Y_{IL10}).

- The concentration of the pro-inflammatory IL-6 up-regulates the activated phagocytic cells (N) and IL-10. IL-6 also down-regulates TNF-α and auto -up-regulates.
- The concentration of the pro-inflammatory TNF-α adds an up-regulating effect of the activated phagocytic cells (N), IL-6 and IL-10. TNF-α is auto-up-regulating.
- The concentration of the anti-inflammatory cytokine IL-10 down-regulates the pro-inflammatory activated phagocytic cells (N), IL-6 and TNF-α. IL-10 inhibits its elimination for large concentrations.
- The tissue damage driven non-accessible IL-10 promoter (Y_{IL10}) contributes to a delayed increase in IL-10.
- The state representing slow acting anti-inflammatory mediators (C_A) down-regulates the activated phagocytic cells (N), and the pro-inflammatory cytokines IL-6 and TNF-α.

These are the major mechanisms involved in the acute inflammatory response, suggested by Roy et al. (2009), thus the dynamics can mathematically be described by:

$$\frac{dP(t)}{dt} = -d_p \cdot P(t) \tag{2.1a}$$

$$\frac{dN(t)}{dt} = k_N \cdot \frac{R(t)}{x_N + R(t)} - d_N \cdot N(t) \tag{2.1b}$$

$$\frac{dD(t)}{dt} = k_D \cdot \frac{N(t)^6}{x_D^6 + N(t)^6} - d_D \cdot D(t) \tag{2.1c}$$

$$\frac{dC_A(t)}{dt} = k_{CA} \cdot N(t) - d_{CA} \cdot C_A(t) + s_{CA} \tag{2.1d}$$

$$\begin{aligned}\frac{dIL6(t)}{dt} = {} & k_{IL6} \cdot \left(\frac{N(t)^4}{x_{IL6}^4 + N(t)^4} \right) \cdot [1 + k_{IL6TNF} \cdot fUP_{IL6TNF}(t) + k_{IL6IL6} \cdot fUP_{IL6IL6}(t)] \\ & \cdot fDN_{IL6IL10}(t) \cdot fDN_{IL6CA}(t) - d_{IL6} \cdot IL6(t)\end{aligned} \tag{2.1e}$$

$$\begin{aligned}\frac{dTNF(t)}{dt} = {} & k_{TNF} \cdot N(t)^{1.5} \cdot [1 + k_{TNFTNF} \cdot fUP_{TNFTNF}(t)] \cdot fDN_{TNFCA}(t) \\ & \cdot fDN_{TNFIL10}(t) \cdot fDN_{TNFIL6(t)} - d_{TNF} \cdot TNF(t)\end{aligned} \tag{2.1f}$$

$$\begin{aligned}\frac{dIL10(t)}{dt} = {} & k_{IL10} \cdot \left(\frac{N(t)^3}{x_{IL10}^3 + N(t)^3} \right) \cdot [1 + k_{IL10IL6} \cdot fUP_{IL10IL6}(t) + k_{IL10TNF} \\ & \cdot fUP_{IL10TNF}(t)] - d_{IL10} \cdot fDN_{IL10d}(t) \cdot IL10(t) + Y_{IL10}(t) + s_{IL10}\end{aligned} \tag{2.1g}$$

$$\frac{dY_{IL10}(t)}{dt} = k_{IL102} \cdot \frac{D(t)^4}{x_{IL102}^4 + D(t)^4} - d_{IL102} \cdot Y_{IL10}(t) \tag{2.1h}$$

where

$$\begin{aligned}R(t) = {} & [k_{NP} \cdot P(t) + k_{ND} \cdot D(t)] \cdot [(1 + k_{NTNF} \cdot fUP_{NTNF}(t)) \\ & \cdot (1 + k_{NIL6} \cdot fUP_{NIL6}(t))] \cdot fDN_{NCA}(t) \cdot fDN_{NIL10}(t)\end{aligned} \tag{2.2}$$

In general the parameters k_i represent production/activation rates, the parameters d_i represent elimination/clearance rates and the parameters x_i are the half-saturation constants determining the level of the variables i, at which the corresponding up-regulating or down-regulating function will reach half of its saturation value, where $i \in \{P, N, D, C_A, IL6, TNF, IL10, Y_{IL10}\}$. The up- and down-regulating functions mentioned are $fUP_{ij}(t)$ and $fDN_{ij}(t)$ respectively, which represent the up- and down-regulating effects of inflammatory mediator j on mediator i. The functions are Michaelis-Menten type equations or Hill functions and are bound between values of 0 and 1. The functions are presented in Appendix A.1.

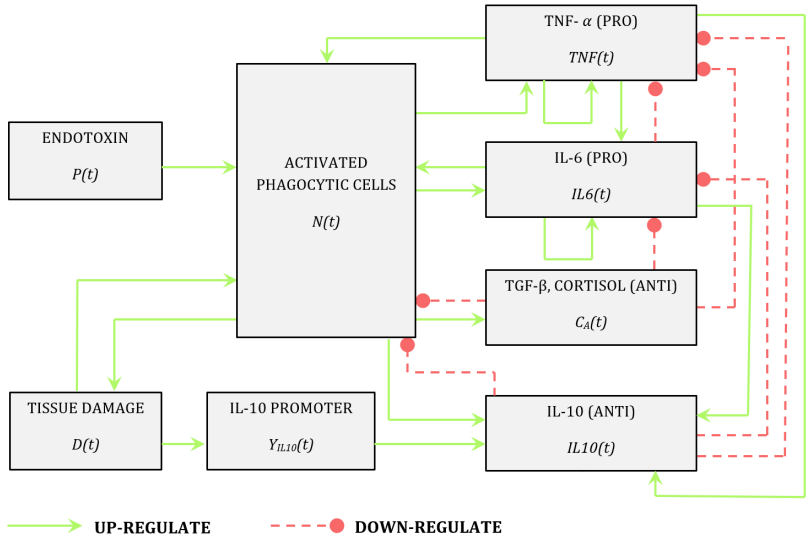

Figure 2.1: Diagram of the dynamics in the model of acute inflammatory response proposed by Roy et al. (2009). The green solid lines represent up-regulating interactions, while the red dashed lines illustrate down-regulating interactions between the variables.

The interactions between the eight variables are visualised in Figure 2.1. From left, by introducing endotoxin to the system, the response is initiated by up-regulating the number of activated phagocytic cells. The phagocytic cells up-regulates the cytokines TNF-α, IL-6, IL-10 and the slow acting inflammatory mediators (placed to the right). Furthermore it up-regulates the tissue damage marker, which up-regulates IL-10 through Y_{IL10}. Up-regulation of the cytokines initiates several interactions between these and feedback on the activated phagocytic cells.

Some of the mathematical equations in the model are complex and there is no clear biological reasoning for most of the specific modelling choices, which

makes the justification of the model development unclear. In the equation for the total number of phagocytic cells (N), four Michaelis-Menten functions are incorporated in yet another Michaelis-Menten function, to mention one example of a complex model choice not justified. No biological reasoning for including the IL-10 promoter Y_{IL10} in the model is presented. The variable is included to capture the dynamics of the damage-marker effects on IL-10, however there is not provided any evidence for the existence of such chemical substance. As mentioned, the model contains 46 parameters, which makes the fit of the model strongly overparametrised. This serves as a reason for investigating model reduction.

Besides the unexplained and remarkable model choices, the structure of the equations seems to follow the form of a stimulating or inhibiting part constructed mostly by one or more of Michaelis-Menten type equations or Hill-functions with varying order. In addition, all the equations contain a clearance rate, described by a linear term (except in the case for IL-10).

The parameters of the model were calibrated to data for rats receiving endotoxin at three different dose levels. The parameters were first estimated for the two data sets for endotoxin doses 3 and 12 mg/kg and next validated by comparing the model predictions to the data obtained for rats receiving an endotoxin dose of 6 mg/kg[29].

In Appendix A.2 the model is studied in details. First, the model was simulated and then compared to data. The reduced six dimensional model presented in the following section is derived from the extensive work presented in Appendix A.2.1-A.2.6. The equations were analysed one at a time to examine the significance of each term and the biological reasoning.

Summing up, the equation for P is changed to depend on the number of phagocytic cells, which seems reasonable from a biological perspective. The equation for N is simplified by changing the Michaelis-Menten function in R to a linear dependence. The equation is further simplified, by removing the dependence of $IL6$ and D due to insignificant observed influence. The simplification of the equation of TNF is constituted by changing the power of N from one and a half to one, changing the order of the Hill function in C_A from six to four and removing of the dependence of $IL6$ and $IL10$. The Michaelis-Menten functions in N and $IL6$ is changed to a linear and a fourth order dependence respectively, while the dependence of C_A is removed in the equation for $IL6$. The equation for $IL10$ is modified by changing the main contributor to the second peak from Y_{IL10} to C_A. In addition, the dependence of TNF in the equation is removed. There are no simplifications introduced in the equation for C_A. But since the dependence of D and Y_{IL10} is removed in all the other equations, they are eliminated from the system. All together, these changes results in a reduced six

dimensional model containing 30 parameters.

The reduced model is presented and studied in the following section, leading to a further simplified five dimensional model.

2.3 Reduced Rat Models

A number of modifications and simplifications have been introduced to the eight dimensional model proposed by Roy et al. (2009) (see Appendix A.2), resulting in a reduced six dimensional model. In this section, the six dimensional model is presented, compared to the eight dimensional model and afterwards a further simplified five dimensional model will be proposed.

2.3.1 Six Dimensional Model

The changes in the model induce a reduction of the described eight dimensional system to a six dimensional system disregarding the variables D and Y_{IL10} (the tissue damage marker and the tissue driven IL-10 promoter respectively). In the following, the six dimensional model is presented and compared both visually and numerically to the eight dimensional model and the rat data. Finally it is shown, that the six dimensional model can be reduced to a five dimensional model, removing the variable $IL6$. Even though the cytokine IL-6 is removed from the model, the dynamics of TNF-α and IL-10 are maintained.

The difference between the variables and their interactions in the original model and the reduced model is visualised in Figure 2.2. The diagram illustrates the removed and the two added interactions. As seen, nine interactions and two variables are removed from the original model and only two new interactions are introduced, namely a down-regulating effect of N on P and an up-regulating effect of C_A on $IL10$.

Besides reducing the dimension of the system, the simplification of the equations implied a major reduction in the total number of parameters. The number of parameters are reduced from 46 to 30.

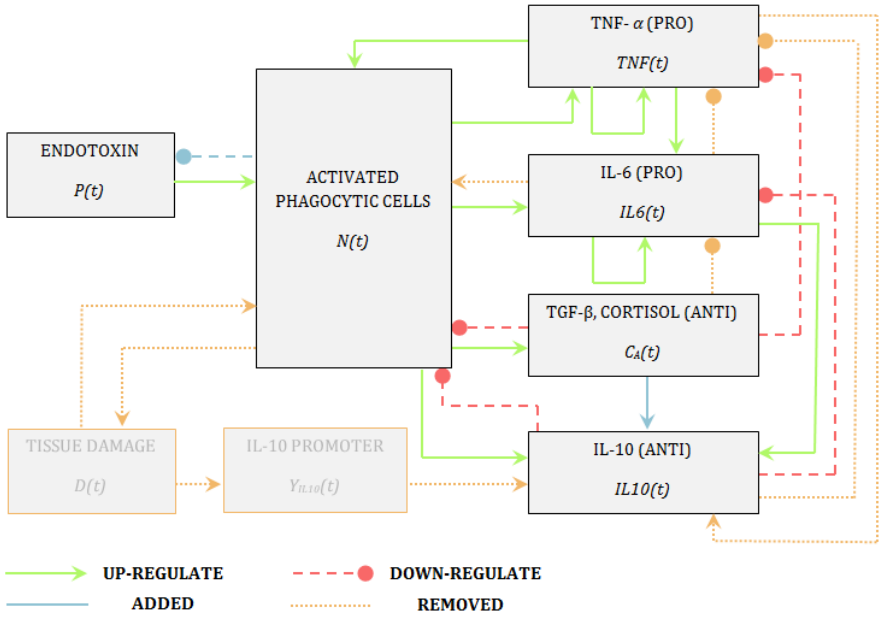

Figure 2.2: Diagram showing the difference between the original model proposed by Roy et al. (2009) and the reduced model (Model (2.3)). The blue color of the arrows between P and N, and C_A and $IL10$ illustrates the two new introduced interactions, while the yellow dashed lines represent the nine interactions which are removed in the reduced model. Furthermore the two variables D and Y_{IL10} only appear in the original model and not in the reduced model.

The reduced six dimensional system can now mathematically be written as:

$$
\begin{aligned}
\frac{dP}{dt} &= -d_p P \cdot N \\
\frac{dN}{dt} &= k_N \left(\left(1 + \frac{k_{NTNF} TNF}{x_{NTNF} + TNF} \right) \frac{x_{NCA}}{x_{NCA} + C_A} \cdot \frac{x_{NIL10}}{x_{NIL10} + IL10} \right) \cdot P - d_N N \\
\frac{dC_A}{dt} &= k_{CA} \cdot N - d_{CA} C_A + s_{CA} \\
\frac{dIL6}{dt} &= N^4 \cdot \left(k_{IL6} + \frac{k_{IL6TNF} TNF}{x_{IL6TNF} + TNF} + k_{IL6IL6} \cdot IL6 \right) \\
&\quad \cdot \frac{x_{IL6IL10}}{x_{IL6IL10} + IL10} - d_{IL6} IL6 \\
\frac{dTNF}{dt} &= N \cdot \frac{x_{TNFCA}^4}{x_{TNFCA}^4 + C_A^4} \left(k_{TNF} + \frac{k_{TNFTNF} TNF}{x_{TNFTNF} + TNF} \right) - d_{TNF} TNF \\
\frac{dIL10}{dt} &= \frac{N^3}{x_{IL10}^3 + N^3} \left(k_{IL10} + \frac{k_{IL10IL6} IL6^4}{x_{IL10IL6}^4 + IL6^4} \right) \\
&\quad - d_{IL10} \frac{x_{IL10d}}{x_{IL10d} + IL10} IL10 + \frac{k_{IL10CA} C_A^6}{x_{IL10CA}^6 + C_A^6} + s_{IL10}.
\end{aligned}
\tag{2.3}
$$

In Figure 2.3 a diagram of the interactions in the reduced model is shown. This diagram shows the simplification of the model, containing two variables and nine interactions less, only introducing two new interactions.

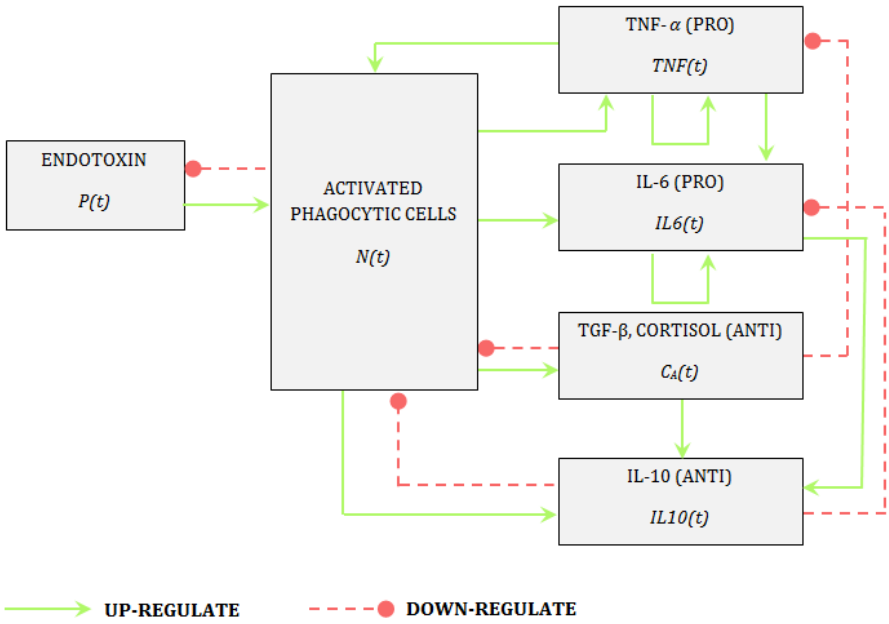

Figure 2.3: Diagram of the dynamics in the reduced six dimensional Model (2.3). The green solid lines represent the up-regulating interactions and the red dashed lines represent the down-regulating interactions between the variables in the model.

In the following, simulations of the reduced model are compared to both the original model and the rat data in an attempt to partly validate the model. The parameters used for simulating the six dimensional model can be found in Appendix A.6. In Figure 2.4-2.6, simulations of the reduced six dimensional model (Model (2.3)) are visually compared to both simulations of the original model (Model (2.1)-(2.2)) and the rat data.

In Figure 2.4, the simulation of endotoxin dose 3 mg/kg is shown. The reduced and the original model perform equally good for $IL6$, where none of them seem to capture the second data point. For TNF, the original model captures the second and fourth data point slightly better, due to the later peak of the con-

centration for the reduced model, however, the response reaches the maximum represented by the third data point. The response of $IL10$ is well modelled by both the original and the reduced model for the first four data points, however the original model captures the two last data point better, while the reduced model tends to overestimate slightly. Both model fits the data for endotoxin of dose 3 mg/kg well.

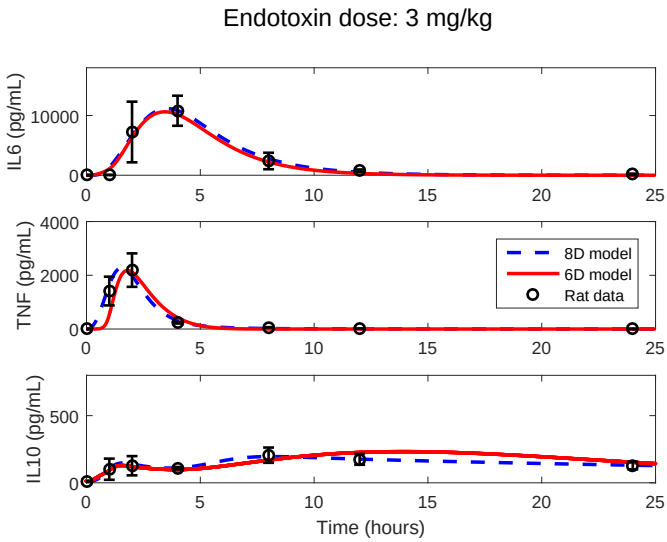

Figure 2.4: Comparison of the original eight dimensional model of acute inflammatory repsonse proposed by Roy et al. (2009) (Model (2.1)-(2.2), blue dashed line), the reduced and simplified six dimensional model (Model (2.3), red solid line) and rat data (black circles) for endotoxin dose 3 mg/kg. For further discussion, see Section 2.3. The data are a mean of measurements from four rats and the standard deviation at each data point is shown.

The simulation of endotoxin dose 6 mg/kg is shown in Figure 2.5. Neither of the model simulations captures the second data point of $IL6$, however the original model agrees better with the the third data point. For the TNF response, the original model is not close to fit the second data point and even though the reduced model does not agree with the data point as well, it is somewhat closer. The consistency between the second and fifth data point and the original model for $IL10$ seems to be somewhat better, compared to the reduced model. However both models seem to overestimate the response of $IL10$ for the decreasing period.

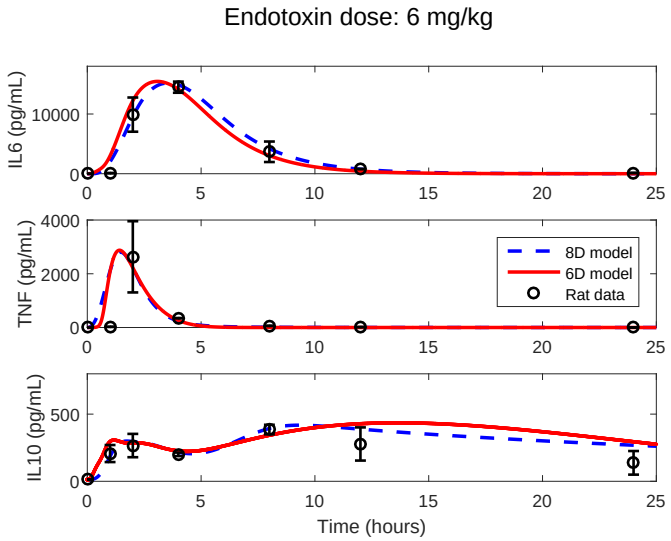

Figure 2.5: Comparison of the original eight dimensional model of acute inflammatory repsonse proposed by Roy et al. (2009) (Model (2.1)-(2.2), blue dashed line), the reduced and simplified six dimensional model (Model (2.3), red solid line) and rat data (black circles) for endotoxin dose 6 mg/kg. For further discussion, see Section 2.3. The data are a mean of measurements from four rats and the standard deviation at each data point is shown.

Finally, the simulations are compared for endotoxin dose 12 mg/kg, seen in Figure 2.6. The reduced model is not fitting the second data point of $IL6$ well, but mimics the dynamics of the remaining data points convincingly. There is only a slight difference between the outcome of the two models for TNF, amounting of a slightly higher response and a slightly earlier peak time. The simulations for $IL10$ reveals an overestimation by the reduced model of the second data point, however the last four data points seems to be perfectly fitted by the model.

Considering all simulations for the different doses of endotoxin, the original model appears to fit the data better than the reduced model. But the reduced model contains two variables, 16 parameters and a lot of interactions less than the model proposed by Roy et al. (2009). In addition, since the parameters in the reduced model are estimated manually, the model fit could be improved by fitting all parameters simultaneously. However, since the aim is to find a model describing the acute inflammatory response of humans, this is not done. Later in this thesis, the model will be modified further, when it is coupled to a model describing the HPA axis. So even though the model fit is not perfect, the model

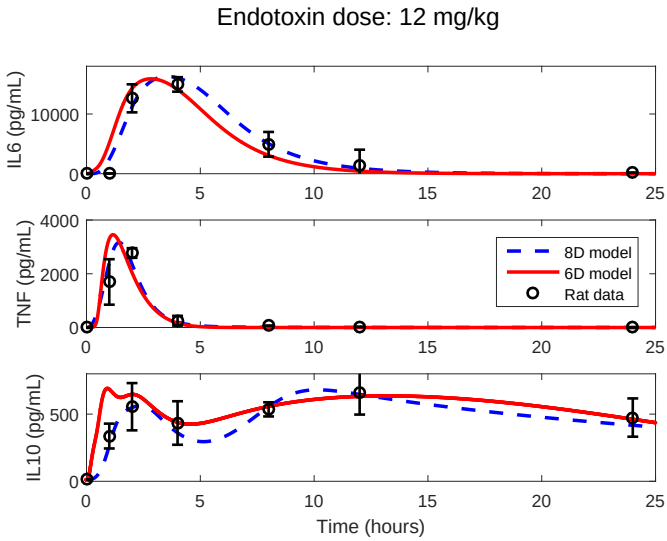

Figure 2.6: Comparison of the original eight dimensional model of acute inflammatory repsonse proposed by Roy et al. (2009) (Model (2.1)-(2.2), blue dashed line), the reduced and simplified six dimensional model (Model (2.3), red solid line) and rat data (black circles) of endotoxin dose 12 mg/kg. For further discussion, see Section 2.3. The data are a mean of measurements from four rats and the standard deviation at each data point is shown.

captures the dynamics of the three cytokines.

To compare the models quantitatively rather than visually, the Akaike Information Criterion (AIC) is calculated. The AIC value of a model is a measure of the goodness of fit, meaning that the amount of lost information when modelling a real system becomes comparable. The criterion can be used to compare two different models of the same data. The AIC value takes the number of parameters into account, when measuring the goodness of fit, by including a penalty-term for the number of parameters. The model achieving the lowest AIC value is preferable. The AIC value can according to Cobelli and Carson (2008) be calculated by:

$$AIC = J + 2p, \tag{2.4}$$

where p is the total number of parameters in the model and J is the weighted

residuals of the model given by:

$$J = \sum_{j=1}^{l} \frac{1}{\max_i(y_{ji})^2} \sum_{i=1}^{k} (y_{ji} - y_j(t_i, q))^2, \tag{2.5}$$

where y_{ji} is the i'th data point in the j'th data set. $\max_i(y_{ji})$ is the maximum value of the data over all times points in the j'th data set (noticing that the chosen weight is making the term dimensionless), $y_j(t_i, q)$ represents the model prediction at time point t_i given the parameters contained in the vector q and the total number of data sets, are denoted by l. For the original model the total number of parameters is $p = 46$ while it is $p = 30$ for the reduced model. There is three dose levels for each of the three of the variables, thus $l = 9$, while $k = 7$ indicates that there is 7 data points for each dose level for each variable.

The calculated weighted residuals is $J = 1.09$ for the original model, while the value is $J = 2.50$ for the reduced model. The residual values are smallest for the original model, as expected, since the model visually fits the data slightly better than the reduced model. Calculating the AIC values for the model gives:

$$AIC_{[ROY]} = 93.09$$

and

$$AIC_{[6D]} = 62.50.$$

Since the reduced model achieves the lowest AIC value, it is preferable to the original model when modelling this data. Even though the original model seems to fit the data better, the reduced model contains fewer parameters and from an AIC perspective, the reduced model fits the data best, with a minimum number of parameters.

This shows that this data of the dynamics of three cytokine concentrations in rats exposed to endotoxin, can be described by a six dimensional model rather than an eight dimensional model.

In the following section, the model is reduced further to a five dimensional model, removing the variable $IL6$ from the system.

2.3.2 Five Dimensional Model

The reduced six dimensional model presented in the previous section, describes the acute inflammatory response convincingly compared to the rat data. Modelling physical phenomena is indeed about simplifying systems up to a certain

point, still describing the phenomena in an adequate way. Since the six dimensional model is a simplification of the eight dimensional model proposed by Roy et al. (2009), it is of interest to see whether the model can be reduced further, without loosing any information of the system.

In the reduced model, six variables appears: P, N, $IL6$, TNF, $IL10$ and C_A. P describes the concentration of endotoxin, which activates the specific immune response investigated by the model. Since it is of interest to study the response to different doses of endotoxin amongst other things, this variable should be in the model.

The presence of the activated phagocytic cells denoted by N is crucial for describing the elimination of the endotoxin challenge. N describes the engulfing cells of the body, which means that the endotoxin would not be engulfed without the presence of these cells. Thus this variable should not be removed from the model either.

The variable C_A describes a state of slow anti-inflammatory mediators. Even though there is no measured data to compare with, the variable covers the hormone cortisol and since the aim of this work is to couple a model of the acute inflammatory system with a model of the HPA axis, where the main component is the secretion of cortisol, it seems reasonable to preserve the variable in the model.

Finally, considering the three variables representing the cytokines in the model, $IL10$ describes an anti-inflammatory cytokine while both $IL6$ and TNF describes pro-inflammatory cytokines. Data is provided for all three cytokines, however, since IL-10 is the only purely anti-inflammatory cytokine, it should be kept in the model. Which leaves the two pro-inflammatory cytokines IL-6 and TNF-α which appear in the equation for $IL10$ and in the equations for N and $IL6$, respectively. TNF-α is considered as a necessary and sufficient mediator of acute inflammation[33]. In addition, it turns out that the impact of $IL6$ on the rest of the system is minor (see Figure 2.7). Thus it is chosen to remove $IL6$ from the model in the aim of an even more simplified model of the acute inflammatory system.

The removal of the variable $IL6$ from the model is fairly easy. It only appears in the equation for $IL10$. By removing the fourth order term of $IL6$ from here, it no longer effects the other variables in the system. Furthermore, the elimination of the term and the equation for $IL6$ implies a reduction of eight parameters in total. The reduced five dimensional model is now mathematically described by:

$$
\begin{aligned}
\frac{dP}{dt} &= -d_p P \cdot N \\
\frac{dN}{dt} &= k_N \left(\left(1 + \frac{k_{NTNF} TNF}{x_{NTNF} + TNF} \right) \frac{x_{NCA}}{x_{NCA} + C_A} \cdot \frac{x_{NIL10}}{x_{NIL10} + IL10} \right) \cdot P - d_N N \\
\frac{dC_A}{dt} &= k_{CA} \cdot N - d_{CA} C_A + s_{CA} \\
\frac{dTNF}{dt} &= N \cdot \frac{x_{TNFCA}^4}{x_{TNFCA}^4 + C_A^4} \left(k_{TNF} + \frac{k_{TNFTNF} TNF}{x_{TNFTNF} + TNF} \right) - d_{TNF} TNF \\
\frac{dIL10}{dt} &= \frac{N^3}{x_{IL10}^3 + N^3} k_{IL10} - d_{IL10} \frac{x_{IL10d}}{x_{IL10d} + IL10} IL10 + \frac{k_{IL10CA} C_A^6}{x_{IL10CA}^6 + C_A^6} + s_{IL10}.
\end{aligned}
\tag{2.6}
$$

The equations are the same as for the six dimensional model, except the eliminated fourth order term of $IL6$ in the equation for $IL10$. Removing the term from the six dimensional model, while keeping the equation for $IL6$ in the model, induces significant over-estimations of the $IL6$ levels for endotoxin doses 6 and 12 mg/kg, which might be improved by changing some parameter values.

The interactions between the dependent variables in the reduced five dimensional model, is summarised in the following bullets:

- The concentration of endotoxin (P) initiates the response by up-regulating and activating the total number of activated phagocytic cells (N).
- Activated phagocytic cells (N) up-regulates the pro-inflammatory cytokine (TNF) and the anti-inflammatory mediators ($IL10$ and C_A), while it inhibits the concentration of endotoxin.
- The concentration of the pro-inflammatory TNF-α is auto-up-regulating and adds an up-regulating effect of the activated phagocytic cells (N).
- The concentration of the anti-inflammatory cytokine IL-10 down-regulates the pro-inflammatory activated phagocytic cells (N) and TNF. IL-10 also has an inhibitory effect on its own elimination for large concentrations of IL-10.
- The state representing slow acting anti-inflammatory mediators (C_A) down-regulates the activated phagocytic cells (N), and the pro-inflammatory cytokine TNF-α, while it up-regulates the anti-inflammatory cytokine IL-10.

The elimination of $IL6$ means a reduction of the number of parameters by eight. The five and six dimensional model is only compared to the data of TNF-α and IL-10. In Figure 2.7, the simulation of the five dimensional model is compared to the simulation of the six dimensional model and the rat data for TNF-α and IL-10 concentrations, respectively. There is almost no difference in the model

outcome, when comparing simulations of endotoxin dose 3 mg/kg. However, there is a slightly change in the IL-10 level of endotoxin dose 6 and 12 mg/kg, but the fit is equally good compared to the fit of the six dimensional model. The simulations of the five dimensional model presented in Figure 2.7 are obtained by using the same parameter values as for the six dimensional model.

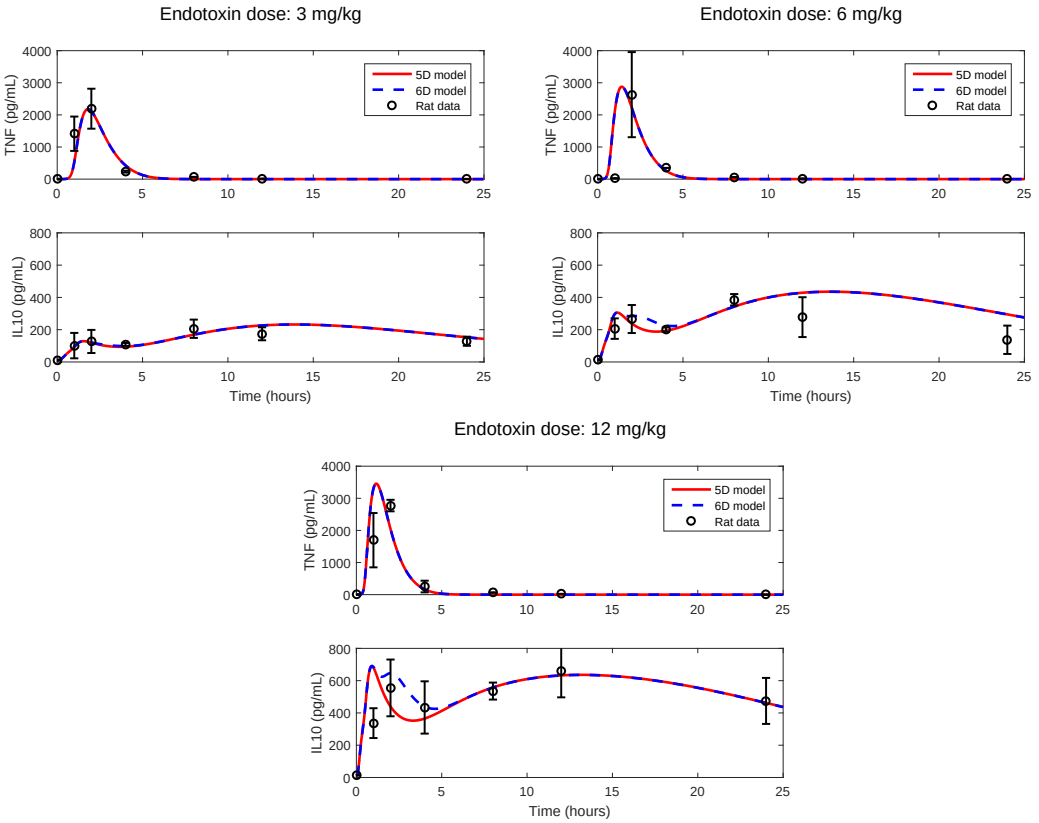

Figure 2.7: Simulation of the six dimensional (dashed blue line) and five dimensional model (red solid line) compared to the rat data (black circles). The difference between the models is the elimination of the variable $IL6$, which only induces a small change in the output for $IL10$ for endotoxin dose levels 6 and 12 mg/kg. The data are a mean of measurements from four rats and the standard deviation at each data point is shown.

The residuals and AIC values can be calculated in a similar way as in Section 2.3, however, only comparing to the data sets of TNF-α and IL-10. There is no greater change between the model outputs, which means that the residuals for the models are similar. The weighted residuals are $J = 2.04$ and $J = 2.26$

for the five and six dimensional model, respectively. This gives AIC values of $AIC_{[5D]} = 46.04$ and $AIC_{[6D]} = 62.26$. The AIC value for the five dimensional model is clearly preferable from an AIC perspective, which is the result of the large parameter reduction. Thus the reduction of eight parameters (and one variable) induces a small decrease in the weighted residuals, but a major decrease in the AIC value.

Thus the five dimensional model describes the dynamics of TNF-α and IL-10 in the data better than the six dimensional. In the rest of the thesis, the five dimensional reduced model will be considered as the prefered model of the acute inflammatory system.

In the following, it is shown that there exists an attracting trapping region for the model and that it satisfies positivity. Finally the model is partly validated by investigating some residuals plots.

2.3.3 Positivity and Trapping Region

In this section the existence of an attracting trapping region T_R is shown together with the proving of positivity.

Positivity of a biological model is crucial. In a mathematical model of the acute inflammatory system, it means that, if the concentration at a certain time is non-negative, it stays non-negative for all later times: Let $X(t) = [P(t), N(t), C_A(t), TNF(t), IL10(t)]'$. By definition, the Model (2.6) is said to fulfil positivity, if $X(t_0) \in (\mathbb{R}_+ \cup \{0\})^5$ implies $X(t) \in (\mathbb{R}_+ \cup \{0\})^5$ for all $t > t_0$.

When modelling a biological system, positivity is not the only important feature. It is also important to ensure, that the solutions of the model are finite. By creating a trapping region, it is possible to show, that the solutions initialised in the trapping region can not escape.

In the following, the model is only considered for positive parameter values and non-negative initial conditions. The model features a trapping region T_R, which means that for any solution $X(t_0) \in T_R$ then $X(t) \in T_R$ for all $t > t_0$. Furthermore, it is shown that the trapping region is attracting, hence solutions starting outside T_R is attracted into the region. Before defining the trapping region, the existence and uniqueness of the solutions are shown.

Considering the Model (2.6) on the form

$$\begin{aligned} \dot{x}_1(t) =& f_1(x_1(t), ..., x_5(t)) \\ & \vdots \\ \dot{x}_5(t) =& f_5(x_1(t), ..., x_5(t)), \end{aligned} \tag{2.7}$$

with initial conditions $X(t_0) = X_0$. From the *theorem of existence and uniqueness*[7] it follows, that for a given $t_0 \in \mathbb{R}$ and $X_0 \in \mathbb{R}^5$, the System (2.7) has one unique solution $X(t)$ satisfying $X(t_0) = X_0$ if the partial derivatives of the functions $f_1, .., f_5$ are continuous. It follows from direct inspection, that the partial derivatives of the functions $f_1, .., f_5$ are indeed continuous.

In the following, first the lower bound of the trapping region is found, which also demonstrates the positivity of the model and secondly the upper bound of the trapping region is found.

For $P = 0$, it is clear that $\frac{dP}{dt} = 0$, this means that for $P(t_0) \geq 0$ then $P(t) \geq 0$ for all $t > t_0$ due to the uniqueness of the solution.

Considering the equation for N, which is slightly more complicated, the term consisting of three Michaelis-Menten functions is always positive. This means that $dN/dt \geq 0$ for $N = 0$ since $P \geq 0$. Thus $N(t) \geq 0$ for $N(t_0) \geq 0$ due to the uniqueness of the solution.

The equation for C_A satisfies strict positivity, since $C_A = 0$ means that $\frac{dC_A}{dt} > 0$ which is caused by the constant term s_{CA} and the fact that $N \geq 0$. Thus as a result of the uniqueness of the solution, $C_A(t) > 0$ for $C_A \geq 0$.

The variable TNF also respects positivity, since $N \geq 0$ and the fourth order hill function in C_A is also positive, which means that for $TNF = 0$ the term $\frac{dTNF}{dt} \geq 0$. Hence, $TNF(t) \geq 0$ for $TNF(t_0) \geq 0$ because of the uniqueness.

At last, $IL10$ fulfils strict positivity, as a result of the constant term in the equation. Thus, once again, as a result of the uniqueness of the solution, $IL10(t) > 0$ for $IL10(t_0) \geq 0$.

This establishes the lower bounds of T_R, the upper bounds of T_R can be determined by the following calculations.

As mentioned, $P = 0$ means that $\frac{dP(t)}{dt} = 0$ for all t. However, if $P(t_0) > 0$ then $\frac{dP(t)}{dt} \leq 0$ for all $t > t_0$, such that $M_P \equiv P(t_0)$ constitutes an upper limit for P.

Considering the upper limit for N, then

$$\begin{aligned}\frac{dN}{dt} &= k_N\left(1+\frac{k_{NTNF}TNF}{x_{NTNF}+TNF}\right)\frac{x_{NCA}}{x_{NCA}+C_A}\frac{x_{NIL10}}{x_{NIL10}+IL10}\cdot P - d_N N\\ &\leq k_N\left(1+k_{NTNF}\right)P - d_N N\\ &\leq k_N\left(1+k_{NTNF}\right)M_P - d_N N.\end{aligned}$$

Defining $M_N \equiv \frac{k_N(1+k_{NTNF})M_P}{d_N}$ then $N(t) \leq \max\{N(t_0), M_N\}$ for all $t > t_0$.

In a similar way, it can be shown that:

$$\frac{dC_A}{dt} < 0 \qquad \text{for} \qquad C_A > \max\{C_A(t_0), M_{CA}\},$$

where $M_{C_A} \equiv \frac{k_{CA}M_N+s_{CA}}{d_{CA}}$ and

$$\frac{dTNF}{dt} < 0 \qquad \text{for} \qquad TNF > \max\{TNF(t_0), M_{TNF}\},$$

where $M_{TNF} \equiv \frac{(k_{TNF}+k_{TNFTNF})\cdot M_N}{d_{TNF}}$ while

$$\frac{dIL10}{dt} < 0 \qquad \text{for} \qquad IL10 > \max\{IL10(t_0), M_{IL10}\},$$

where $M_{IL10} \equiv \frac{(k_{IL10}+k_{IL10CA}+s_{IL10})x_{IL10d}}{d_{IL10}x_{IL10d}-(k_{IL10}+k_{IL10CA}+s_{IL10})}$ for $d_{IL10}x_{IL10d} > (k_{IL10} + k_{IL10CA} + s_{IL10})$.

This means that there exists a trapping region $T_R = [0, M_P] \times [0, M_N] \times [0, M_{C_A}] \times [0, M_{TNF}] \times [0, M_{IL10}]$. Thus positivity and limitation of the solutions are ensured. Furthermore, the trapping region is attracting for all solutions $X(t_0) \in (\mathbb{R}_+ \cup \{0\})^5 \backslash T_R$ starting outside T_R, observed from the above calculus.

2.3.4 Residual Plots

When developing a mathematical model to describe a biological phenomena expressed by measurements, it is important to validate the model adequacy. Graphically and numerically the model has been validated according to the data in Section 2.3.2. However, also the assumption of structureless and normality of the error-terms must be investigated.

In Figure 2.3.4, the Q-Q plot (quantile-quantile plot) is shown in (a), (c) and (e). Here the theoretical quantiles of the normal distribution are plotted against the quantiles of the residuals. If the points lay on the strait line, the underlying errors can be assumed to be normally distributed. When evaluating the visualisation, the central values rather than the extreme values should be emphasised [24], which means that the assumption is not rejected in this case. Another

way to check the normality, is to plot a histogram of the errors. If the residuals look like a normal distribution and are centred around zero, the assumption holds, however, due to small sample sizes, this shape of the histogram can be different, even though the assumption is not violated. Thus plotting of the histograms are omitted.

In Figure 2.3.4 (b), (d) and (f), the standardised residuals are plotted against the predicted values of TNF and IL-10 respectively. The standardised residuals are defined as

$$R_i = \frac{r_i}{\tilde{\sigma}_r}, \tag{2.8}$$

where r_i is the i'th residual and $\tilde{\sigma}_r$ is the estimated standard deviation of the residuals[24]. As a rule of thump, approximately 95 percent of the standardised residuals should fall within the interval from $[-2, 2]$, while all of them should be in the interval $[-3, 3]$, not to be considered as a potential outlier. When plotting the standardised residuals against the predicted values, no structure or pattern should be visible, which is also the case in Figure 2.3.4. This suggests that the model correct.

In all, the five dimensional model seem to be a adequate model describing the dynamics of TNF-α and IL-10 as biomarkers for the acute inflammatory response as a reaction of invading endotoxin. Keeping in mind, that the data is collected from rats, the model is calibrated to describe the response in rats. However, the response of TNF-α are similar in humans considering both concentration- and time-dependence[11,18,34]. The response of IL-10 to LPS (endotoxin) in humans is described by Kemna et al. (2005), where a peak within the first four hours is observed similar to the simulated rat model. However, the response is only shown for the first four hours, which leaves neither validation nor rejection of two peaks of $IL10$[18]. Only one peak of the concentration of IL-10 as a response to LPS is observed in humans according to the experiment in 1996 by van der Poll et al., noticing that only 2 ng/kg was injected, thus the concentration is far less than the concentrations considered in the rat model. The peak of IL-10 in this experiment arose three hours after injection and the response ended within six hours[34].

Despite that the five dimensional model is developed to describe the response in rats, it seems to give a suitable qualitative description of the dynamics of the response in humans too. Therefore it will be used as a starting point for the coupled model presented later.

In the following chapter, a model describing the interactions of the hormones released by the Hypothalamic-Pituitary-Adrenal axis is studied.

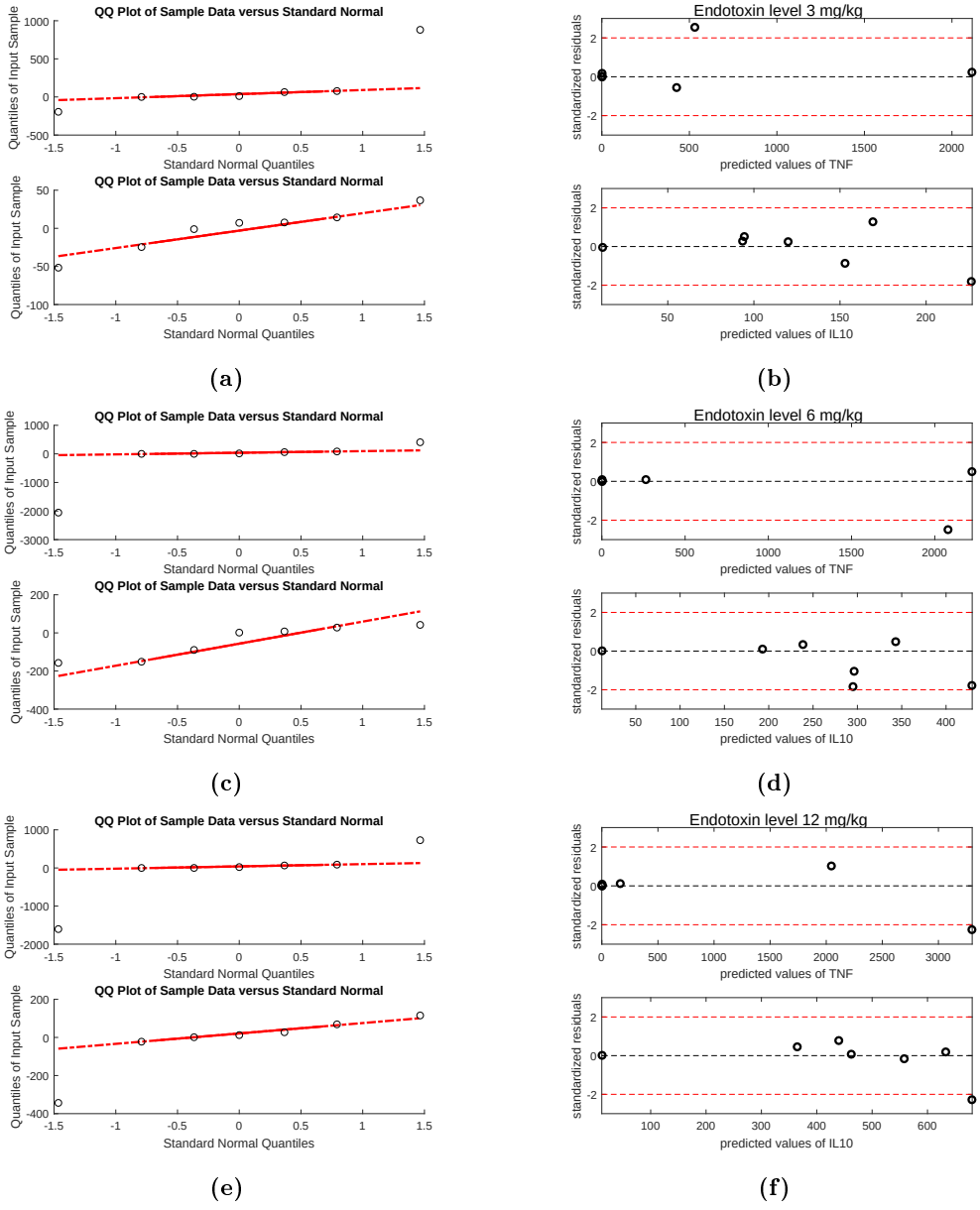

Figure 2.8: Residual plots of the five dimensional model presented in Section 2.3.2. To the left: Q-Q plots, validating the normality of the residuals by forming a straight line, when emphasising the center points. To the right: The standardised residuals plotted against the predicted values of the model. No structural pattern and all values between $[-3, 3]$ suggest a good model, with no outliers.

Chapter 3

Hypothalamic-Pituitary-Adrenal Axis

The hypothalamic-pituitary-adrenal axis (HPA axis) regulates the level of glucocorticoid hormones in the blood. The hormone called cortisol, is essential for several processes of the body. Especially, the regulation of cortisol is linked to the maintenance of body homeostasis as a response to both mental and physical stress (such as injected LPS). Besides this, the secretion and clearance of cortisol plays a role in the acute inflammatory response, where it acts as an anti-inflammatory mediator in the system.[32,33]

The secretion of cortisol is regulated by a feedback system. In the brain, Hippocampus stimulates hypothalamus to secrete corticotropin releasing hormone (CRH), which is transported to the pituitary resulting in a release of adrenocorticotropic hormone (ACTH). Then ACTH is moved through the blood circulation to the adrenal cortex, where it stimulates the production and release of cortisol. Cortisol feeds back on hypothalamus and inhibits the release of CRH and thereby ACTH, leading to a decrease of cortisol.[13,22,26]

The secretion of cortisol has been studied in many cases revealing both circadian and ultradian oscillations in the concentration[26]. Also the release of

ACTH follows similar patterns. The circadian rhythm of cortisol is observed in humans, by low concentrations of cortisol in the very early hours of the day, which increases during early morning hours to a maximum peak around noon, whereupon the concentrations roughly decreases to a low level during the night. The circadian clock causing the circadian rhythm is superiorly synchronised by the suprachiasmatic nuclei (SCN), located in the hypothalamus in the brain[1].

In this chapter, different modelling approaches of the HPA axis are presented, after which a three dimensional model describing the dynamics of CRH, ACTH and cortisol of the HPA axis is studied in details. This lead to an adequate model, describing the dynamics in humans.

3.1 Modelling Approaches

Up till today, no commonly used model of the interactions in the HPA axis has been published. There exist different opinions on the origin of the circadian and ultradian rhythms observed in data for ACTH and cortisol in humans.

In the work accomplished by Jelić et al. (2005), it is assumed that changes in the dynamics of CRH are negligible thus the overall dynamics of the HPA axis activity can be described by a two dimensional model featuring ACTH and cortisol as variables. The model produces ultradian rhythms in the model simulation of cortisol, which is generated by large time delays. In this paper, the circadian rhythm of cortisol is modelled as an external periodic function, while the model is not calibrated to data and the concentration of CRH is assumed constant as mentioned.[16]

A two dimensional model describing the dynamics of ACTH and cortisol was proposed by Conrad et al. (2009). The model contains 7 parameters, an external input and the two compartments in the model covers a pooled influence of CRH and ACTH (interpreted as plasma ACTH) and cortisol. While the CRH-ACTH variable stimulates cortisol, the cortisol variable has both a positive and negative feedback on the CRH-ACTH variable. Besides analysing the model mathematically, the parameters are fitted to data. The data consists of the mean of ACTH and cortisol concentrations of 20 humans receiving 1 μg/kg CRH at time $t = 0$. Even though the model fits the data very well, only the circadian rhythm of ACTH and cortisol is seen in the data and explained by the model, thus the ultradian rhythms are not considered.[10]

A four dimensional model including the variables CRH, ACTH, cortisol and glucocorticoid receptors (GR) in the pituitary is presented by Gupta et al. (2007).

The authors postulates that the inclusion of the dynamics of the GR synthesis in the pituitary demonstrates bistability of the HPA axis. However, the validation of the model seems very weak. The model is validated by simulating the cortisol level by feeding experimental human ACTH data into the equation for cortisol. Therefore it is not surprising, that the model predictions come very close to the measured cortisol data, predicting both the observed circadian and ultradian rhythms, since the dynamics of cortisol closely follows that of ACTH. The ACTH prediction of the model is not validated, arguing that the hypothalamic derived CRH cannot be measured and therefore there is no CRH data to feed into the ACTH equation. However, when not feeding the data into the cortisol equation, simulations of the closed model did not produce any oscillations.[13]

A model developed for distinguishing between normal humans and humans diagnosed with either depression or Post-traumatic Stress Disordered (PTSD) is proposed by Sriram et al. (2012). The authors seek to use the dynamics of cortisol as a biomarker for psychiatric disorders. It is claimed, that the model can produce ultradian rhythms of cortisol, however, this is not observed in simulations of the model. Furthermore the simulations of subjects suffering from depression and PTSD fits the given data set much better than the simulation of cortisol concentrations for normal subjects.[31]

Andersen et al. (2013) present a three dimensional model describing the dynamics of the CRH, ACTH and cortisol concentrations. After a comprehensive mathematical analysis of the model, it is shown that no periodic solutions exists for physiological reasonable parameter values. However, it is found that the system has either one stable equilibrium (representing normal cortisolemic) or two stable (representing hypercortisolemic and hypocortisolemic depression) and one unstable equilibrium (representing normal cortisolemic) depending on perturbation of the parameters. Thus this result could be used as a possible biomarker for depressed humans.[2]

In recent work by Hosseinichimeh et al. (2015), several different model approaches of the dynamics of the HPA axis are reviewed in the aim of finding the model which fits a chosen data set best (assuming, that the data used for testing has not been used as calibrating data for any of the models). Five models, published before 2015, representing the human HPA axis and capturing the interactions and their evolution over time, are compared. It is noticeable, that the validation of the models are performed by using the data of either cortisol or ACTH, respectively, to predict the simulations of the other (called partial prediction method in the article). Based on statistically calculations of these results, the authors conclude that the model proposed by Andersen et al. (2013) provides the best overall fit. In the aim of improving the fit of this model, the authors recalibrates the model to data by the partial prediction method, also including a circadian rhythm in the equation for cortisol described by an indi-

vidualised third order function of time. However, it is found that without the inclusion of individualised circadian rhythm, the re-calibrated, closed model was not capable of producing ultradian oscillations.[15]

A three dimensional model capable of producing both circadian and ultradian rhythms in the concentrations of CRH, ACTH and cortisol was proposed by Ottesen (2011) (presented at the IFAC Congress). The model generates the circadian rhythm by an endogenous function in time incorporated in the equation for CRH. Furthermore, the production of CRH is modelled to up-regulate its own production, in accordance with experimental evidence in the literature, unlike the previous considered models. The model has not yet been fitted to data, thus the author is investigating different methods for estimating the parameters in the model.[25]. The reason why the model is not included in the meta-analysis by Hosseinichimeh et al. (2015), is that the model is not published yet.

The three dimensional model presented by Ottesen (2011) seems to be the only model among the considered, which produces both circadian and ultradian rhythms. Based on this, the model seems to be the most adequate model, describing the dynamics of the HPA axis in humans. The model will be investigated and studied in details in the following. First the model is presented and simulated, then the existence and uniqueness of the solutions is shown. In addition, the existence of a trapping region and positivity of the model is proved. Furthermore, some approximations are done and the dynamics of the system is studied, keeping the time varying circadian input function constant, making the system autonomous. Hereafter, the time varying system is simulated and compared to data of humans characterised as normal (contrary to depressed) and finally, parameter estimation and residual analysis of the model are carried out.

3.2 Human Model of the HPA Axis

In this chapter, a model describing the dynamics of the hormones CRH, ACTH and cortisol in the HPA axis in humans is presented and analysed.

Inspired by the model proposed by Ottesen (2011) and the work accomplished by Rasmussen et al. (2015), a simple model of the interactions of the HPA axis

can be presented by

$$\begin{aligned}
\frac{dCRH(t)}{dt} &= a_0 + C(t)\frac{a_1}{1+a_2 Cortisol(t)^2}\frac{CRH(t)}{\mu + CRH(t)} - \omega_1 CRH(t) \\
\frac{dACTH(t)}{dt} &= \frac{a_3 CRH(t)}{1+a_4 Cortisol(t)} - \omega_2 ACTH(t) \\
\frac{dCortisol(t)}{dt} &= a_5 ACTH(t)^2 - \omega_3 Cortisol(t),
\end{aligned} \tag{3.1}$$

where

$$C(t) = N_c \left(\frac{t_m^k}{t_m^k + \alpha^k} \cdot \frac{(T - t_m)^l}{(T - t_m)^l + \beta^l} + \epsilon \right), \tag{3.2}$$

which simulates one single period of the circadian rhythm. The time unit is minutes and t_m can be calculated as $t_m = (t - \delta)$ modulo 1440. t_m denotes the time modulo 24 hours shifted by δ. $T = 1440$ min and N_c is a normalisation constant.

The model can visually be described as seen in Figure 3.1. The secretion of CRH is affected by the circadian rhythm and is auto-up-regulating. When CRH is released, it stimulates the release of ACTH. An up-regulation of ACTH further stimulates the production and release of cortisol which at last inhibits the secretion of CRH and ACTH by feedback mechanisms.

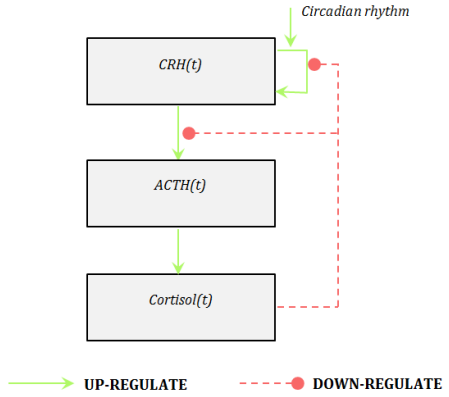

Figure 3.1: Diagram of the dynamics in Model (3.1)-(3.2). The model contains three variables CRH, $ACTH$ and $Cortisol$. From hypothalamus CRH is secreted, causig an auto-up-regulation and an up-regulation of ACTH. The up-regulation of ACTH in the pituitary initiates an up-regulation of cortisol released from the adrenal. Then feedback mechanisms inhibit both CRH and ACTH. A circadian rhythm affects the system from SCN and enters through regulation of the auto-up-regulation of CRH.

In Figure 3.2 a simulation of Model (3.1)-(3.2) over three days is shown. Both the circadian and ultradian oscillations are seen for all three variables. The time

$t = 0$ indicates midnight. The circadian function $C(t)$ results in an increase of the concentration of CRH. $C(t)$ increases until approximately 8 a.m. and declines after noon. This pattern repeats every 24 hour. Notice that the model has a transient period covering the first day, before it tends to the steady state solution. The parameters used for the simulation can be found in Appendix B.1.

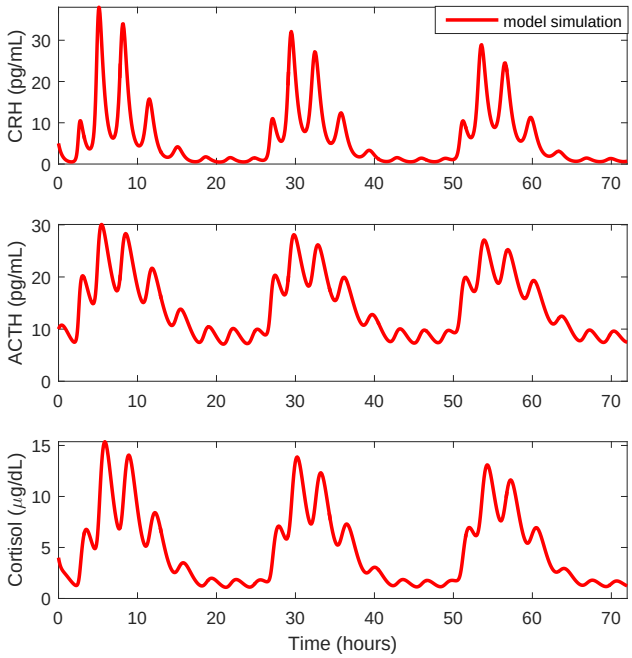

Figure 3.2: Simulation of HPA axis model ((3.1)-(3.2)) over three days. For all three variables both circadian and ultradian oscillations are observed.

There are some differences between the model proposed by Ottesen (2011), the reduced version studied in Rasmussen et al. (2015) and the model presented in this thesis. The model proposed by Ottesen (2011) multiplies the parameter a_0 by the circadian rhythm in the equation for CRH, while the inhibition term of CRH consists of both a first and second order term in $Cortsiol$. Furthermore, there is also included a first order term of $ACTH$ in the equation for $Cortsiol$ contributing to the up-regulation. The work by Rasmussen et al. (2015) shows that these three terms in the model does not contribute to a change in the model outcome within the physiological range of the parameters, and therefore

the model can be reduced by removing these terms.

The model presented in this thesis resembles the reduced model, however there are some modifications. The parameter a_0 is included in the equation for CRH to model a basic level of secretion of CRH, which might seem reasonable from a biological perspective, since it also ensures positivity of the model. Furthermore, the auto-up-regulation of CRH is described by a Michaelis-Menten function compared to the linear description in the reduced model. This means that the increase of CRH is limited since the Michealis-Menten function has a saturation for large concentrations of CRH and hence it guarantees boundedness of the solutions. At last, an inspection of the function describing circadian rhythm used in the reduced model revealed a discontinuity of the function when repeating the rhythm. From a biological point of view, such a discontinuous 'circadian clock' seems very unrealistic. Therefore, a continuous and normed function described by Hill-functions is used instead of the discontinuous and unnormed function described by a product of time to the power of three and an exponential term.

3.2.1 Variables and Parameters

The variables and parameters are presented and discussed in this section, since the biological interpretation of the parameters in the model gives more insight to the system.

CRH and $ACTH$ denotes the concentrations of CRH and ACTH in pg/mL, respectively, while $Cortisol$ represents the concentration of cortisol in μg/dL.

$C(t)$ models the observed circadian rhythm of the system caused by the 'circadian clock' synchronised by the *SCN*. This function models a single period of the circadian rhythm, repeating itself after 24 hours. It is described by the product of two Hill functions. α and β represent the times at which the corresponding increasing or decreasing Hill-function reaches half the saturation. k changes the steepness of the increasing Hill-function at the half saturation point $t = \alpha$, while l changes the steepness of the decreasing Hill-function at $t = \beta$. Hence, raising the k and l values clarifies the s-shape of the Hill-functions and changes the steepness of the increase or decrease. ϵ represents the basic contribution from the 'circadian clock', which occurs during the night. δ describes the time shifting of the circadian rhythm observed in different subjects.

a_0 describes the basic secretion of CRH which only makes a greater contribution to the system, if the concentration of CRH is low, therefore it should be set to a small number. a_1 represents the strength of the auto-up-regulation of CRH, in this way it symbolises the synthesis of CRH under influence of the 'circadian

clock' modelled by $C(t)$ as mentioned. a_2 is multiplied by $Cortisol$ and controls the inhibition of the synthesis of CRH through cortisol. The inhibition of CRH is modelled by a second order term in $Cortisol$. Considering the mechanism as a chemical reaction, this can be interpreted as a cooperative effect. This model choice means that small concentrations of cortisol ($Cortisol \ll 1$) has a minor influence, while the effect of large concentrations ($Cortisol \gg 1$) is more extensive. μ, in the Michaelis-Menten function involving CRH, is the half-saturation constant. Thus μ determines the level of CRH at which the Michaelis-Menten function will reach half of its saturation value.

The strength of the stimulation of $ACTH$ by CRH in the absence of cortisol is denoted a_3, while a_4 represents the magnitude of the inhibition of the synthesis of ACTH by $Cortisol$.

a_5 describes the stimulation of cortisol by ACTH. $ACTH$ is included in the equation in squared form, which can be interpreted as a cooperative effect. From a chemical reaction perspective, this is similar to the inhibition of CRH by cortisol.

The parameters ω_1, ω_2 and ω_3 are interpreted as the elimination rates of CRH, ACTH and cortisol respectively.

In the following sections, the model is investigated analytically to prove existence and uniqueness of the solution and the existence of an attracting, trapping region.

3.2.2 Existence and Uniqueness

In this section, existence and uniqueness of the solution to the System (3.1)-(3.2) is proved. This result is used when finding the trapping region of the model in the next section.

Consider the System (3.1)-(3.2) on the form

$$\begin{aligned} \frac{du(t)}{dt} &= f(u,t) \\ u(t_0) &= u_0, \end{aligned} \tag{3.3}$$

where $u(t) = [CRH(t), ACTH(t), Cortsiol(t)]'$, u_0 denotes the initial condition and $f(u,t)$ is a vector containing the right-hand-side of the System (3.1).
It follows that $f(u,t)$ is Lipschitz continuous in u over any domain

$$\mathcal{D} = \{(u,t) | \parallel u - u_0 \parallel \leq a, t_0 \leq t \leq t_1\}$$

with $a > 0$ and $t_1 > t_0$, i.e. there exists a constant $\mathcal{L} \geq 0$ such that

$$\| f(u,t) - f(u^*,t) \| \leq \mathcal{L} \| u - u^* \|$$

for all (u,t), $(u^*,t) \in \mathcal{D}$, see Appendix B.2 for details.
Thus it follows from the *Existence and Uniqueness Theorem* that there exists a unique solution to (3.3) for all finite time intervals $[t_0, t_2]$[20].

3.2.3 Trapping Region

In the previous section, existence and uniqueness of the solution to (3.1)-(3.2) were shown. This result is now used to prove the existence of an attracting, trapping region T_R for the system.

Define $u(t) = [CRH(t), ACTH(t), Cortisol(t)]'$ as a solution to the System (3.1)-(3.2) and assume that all parameter values are positive and the initial conditions are non-negative. It follows that for any $u(t_0) \in (\mathbb{R}^+ \cup \{0\})^3 \backslash T_R$ then $u(t) \in T_R$ for $t > t_1$, for some $t_1 > t_0$ where $T_R = [0, M_{CRH}] \times [0, M_{ACTH}] \times [0, M_{Cortisol}]$.

To prove the existence of T_R, first the lower bounds are found. This also ensures positivity of system.

Consider the CRH-equation for $CRH = 0$, which gives $\frac{dCRH(t)}{dt} = a_0 > 0$. This means that the solution cannot cross the plane $\{u \in \mathcal{R}^3 | u_1 = CRH = 0\}$ in negative direction due to the uniqueness of the solution. So for a given $CRH(t_0) \geq 0$ then $CRH(t) > 0$ for all $t > t_0$.

Then considering the $Cortisol$-equation for $Cortsiol = 0$ which yields $\frac{dCortisol(t)}{dt}$ $= a_5 ACTH(t)^2 \geq 0$. Hence $Cortisol(t_0) \geq 0$ implies that $Cortisol(t) \geq 0$ for all $t > t_0$ due to the uniqueness of the solution.

For $ACTH = 0$ it is observed that $\frac{dACTH(t)}{dt} = \frac{a_3 CRH(t)}{1+a_4 Cortisol(t)} \geq 0$ since $CRH(t) \geq 0$ and $Cortisol(t) \geq 0$ for all $t > t_0$. Then it follows from the uniqueness of the solution, that $ACTH(t) \geq 0$ for $ACTH(t_0) \geq 0$ and $t > t_0$.

This constitute the lower bounds of T_R, the upper bounds are found by:

$$\begin{aligned}
\frac{dCRH}{dt} &= a_0 + C(t) \frac{a_1}{1 + a_2 Cortisol^2} \frac{CRH}{\mu + CRH} - \omega_1 CRH \\
&\leq a_0 + \frac{a_1}{1 + a_2 Cortisol^2} - \omega_1 CRH \\
&\leq a_0 + a_1 - \omega_1 CRH.
\end{aligned}$$

Thus $\frac{dCRH}{dt} < 0$ for $CRH > \frac{a_0+a_1}{\omega_1} \equiv M_{CRH}$, which means that $CRH(t) \leq \max\{CRH(t_0), M_{CRH}\}$ for all $t > t_0$.

Similarly, it can be shown that for all $t > t_0$ the following holds:

$$\frac{dACTH}{dt} < 0 \qquad \text{for} \qquad ACTH > \frac{a_3 M_{CRH}}{\omega_2} \equiv M_{ACTH}$$

and

$$\frac{dCortisol}{dt} < 0 \qquad \text{for} \qquad Cortisol > \frac{a_5 M_{ACTH}^2}{\omega_3} \equiv M_{Cortisol}.$$

This proves that there exists an attracting trapping region T_R, where solutions starting outside $T_R = [0, M_{CRH}] \times [0, M_{ACTH}] \times [0, M_{Cortisol}]$ are attracted into the region and solutions inside cannot leave the region.

3.2.4 Reduction and Dynamics of the System

In this section, the model is reduced by one parameter. Furthermore, the dynamics of the system is investigated for fixed values of the function $C(t)$ describing the circadian rhythm.

To get a better understanding of the influence of the parameters in the model, the parameters were varied one at a time, by decreasing and increasing the value by 50% respectively. The figures are shown in Appendix B.3. This is used to investigate the sensitivity of the parameters and later to manually fit the parameters to mimic the data as convincingly as possible, to give good and reliable initial guesses of the parameters used for the parameter estimation process. When studying the plots, it is seen that both a_3 and a_4 have minimal influence after the transient period on the model output of $ACTH$ and $Cortisol$, which is the two variables with available data. Furthermore, the change in the model outcome for all three variables when varying μ is insignificant. This suggests that the Michaelis-Menten function in CRH can be well approximated by a linear term, since the half-saturation constant $\mu \gg CRH$ in the physiological range of CRH. This approximation is also implemented in both the model proposed by Ottesen (2011) and the reduced model by Rasmussen et al. (2015). This reduces the model by one parameter:

$$\begin{aligned} \frac{dCRH(t)}{dt} &= a_0 + C(t)\frac{a_1 CRH(t)}{1 + a_2 Cortisol(t)^2} - \omega_1 CRH(t) \\ \frac{dACTH(t)}{dt} &= \frac{a_3 CRH(t)}{1 + a_4 Cortisol(t)} - \omega_2 ACTH(t) \\ \frac{dCortisol(t)}{dt} &= a_5 ACTH(t)^2 - \omega_3 Cortisol(t) \end{aligned} \quad , \tag{3.4}$$

where

$$C(t) = N\left(\frac{t_m^k}{t_m^k + \alpha^k} \cdot \frac{(T - t_m)^l}{(T - t_m)^l + \beta^l} + \epsilon\right). \tag{3.5}$$

The model is of three dimensions, which allows explicit investigation of the dynamics of the system. However, the system is non-autonomous and non-linear, which makes the analytical and theoretical investigation limited.

The system is examined for constant values of the function describing the circadian rhythm, which might reflect the dynamic of the system at that particular time point.

$C(t)$ is a bounded function, with a slow variation over time compared to the ultradian time-scale of the three variables as seen in Figure 3.3. This slow time variation suggests an investigation of the system for different fixed values of $C(t)$ in the interval $I = [\min_{0\leq t}\{C(t)\},\ \max_{0\leq t}\{C(t)\}] = [0.0192,\ 1]$, for the default parameter values reported in Appendix B.4. In the following, the system is investigated for fixed values of $C(t) = C_0 \in I$.

The equilibrium points of the system for constant $C(t) = C_0$ are found by solving

$$\frac{dCRH}{dt} = 0, \quad \frac{dACTH}{dt} = 0 \quad \text{and} \quad \frac{dCortisol}{dt} = 0 \tag{3.6}$$

for all $0 \leq t$. In this case, only one real, positive solution, $x^* = [CRH^*, ACTH^*, Cortisol^*]'$, to (3.6) is found. The solution depends explicit on time and can be found as a solution of a polynomial of degree seven.

By linearising the system, it is possible to investigate the dynamics close to equilibrium by a linear approximation. The linearisation of the system $dx/dt = f(x)$ at equilibrium x^* is given by $dy/dt = J(x^*)y$ where $y = x - x^*$ and $J(x^*)$ is the Jacobian matrix defined by

$$J(x^*) = \begin{bmatrix} \frac{df_1(x)}{dx_1} & \cdots & \frac{df_1(x)}{dx_n} \\ \vdots & \ddots & \vdots \\ \frac{df_n(x)}{dx_1} & \cdots & \frac{df_n(x)}{dx_n} \end{bmatrix}\Bigg|_{x=x^*}$$

By determining the eigenvalues of $J(x^*)$, it is possible to investigate the stability of the given equilibrium. For the System (3.4)-(3.5) with fixed $C(t) = C_0$, the Jacobian matrix is given by

$$J = \begin{bmatrix} \frac{a_1 C_0}{1+a_2 Cortisol^{*2}} - \omega_1 & 0 & -2C_0 \frac{a_1 CRH^* a_2 Cortisol^*}{(1+a_2 Cortisol^{*2})^2} \\ \frac{a_3}{1+a_4 Cortisol^*} & -\omega_2 & -\frac{a_3 a_4 CRH^*}{(1+a_4 Cortisol^*)^2} \\ 0 & 2a_5 ACTH^* & -\omega_3 \end{bmatrix}.$$

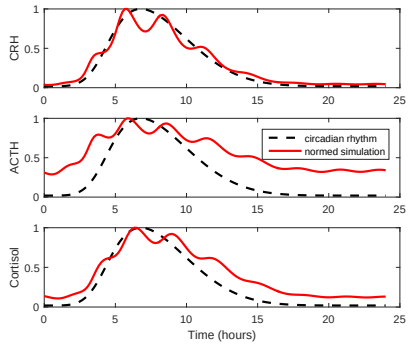

Figure 3.3: The time variation of the circadian rhythm $C(t)$ compared to the ultradian time variation of a normed simulation of the concentrations of CRH, ACTH and cortisol. $C(t)$ has a slower time variation than the ultradian variation of the three hormones of the HPA axis.

The eigenvalues of the Jacobian matrix for the equilibrium $CRH = CRH^*$, $ACTH = ACTH^*$ and $Cortisol = Cortisol^*$ are studied numerically for different fixed values of $C_0 \in I$. The eigenvalues of the Jacobian matrix of the given equilibrium are all of the form

$$\lambda_1 = -a + ib, \quad \lambda_2 = -a - ib, \quad \text{and} \quad \lambda_3 = -c \tag{3.7}$$

for fixed $C_0 \in I$, where a, b and $c > 0$. There is one negative eigenvalue and two complex conjugated eigenvalues with negative real part. This means that the equilibria are a hyperbolic sink-focus, and the points are stable for the default parameter values. The numeric value of the eigenvalues only changes slightly, contrary to the changes of the numeric values of the equilibria for different values of C_0 (see table 3.1).

Table 3.1: Numeric values of the eigenvalues λ_1, λ_2 and λ_3 associated with the equilibria $[CRH^*, ACTH^*, Cortsiol^*]$ for various fixed values of $C(t) = C_0 \in I$ for the default parameter values presented in Appendix B.4. The eigenvalues are given with four decimals after the leading decimal.

C_0	$[CRH^*, ACTH^*, Cortisol^*]$	λ_1, λ_2	λ_3
0.019	$[0.9, 8.6, 1.5]$	$-9.237 \cdot 10^{-4} \pm i \cdot 3.407 \cdot 10^{-2}$	$-4.921 \cdot 10^{-2}$
0.250	$[6.4, 16.3, 5.2]$	$-4.183 \cdot 10^{-4} \pm i \cdot 3.415 \cdot 10^{-2}$	$-4.932 \cdot 10^{-2}$
0.500	$[10.7, 19.3, 7.4]$	$-3.826 \cdot 10^{-4} \pm i \cdot 3.415 \cdot 10^{-2}$	$-4.933 \cdot 10^{-2}$
0.750	$[14.5, 21.4, 9.0]$	$-3.689 \cdot 10^{-4} \pm i \cdot 3.416 \cdot 10^{-2}$	$-4.933 \cdot 10^{-2}$
1.000	$[17.9, 23.0, 10.4]$	$-3.614 \cdot 10^{-4} \pm i \cdot 3.416 \cdot 10^{-2}$	$-4.933 \cdot 10^{-2}$

In Figure 3.4 the equilibria for different fixed values of $C(t) = C_0 \in I$ are

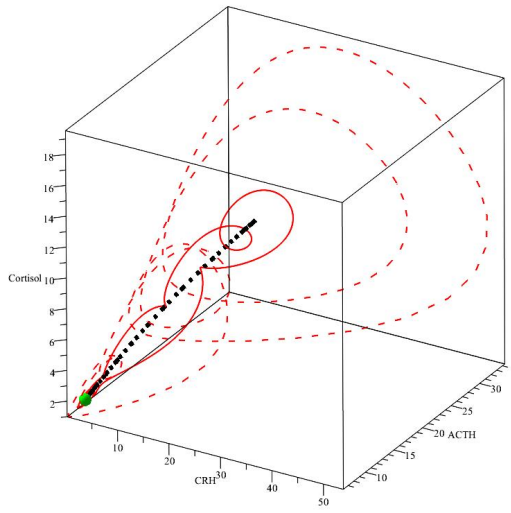

Figure 3.4: The phase space of the HPA system. The equilibria for fixed values of $C(t) = C_0 \in I$ is marked by black dots. The green circle indicates the equilibrium corresponding to the system for fixed $C(0) \approx 0.0192$. The orbit represents a solution curve, where the dashed part illustrates the transient period.

shown. It is seen, how the equilibria occurs at different positions in the phase space for different choices of C_0. The equilibrium represented by the green circle illustrates the equilibrium for the system with fixed $C(t) = 0.0192$ for time $t = 0$ and $t = 1440$. A solution curve is also shown in the figure. It is seen how the solution twists around the temporarily equilibrium points for fixed C_0. The solution curve is shown for two days, where the dashed orbit represents the transient period.

3.2.5 Simulation of the Human Model

In the following, Model (3.4)-(3.5) is simulated and compared to data. Additionally, the fit of the model is improved and the model is validated through residual plots.

The model is simulated and compared to data for ACTH and cortisol concentrations obtained from humans. Before presenting the simulations, the data is

smoothened and the influence of the parameters in the model is investigated.

The data come from a study described by Carroll et al. (2007), where 17 'normal' and 12 depressive humans were included. Since it is not of interest to investigate the ACTH and cortisol concentrations in relation to depression in this thesis, only the data for the 'normal' humans will be considered. Concentrations were measured within ten minute intervals over 24 hours, which highlights the ultradian pulses in both ACTH and cortisol. The measured concentrations of cortisol and ACTH are within the ranges $0.1 - 24$ μg/dL and $1 - 94$ pg/mL, respectively.

However, the high sampling frequency imposes amplified noise. The main purpose of this model is to describe the circadian and ultradian rhythms seen in data and not the small fluctuations, which can be considered as noise due to measuring errors, etc. Therefore, the data is smoothened using a moving average method. By calculating the average of each data point and its neighbours, the data is smoothened. In this case, a span of five is used resulting in $y_n = (y_{n-2} + y_{n-1} + y_n + y_{n+1} + y_{n+2})/5$ for $n = 3, ..., n_d - 2$, where n_d is the number of data points. The two end points are not smoothed and the two points $n = 2$ and $n = n_d - 1$ is calculated as an average of the two nearest neighbours and the point itself. The result of smoothen data for one of the subjects can be seen in Figure 3.5.

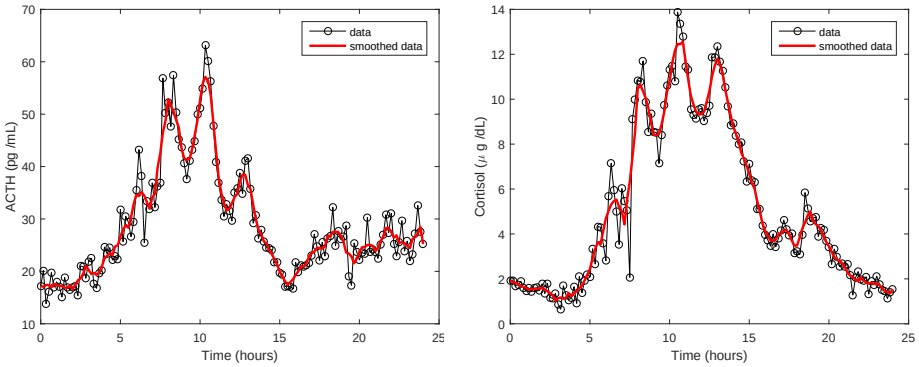

Figure 3.5: The red solid line represents the smoothened data, using a moving average filter with a span of five. The noise from the original data (black, circled line) is reduced.

Eight normal subjects are used for the calibration of parameters. The data is fitted separately, to avoid an elimination by averaging the ultradian rhythm observed in the individual measurements. In Figure 3.6, simulations of the ACTH and cortisol concentrations for eight subjects are shown. The results are obtained by manually changing the parameters in accordance to the knowledge of

the influence achieved by the plots in Appendix B.3.

When manually fitting the subjects, it is clear, that at least two parameters are very important when trying to fit all eight data sets. The parameter a_5 changes the ACTH level, which base level varies significantly for some of the subjects, without changing the level of cortisol to a greater extend. By only varying two parameters, namely a_5 and δ manually, the plots in Figure 3.6 can be obtained by using the parameter values from Appendix B.4 for the other parameters.

The model outcome mimics the data to some extend, which can be seen in Figure 3.6. However, especially the simulation of the ACTH concentration is very poor for some of the individuals, when comparing to the data as observed for subject (c) and (g). The predictions of the cortisol levels are more convincing and the model simulations captures many of the ultradian rhythms, but a difference in the frequency and magnitude of the oscillations is apparent. The cortisol level for the individual (g) has an early peak, which the model cannot reproduce. The simulations of the individuals (a), (d) and (h) provide reasonable good fits of the data, when only varying the two parameters a_5 and δ.

As mentioned, these results are obtained by only varying two parameters manually. The results are not adequate to postulate that the model describes the dynamics of the HPA axis in humans with these sets of parameter values. Using parameter estimation, permitting variation of more than the two parameters gives much more reliable fits as shown in the following. This leads to the conclusion, that the model is an adequate model describing the interactions in the human HPA axis.

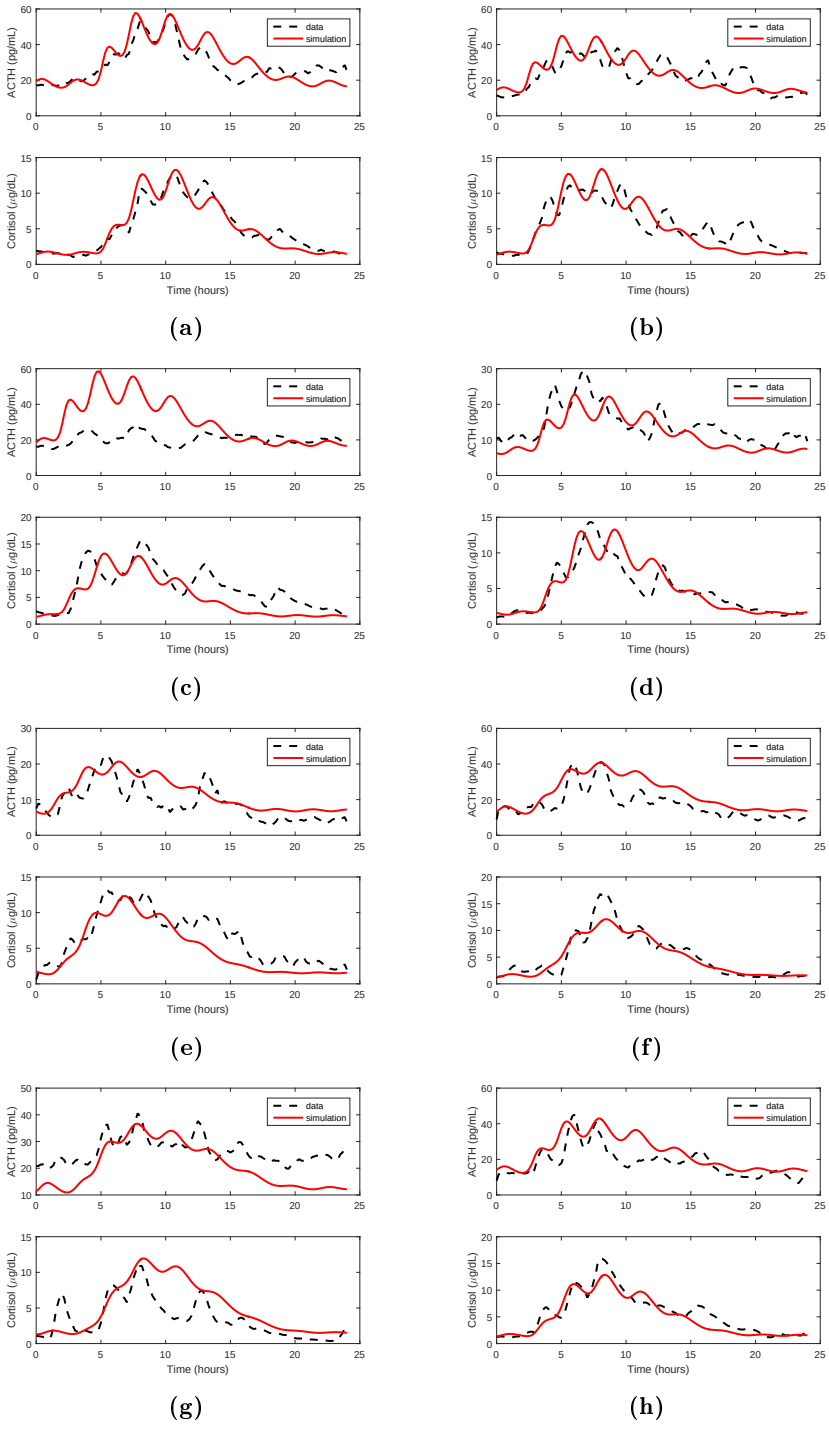

Figure 3.6: Simulation of the HPA axis model ((3.4)-(3.5)) using the parameter values presented in Appendix B.4 for varying a_5 and δ. The simulations are compared to data of ACTH and cortisol concentrations for eight subjects.

3.2.6 Parameter Estimation

In the following, parameter estimation is used to improve the fits of the eight subjects introduced in the previous section. The improvement in the fits are presented visually and numerically, by comparing the sum of squares. Finally, the residual plots are used to validate the model.

The model simulations seen in the previous section seem to fit the data to some extend for some of the subjects. Using parameter estimation of several of the parameters, it is possible to improve the agreement between the model prediction and data.

The parameters are estimated by minimising the dimensionless, weighted sum of squares

$$R_w = \frac{1}{145}\sum_{i=0}^{144}\left(\left(\frac{ACTH_i - y_i}{\overline{ACTH}}\right)^2 + \left(\frac{Cortisol_i - z_i}{\overline{Cortisol}}\right)^2\right), \tag{3.8}$$

where $ACTH_i$ and $Cortisol_i$ represents the i'th data point of the relevant subject, while y_i and z_i are the model predictions of ACTH and cortisol respectively, at time point i. $\overline{ACTH}$ and $\overline{Cortisol}$ denote the mean of the data set for the relevant subject over 24 hours and are used as weights in the function, which is important, since the two data sets are of different scales, but fitted simultaneously.

There are several ways to minimise R_w. One way is to use `MATLAB`'s build-in function `lsqnonlin` which uses the user-specified *Trust-region-reflective* algorithm to search for the minimum of the function. The results, using this algorithm to minimise the sum of squares, are shown in Figure 3.7. The estimation of parameters seems to improve the model prediction. The only simulation which does not agree with data to a satisfactory degree, is subject (g). The simulation does not fit neither the ACTH nor the cortisol data very well, however, this data set also appears to be different, with a lonely and very early peak of cortisol, which is not observed for the other subjects. Thus it may be considered as an outlier. Besides this, the model simulations are adequately, with the greatest problem appearing to be to model the oscillations of the right end tails of both ACTH and cortisol, which is a consequence of periodic model solutions in contrast to data.

To evaluate the improvement using the manually fitted parameters and the estimated parameters, the residuals are compared. In table 3.2 the squared 2-norm R_w from (3.8) is calculated for each of the subjects for both the simulations using the manually fitted parameter values and using the estimated parameter values. Together with this, the relative change in the squared norm of the residuals is calculated. It is no surprise, that the residuals are smaller for the

Table 3.2: The squared 2-norm of the residuals for each subject, calculated for the simulations using the manually fitted parameter values (Manually) and the estimated parameter values (Estimated). The relative change in the residuals reveals that the estimated parameters improve the correspondence between the model simulation and the data to a great extend.

Subject	(a)	(b)	(c)	(d)	(e)	(f)	(g)	(h)
Manually	0.11	0.28	0.78	0.25	0.35	0.28	0.72	0.25
Estimated	0.08	0.16	0.21	0.13	0.17	0.12	0.28	0.13
Relative Change (%)	27	43	73	48	51	57	61	48

estimated parameters, since these parameters are estimated to minimise this quantity. However, the interesting thing is the magnitude of the relative change for all of the subjects and the agreement between the simulations and the data, were many of the ultradian rhythms are mimicked. The solutions for subject (e) and (g) found by parameter estimation are almost without ultrdian oscillations, which may cause the relatively large R_w values. The poor manually fitted values used as initial guess for the parameter estimation may be one of the explanations for this.

The considered weighted residuals, R_w, covers both the residuals of ACTH and cortisol, since the parameters are estimated to fit both simultaneously. The residuals are weighted, such that the magnitude of the residuals becomes equal. The subject with the lowest R_w is subject (a), which also is observed from Figure 3.7, where especially the cortisol level fits the data very well. Also subject (d) and (f) provides very consistent fits of the data. The improvement of the simulation of subject (c) is noticeable, the improvement of the residuals is 73 % and the visualised change is very clear. The results are achieved by varying six of the parameters.

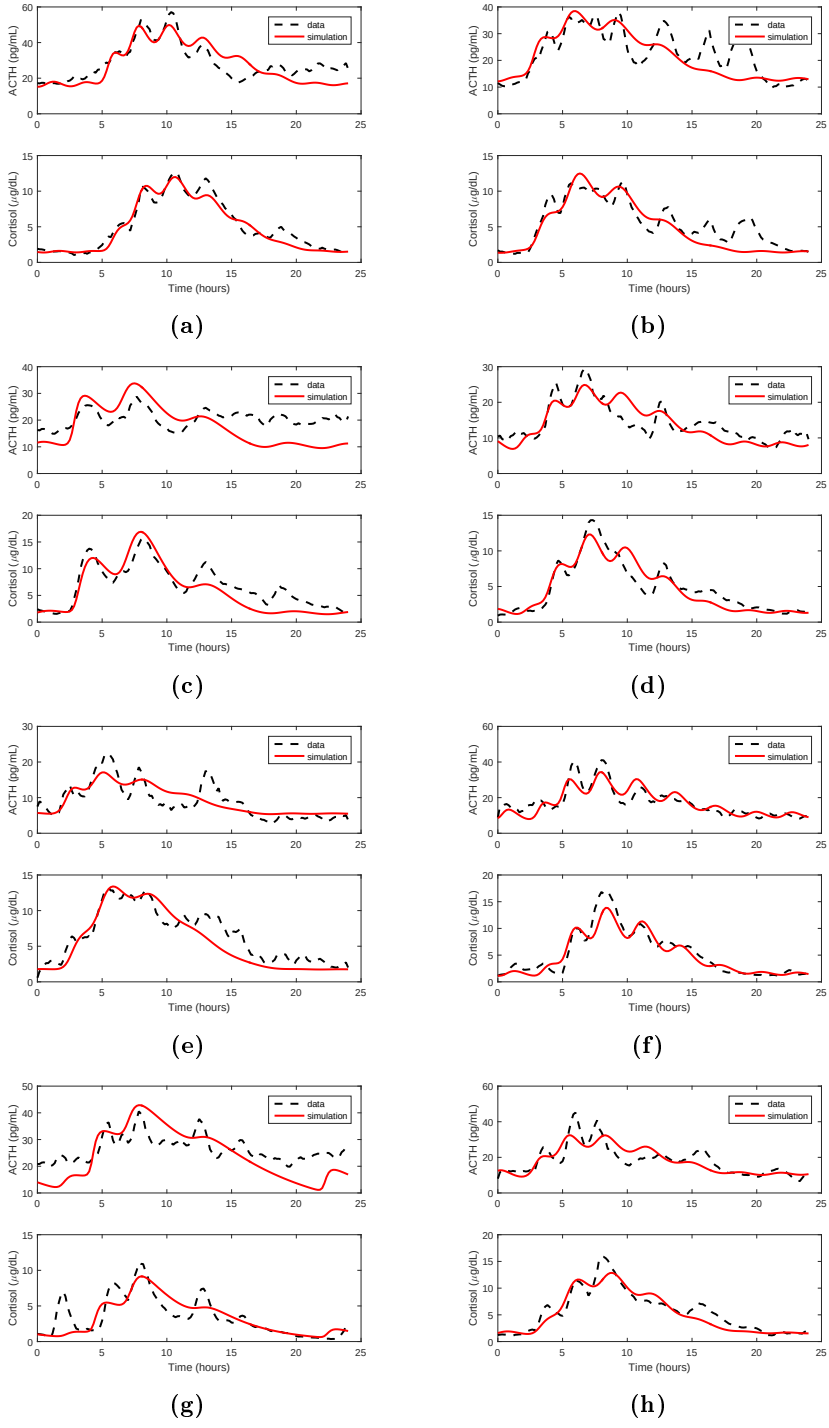

Figure 3.7: Simulation of the HPA axis model using the estimated parameters. The simulations (red solid lines) are compared to data for ACTH and cortisol (black dashed lines). The parameters are estimated individually for each subject.

3.2.7 Residual Plots

In the aim of validating the model adequacy, a visual residual analysis is carried out similar to the analysis of the five dimensional model of the acute inflammatory system in Section 2.3.4.

In Figure 3.8, the model simulation, the standardised residuals against the predicted values, a frequency histogram of the residuals and a Q-Q plot are shown for subject (f). The histogram and Q-Q plot suggest that the residuals are indeed normally distributed, while the standardised residuals do not reveal any structure or outliers to cause any major concern. Similar analysis for the other subjects are made, showing satisfying behaviour of the residuals, however, they are omitted from the report.

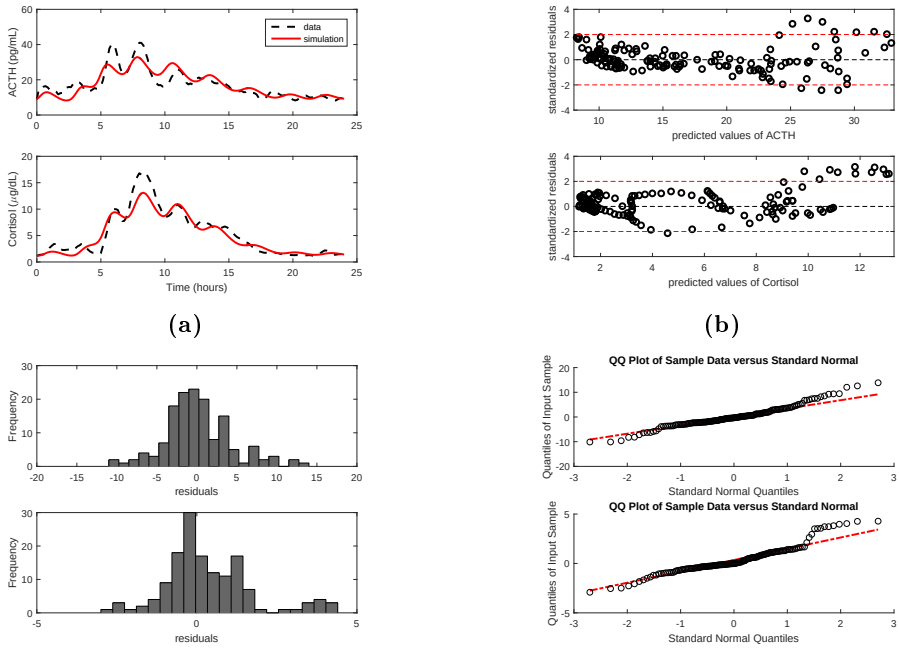

Figure 3.8: Residual plots for subject (f). The frequency histogram of the residuals and the Q-Q plot suggest normally distributed residuals and the standardised residuals plotted against the predicted values are structureless and fall in the interval $[-4, 4]$.

In the previous chapter, an adequate model of the acute inflammatory response

was formulated and now an adequate model describing the interactions of the HPA axis is found. In the following chapter, the two models will be coupled to investigate the coupling between the two subsystems of the human inflammatory system.

Chapter 4

The Coupled Model

In the previous chapters, a model of the acute inflammatory system in rats and a model of the HPA axis in humans has been studied in details and partly validated. Over the years, it has become clear, that there exists a coupling between these two systems. In this chapter, a model describing the interaction is proposed, calibrated to human data and studied for different scenarios.

As mentioned briefly, the interaction between the two subsystems is very important to maintain homeostasis. LPS activates the release of cytokines, which up-regulates the release of cortisol by activating the HPA axis. The released cortisol inhibits further synthesis of the cytokines[32,33]. In this way, the HPA axis is an essential component for returning to homeostasis after a response caused by endotoxin. Furthermore, the level of cortisol in humans has been closely connected with stress[5]. Describing the interaction between these two subsystems can potentially help understanding, prevent and cure diseases associated with the immune system.

So far, the investigation of the interaction between the two systems through mathematical modelling is very limited. There exists no commonly used model, which describes the interaction of the HPA axis and the acute inflammatory system. A very recent work published in December 2015 by Malek et al. tends to describe the dynamics of the HPA axis and some inflammatory cytokines. The authors proposes a model of five delayed differential equations contain-

ing 32 parameters and an external periodic function describing the circadian rhythm of the HPA axis[23]. The aim of the work, was to develop a mathematical model describing the interactions between the two subsystems to study the bi-directional communication. The included variables in the model are two of the inflammatory cytokines: TNF-α and IL-6, two of the hormones of the HPA axis: ACTH and cortisol together with endotoxin (LPS). The model is developed in two steps, first a two dimensional delayed model of the HPA axis (assuming a constant CRH level) is proposed. Then the model is extended by including the inflammatory cytokines and LPS as variables. Both delay parameters in the equations for ACTH and cortisol, are set to $\tau_1 = \tau_2 = 10$ min, which appears as relatively high delays. However, lowering the delay parameters reduces the amplitude of the ultradian rhythms in the simulations. Even though the model consists of five delay differential equations, the model is in fact infinite dimensional. After a combination of finding parameter values in literature and parameter estimation, the model is simulated and compared to data. The data contains measures of TNF-α, IL-6, ACTH and cortisol after an injection of LPS. The model seems to qualitatively capture the structure of the response, however, the actual fit to the data seems very poor. The injection of LPS is simulated as an infusion of 2 IU/kg over 10 min, which is contrary to the study. The subjects in the study, received an injection of 20 IU/kg, which might take far less time to inject, as described in the next section[8]. Malek et al. postulates that no mathematical model of the bi-directional interaction between the acute inflammatory system and the HPA axis has been proposed, even though various studies have been carried out[23].

4.1 Interactions of the Systems

In this section, a connection of the two systems is build as an attempt to describe the main interactions between the two subsystems. The proposed mechanisms are developed partly by biological reasoning and mathematically considerations related to data.

First, the models were non-dimensionalised, to explore the structure of the two subsystems and the effect of different modelling approaches of the mechanisms, see Appendix C.1. Based on this analysis, a specific model has been chosen.

In the following, a few modifications of the two models are presented in details in order to couple the models.

One major change is, that the variable C_A is divided into two parts, describing the effect of TGF-β1 and cortisol, respectively. This means, that the coupled

model contains the following eight variables:

- LPS (P)
- Number of phagocytic cells (N)
- Tumor necrosis factor-α (TNF)
- Interleukin 10 ($IL10$)
- Transforming growth factor-β1 (TGF)
- Corticotropin releasing hormone (CRH)
- Adrenocorticotropic hormone ($ACTH$)
- Cortisol ($Cortisol$).

The specific changes in the affected equations and the biological reasoning are described the following subsections.

4.1.1 The Equation for TNF-α

The acute inflammatory response model is developed and fitted using data from rats, while the HPA model is calibrated to data from humans. It seems reasonable to assume, that there is a difference between these systems in rats and humans. Furthermore, there is a great difference in the concentrations of LPS given to the rats (3, 6 and 12 mg/kg) compared to humans (2 ng/kg). Such a variation in dose, may cause quantitative differences in the responses. Based on this, it seems reasonable to change some of the parameter values in the coupled model.

In addition, the elimination rate of TNF-α is changed from a linear to second order term in order to reproduce data from humans. From a biological perspective, the elimination may be a second order Hill function in TNF, with a large saturation. However, this is not supported by data. Thus the simpler second order term is kept as a possible approximation. The changed elimination term reduces the degeneration of TNF-α for small concentrations. Furthermore, the linear dependence of N in the equation for TNF is changed to a Michealis-Menten function, lowering the sensitivity of the TNF-α response, especially for large N.

4.1.2 The Equation for TGF-β1

It is commonly known that cortisol acts in an anti-inflammatory way[32,33]. The anti-inflammatory effects of cortisol are modelled through a stimulation of TGF. The regulation of the cytokines by cortisol is thereby modelled through the effects of TGF-β1. TGF-β1, amongst other factors, has been shown to modulate the response of the HPA axis by affecting pro-inflammatory cytokines[17]. It has been shown, that elevated cortisol levels results in suppression of TNF-α and stimulation of IL-10[4]. This is consistent, with the modelling choice, since TGF-β1 modulates these effects. The stimulation of TGF-β1 by cortisol is modelled by introducing a Michealis-Menten function in $Cortisol$ in the equation for TGF-β.

4.1.3 The Equation for CRH and ACTH

The influence of the inflammatory system on the HPA axis is modelled by an up-regulation of CRH and ACTH by TNF-α. TNF-α is regarded as an activator of the HPA system[4]. Cytokines are activating the HPA axis at all three levels, however, the hypothalamic level (secreting CRH) is considered as the primary mechanism[4,30].

The effect of TNF-α on CRH is incorporated in the model and for data fitting purposes, the effect on ACTH is also included. The up-regulation of CRH and ACTH are introduced as a linear term (approximating a Michaelis-Menten function) and a second order Hill function, respectively, since it gives a good fit of the data.

4.1.4 The Equation for Cortisol

TGF-β1 has an inhibitory effect on cortisol[21], which is modelled by dividing the up-regulating term in ACTH by a linear term in TGF.

Summing up, the elimination rate of TNF-α is changed from linear to a second order dependence and the up-regulating term in N is changed to a Michealis-Menten function. An inhibiting effect of TGF-β1 is introduced in the equation for cortisol, while an up-regulating term of cortisol is included in the equation for TGF-β1. Furthermore, an up-regulation caused by TNF-α is incorporated in the equations for CRH and $ACTH$ and in addition, some parameter values

of the inflammatory subsystem are changed.

The resulting coupled model is presented in (4.1)-(4.2), where the red color indicates the newly introduced changes.

$$\begin{aligned}
\frac{dP}{dt} &= -d_P P \cdot N \\
\frac{dN}{dt} &= k_N \left(\left(1 + \frac{k_{NTNF} TNF}{x_{NTNF} + TNF} \right) \frac{x_{NTGF}}{x_{NTGF} + TGF} \cdot \frac{x_{NIL10}}{x_{NIL10} + IL10} \right) \cdot P - d_N N \\
\frac{dTGF}{dt} &= k_{TGF} \cdot N + q_1 \frac{Cortisol}{q_2 + Cortisol} - d_{TGF} TGF \\
\frac{dTNF}{dt} &= \frac{N}{xTNFN + N} \cdot \frac{x^4_{TNFTGF}}{x^4_{TNFTGF} + TGF^4} \left(k_{TNF} + \frac{k_{TNFTNF} TNF}{x_{TNFTNF} + TNF} \right) \\
&\quad - d_{TNF} TNF^2 \\
\frac{dIL10}{dt} &= k_{IL10N} \frac{N^3}{x^3_{IL10N} + N^3} + \frac{k_{IL10TGF} TGF^6}{x^6_{IL10TGF} + TGF^6} + s_{IL10} \\
&\quad - d_{IL10} \frac{x_{IL10d}}{x_{IL10d} + IL10} IL10 \\
\frac{dCRH}{dt} &= a_0 + C(t) \frac{a_1 CRH}{1 + a_2 Cortisol^2} + q_3 TNF - \omega_1 CRH \\
\frac{dACTH}{dt} &= \frac{a_3 CRH}{1 + a_4 Cortisol} + q_4 \frac{TNF^2}{q_5^2 + TNF^2} - \omega_2 ACTH \\
\frac{dCortisol}{dt} &= a_5 \frac{ACTH^2}{1 + q_6 TGF} - \omega_3 Cortisol,
\end{aligned} \tag{4.1}$$

where

$$C(t) = N_c \left(\frac{t_m^k}{t_m^k + \alpha^k} \cdot \frac{(T - t_m)^l}{(T - t_m)^l + \beta^l} + \epsilon \right). \tag{4.2}$$

The model describes the most considerable interactions of the main cytokines of the acute inflammatory system and hormones of the HPA axis. The model contains eight variables, four new interactions between the subsystems and seven new parameters resulting in a total of 43 parameters.

The main interactions between the variables can be seen in Figure 4.1. Notice, that the extended model (with a Michaelis-Menten function in CRH instead of a linear term in the equation for CRH) satisfies positivity and there exists an attracting trapping region ensuring boundedness of the solutions. The results are presented in Appendix C.2.

4.2 Calibration of the Model to Human Data

In previous section, a model proposed for the coupled system is presented. In this section, the model is calibrated to human data and compared to the model

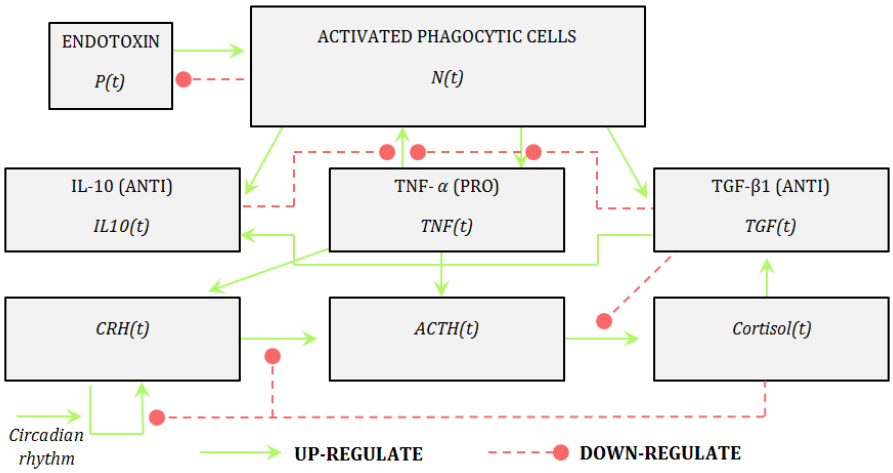

Figure 4.1: Diagram of the main dynamics in the coupled model (Model (4.1)-(4.2)). The green solid lines represent the up-regulating interactions and the red dashed lines represent the down-regulating interactions between the variables in the model.

proposed by Malek et al. (2015).

The data, originates from a study conducted by Clodi et al., designed for investigating the impact of oxytocin on the innate immune system in humans[8]. Data describes the response of TNF-α, ATCH and cortisol to a LPS injection of 20 IU/kg (corresponding to 2 ng/kg) in contrast to the response affected by an additional injection of oxytocin[8]. In this thesis, only the data describing the response in the concentrations in the absence of oxytocin is considered. Each data point is a mean and standard deviation of measurements on 10 healthy men.

The parameters introduced in the coupled model, are manually calibrated to mimic the data. The manually fitted parameters result in an adequate correspondence between the simulation of the model and data. By using parameter estimation on a few *selected* parameters, the fit of the model is improved. The *selected* parameters are chosen as parameters, which varies considerably between individuals. The parameters are the elimination rate of TNF-α (d_{TNF}), the strength of the stimulation of cortisol by ACTH (a_5), the time-shifting of the phase in the circadian function (δ) and the elimination rate of cortisol (ω_3). The response of TNF-α varies for individuals, and d_{TNF} is a possible parameter which might change between individuals causing this difference. In Section 3.2.5 the variation of a_5 and δ between individuals were clarified. The significance

of ω_3 on the simulations has a distinct effect on the ultradian oscillations for all three hormones of the HPA axis (see Appendix B.3), indicating that the system is sensitive to this parameter. The same goes for the elimination rate of CRH (ω_1), however, changing ω_3 provides a better fit to data, while keeping the concentration level of cortisol within the ranges observed from the data in Section 3.2.5. Thus, these parameters might vary considerable between individuals compared to the other parameters and therefore these are chosen as *special* parameters.

The *selected* parameters are estimated, using `nlinfit` in `MATLAB`. The result of the simulation for TNF, $ACTH$ and $Cortisol$ with the estimated parameters and a 95%-confidence band is compared to data in Figure 4.2. The confidence band is constructed by using the function `nlpredci` in `MATLAB`. The confidence band gives an estimate of the uncertainty of the mean of the fitted curve. The confidence band is calculated pointwise rather than simultaneously. The simulation with the estimated parameters mimics the data of TNF-α, ACTH and cortisol (see Figure 4.2). The model fits data, except for a few points.

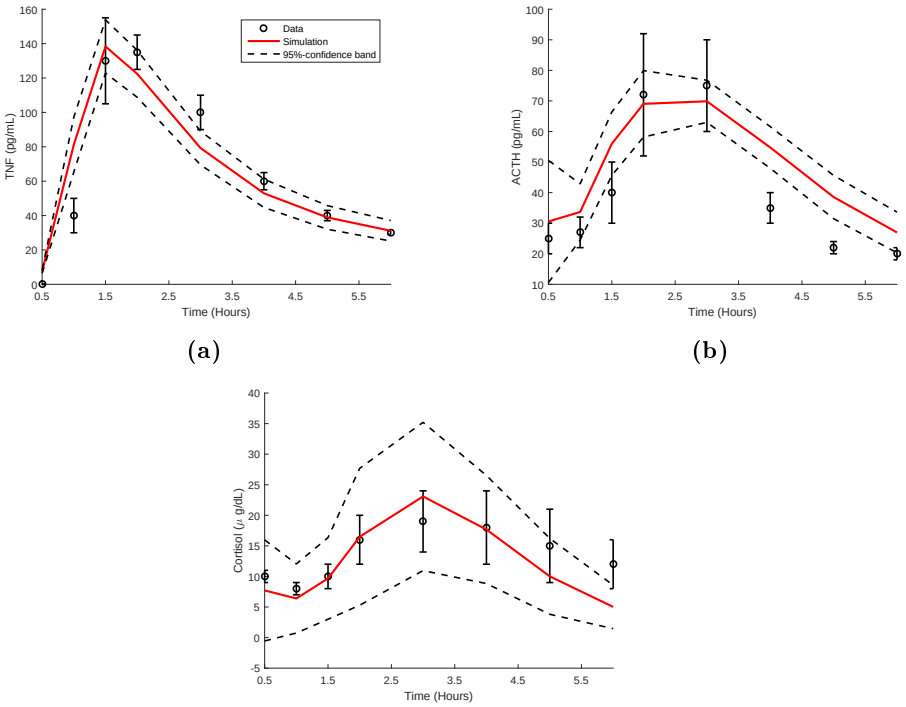

Figure 4.2: Simulation of the coupled model ((4.1)-(4.2)) with the estimated parameters. The red, solid line represents the simulation of TNF, $ACTH$ and $Cortisol$, respectively, and the black, dashed line represents the 95%-confidence band. The data (black circles) are represented as a mean and standard deviation of mesurements from ten subjects at each point. The time indicates hours after LPS injection.

The delayed differential model proposed by Malek et al. (2015) is calibrated to the same data, which gives a good opportunity for comparison of the two models. As mentioned, the model proposed by Malek et al. (2015) simulates the injection of LPS in a different way. The model proposed by Malek et al. (2015) simulates the injection of LPS by an infusion of 2 IU/kg over 10 min, while the injection in the coupled model is simulated by one bolus of 2 ng/kg ($\approx$ 20 IU/kg) over 1 min. Both infusions are started at $t = 13.5$ hour (the coupled model was simulated for one day before the injection day, to get past the transient period). The results of the simulations can be seen in Figure 4.3. Visually, the coupled model provides better fits of TNF and $Cortisol$, while the fits of $ACTH$ are somewhat equally good. Calculating the residuals for both models (similar to equation (3.8) in Section 3.2.6), shows that the coupled model provides at better fit ($R_w = 0.22$) compared to the model proposed by Malek et al. (2015) ($R_w = 0.64$). The parameter values and biological interpretation for the coupled model, used to produce the figures in this section, can be found in Appendix C.3.

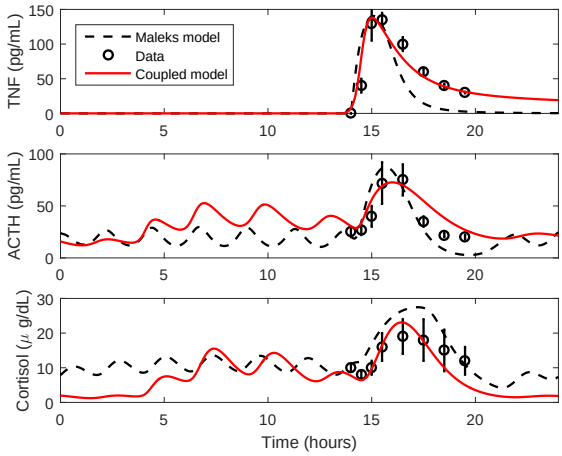

Figure 4.3: Comparison of the coupled model ((4.1)-(4.2)) and the model proposed by Malek et al. (2015) to data. The solid, red curve represents the simulation of the coupled model and the dashed, black curve represents the simulation of the model proposed by Malek et al. (2015). The data (black circles) is represented as a mean and standard deviation of mesurements on 10 subjects at each point. The LPS is injected at $t = 13.5$.

The coupled model provides a better fit to data, than the model proposed by Malek et al. (2015) (both visually and numerically). In the next sections, the coupled model is studied on its own terms. Thus the model is simulated and studied for different scenarios.

4.3 Simulation for Different LPS Doses

In Figure 4.4 and 4.5, model simulations for three different doses are compared to a simulation of the model with no injection of LPS. In Figure 4.4, the LPS is injected at $t = 7.5$ (at the top of the first ultradian rhythm, on the peak the circadian rhythm for cortisol) while the LPS bolus are given at $t = 9$ in Figure 4.5 (just after the first ultradian rhythm, on the peak the circadian rhythm for cortisol). The doses of injected LPS are chosen as 0.4, 2 and 10 ng/kg. The model is studied for these doses, to investigate the response to a dose chosen accordingly to the calibration data and doses higher and lower than this.

The simulations clarify the importance of the ultradian rhythms for small doses of LPS. The peak in cortisol is largest for the smallest LPS dose, when injecting on the top of the ultradian peak. The increase in cortisol for small doses of LPS has a delayed peak, compared to the response for the other doses for both injection times. The magnitude of the response in N is mainly controlled by the concentration of LPS (P). A large dose of P results in a large response of N, which stimulates TGF. The large stimulation of TGF inhibits $Cortisol$, which might be a reason, for the limited response in $Cortisol$ for large doses of LPS. The oscillations of ACTH and cortisol for the day after the injection at time $t = 9$ are also noticeable. For LPS dose 10 pg/kg, the ultradian rhythms are similar to the rhythms for no injected LPS, contrary to the simulations for the small LPS doses, where the ultradian rhythms have smaller amplitude. The circadian rhythm for cortisol is almost unchanged, while the level of ACTH is lifted.

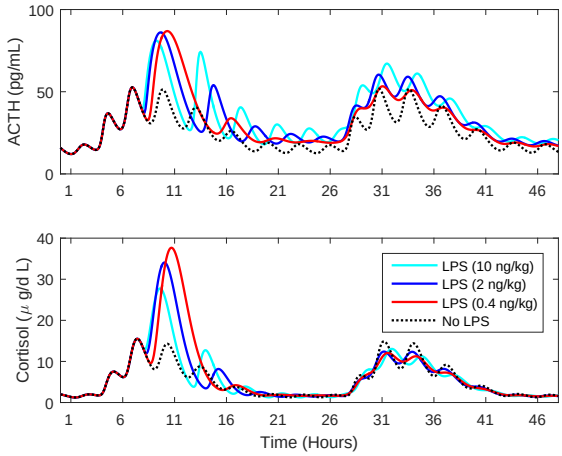

Figure 4.4: Simulation of the coupled model ((4.1)-(4.2)) for different doses of LPS (black dottet: 0 ng/kg, red: 0.4 ng/kg, blue: 2 ng/kg, cyan: 10 ng/kg) injected at $t = 7.5$.

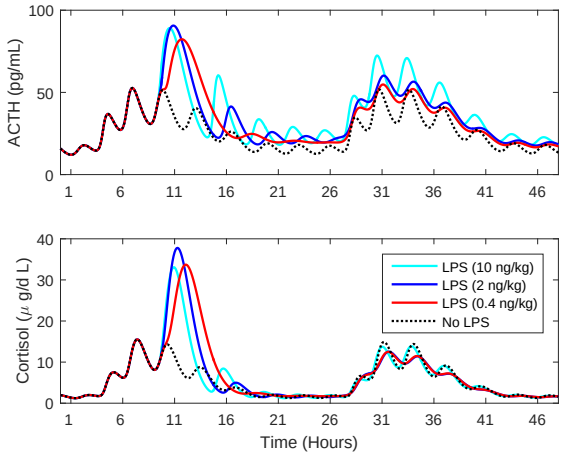

Figure 4.5: Simulation of the coupled model ((4.1)-(4.2)) for different doses of LPS (black dottet: 0 ng/kg, red: 0.4 ng/kg, blue: 2 ng/kg, cyan: 10 ng/kg) injected at $t = 9$.

4.4 Simulation for Different Times of LPS Injection

The model is simulated for LPS injection at different times, to investigate the effect of a LPS injection in relation to the observed ultradian and circadian rhythms in cortisol. In Figure 4.6 simulations of the coupled model ((4.1)-(4.2)) are shown for two days for different injection times.

The injections are given at $t = 6$, when level of cortisol is increasing, $t = 7.8$, just after the first ultradian peak on top of the circadian peak of cortisol, $t = 8.9$, just before the second ultradian peak on top of the circadian peak of cortisol, $t = 9.5$, at the peak of the second ultradian oscillation on top of the circadian peak of cortisol, $t = 16$, where the level of cortisol is decreasing and at last at $t = 24.8$ at the nadir of the cortisol level.

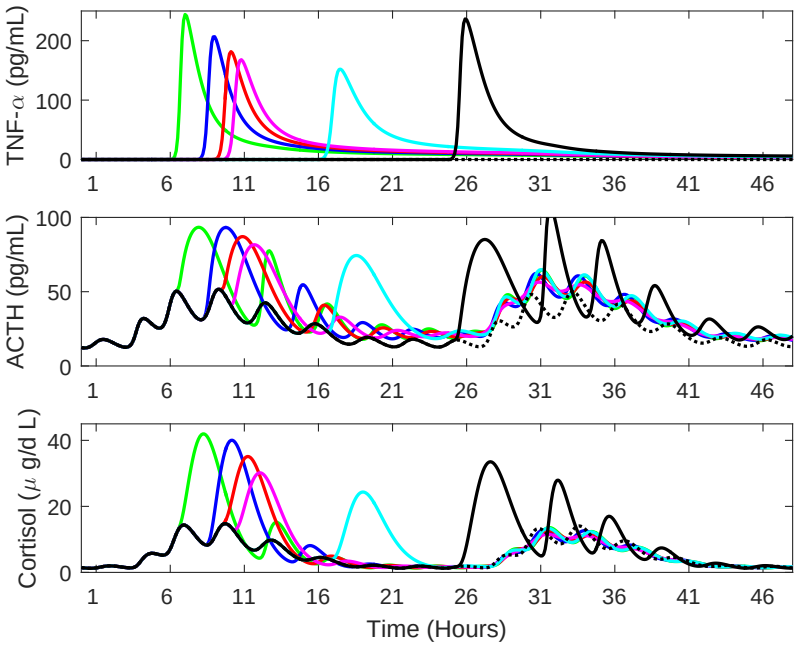

Figure 4.6: Simulation of the coupled model ((4.1)-(4.2)) for different times of injection of LPS (2 ng/kg) compared to the simulation for no injection of LPS (dotted, black line). The model is simualted over two days. The injection times for the simulations is $t = 6$ (green curve), $t = 7.8$ (blue curve), $t = 8.9$ (red curve), $t = 9.5$ (magenta curve), $t = 16$ (cyan curve) and $t = 24.8$ (black curve).

The injected LPS dose is 2 ng/kg for all simulations, except for the dotted curve, which represents the simulation for no injected LPS. The dose is chosen according to the LPS dose of the calibration data. The largest responses in ACTH and cortisol are observed in the early hours of the day, while the lowest responses are observed in the afternoon, where there is a decreasing trend in the circadian rhythms of the concentrations. At the nadir of the circadian rhythm, the response of both ACTH and cortisol are remarkably high compared to the baseline at this time.

4.5 Repeated LPS Injections

In this section, the model is studied for repeated LPS injections. In Figure 4.7, model simulations for no LPS injection, one LPS injection and two LPS injections (with an interval of 24 hours), respectively, are shown. The interval between the injections were chosen, such that the largest effect on the system were observed. In the first simulation, no LPS injection was given. In the second simulation, a LPS bolus of 2 ng/kg was given at $t = 13.5$ (the dose and time of injection was chosen according to the dose and time of injection for the calibration data). The third simulation represents the scenario, where a 2 ng/kg LPS bolus was given at $t = 13.5$ and an additional bolus was given at $t = 37.5$. It is seen, that the endotoxin is eliminated slower after the second LPS bolus. The injection is given before the system is returned to homeostasis, which causes a different response of the system. The response of phagocytic cells (N) is approximately less than half the magnitude for the second injection. The response of TNF-α is also very small, compared to the first response. The response of ACTH and cortisol is non-detectable for the second injection. This illustrates the importance of the system being in homeostasis, when exposed to LSP, such that intolerance is avoided.

The model was also simulated (but not shown) for 10 repeated LPS injections with injection intervals of both one half and one hour, respectively. This resulted in a prolonged low concentration of N and TNF, and a high concentration of TGF and $IL10$ with small oscillations. The LPS was eliminated every time after each injection, which seems reasonable, since the LPS has no ability of reproducing itself.

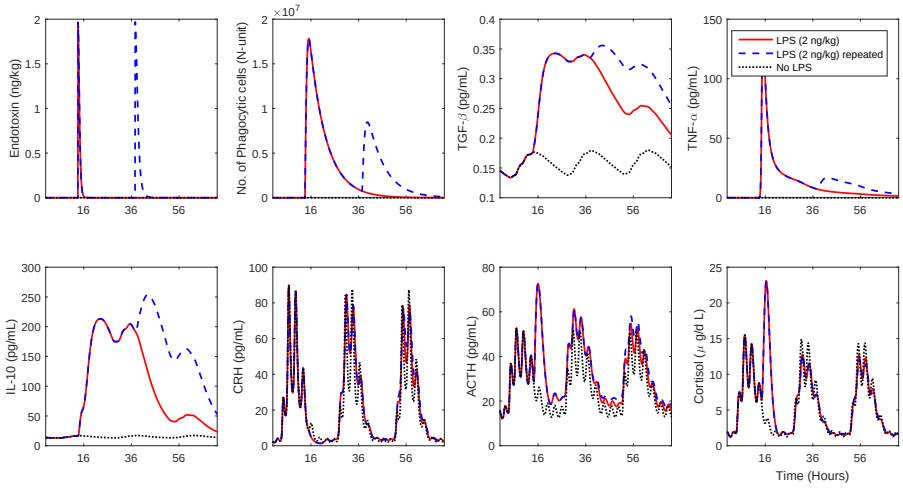

Figure 4.7: Simulation of the system ((4.1)-(4.2)) for repeated LPS injections. The dotted curve represents the simulation for no injection of LPS, the red curve represents the simulation for one bolus of LPS (2 ng/kg) at $t = 13.5$ and the blue dashed curve represents the simulation for two LPS injections of 2 ng/kg with an interval of 24 hours ($t = 13.5$ and $t = 27.5$).

4.6 Effects of LPS Injection During Baseline Level of LPS

The effect of constant infusion of LPS on the systems response to a bolus of LPS is simulated and the result is shown in Figure 4.8. This might be interpreted as a daily pressure from the environment, which all humans are exposed to every day, when breathing in the bus, at the work or in the gym. The constant infusion of LPS is simulated by including a baseline level of 0.1 ng/(kg·hr) of LPS. The dose and time of injection is chosen according to the calibration data as LPS dose of 2 ng/kg injected at time $t = 13.5$ for both the simulation with and without the baseline level of LPS, respectively. The constant infusion of LPS results in elevated levels of phagocytic cells, TGF-β1, TNF-α and IL-10 compared to the simulation of the concentrations for no LPS injections. In addition, the baseline level of LPS lowers the amplitude of the ultradian oscillations in CRH, ACTH and cortisol. The response to an injection of LPS, on the top of a baseline level of LPS results in an absent response of TNF-α, which is also observed for ACTH and cortisol, compared to the responses to the LPS injection with no baseline level of LPS.

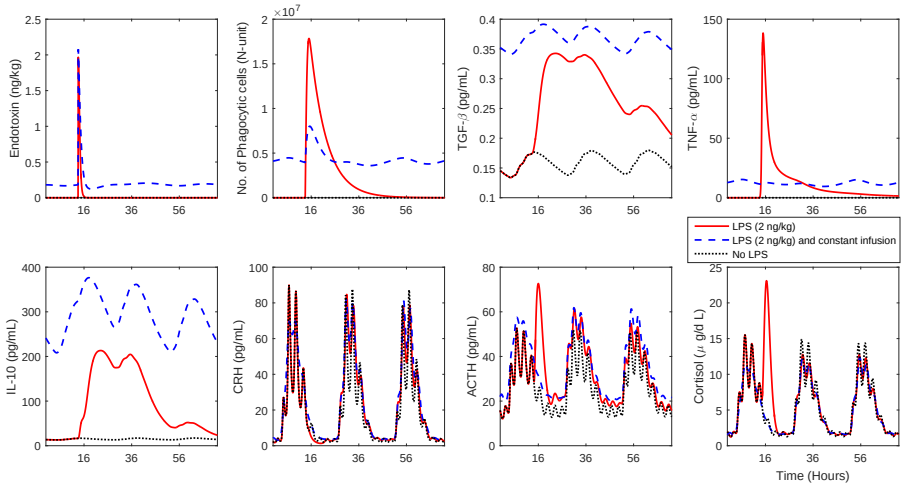

Figure 4.8: Simulation of the coupled model ((4.1)-(4.2)). The three simulations show the reponse of the system to no LPS injection, a LPS injection of 2 ng/kg and a LPS injection of 2 ng/kg on the top of a constant infusion of LPS (0.1 ng/(kg·hr)). The endotoxin is eliminated similarly, but the response of TNF-α, ACTH and cortisol is neglectable for constant LPS infusion.

This highlights the importance of reaming the immune system in homeostasis, since the response to invading (possibly reproducing) bacteria is inhibited when the system is stimulated over longer time.

To sum up, these simulations clarify the importance of dose, time and pre-activation of the immune system in relation to LPS injections.

Chapter 5

Discussion and Conclusion

The aim of this thesis was to formulate an adequate model describing the coupling between the acute inflammatory system and the HPA axis. To formulate a model describing the acute inflammatory response and a model describing the interactions between the hormones in the HPA axis, was included as subsidiary goals.

In the first part of the thesis, an eight dimensional model (proposed by Roy et al. (2009)) describing the interactions between endotoxin (LPS), the phagocytic cells (the eating cells of the immune system), damaged tissue, pro- and anti-inflammatory cytokines (TNF-α, IL-6, IL-10 and C_A) and an unknown Y_{IL10}-promoter was studied in details. The model was developed to document the behaviour of IL-6, TNF$-\alpha$ and IL-10 in rats exposed to different doses of LSP. Simulations of the model fitted data well, however, the model formulation was very complex and without biological reasoning. Therefore, the model was modified and reduced with a special view to simplification and biological rationale. From this, a five dimensional model of the acute inflammatory system was formulated, including the variables P (LPS), N (phagocytic cells), TNF, $IL10$ and C_A (slow acting anti-inflammatory mediators such as TGF-β1 and cortisol). The minimal model mimicked the data of TNF-α and IL-10 and the eight dimensional model only fitted data slightly better. The reduction of the model by three variables, 24 parameters (from 46 to 22) and included biological perspectives, however, make the five dimensional model preferable. Furthermore,

it was proven, that there exists an attracting trapping region for the model and that it satisfies positivity. Thus the solutions to the system are bounded, in accordance with biological expectation. A visual residual analysis was carried out, suggesting no concerns. The model was only calibrated to data from rats, since the attempt to access human data failed. The system in rats and humans are assumed to be somewhat similar. However, rats are nocturnal animals and the rats in the experiments are exposed to much higher doses of LPS compared to humans. This means that the systems are not identical despite their similarities. In the future, it could be interesting to calibrate and validate the five dimension for human data.

In the second part, a model describing the interactions between the hormones (CRH, ACTH and cortisol) of the HPA axis was formulated on a basis of a model proposed by Ottesen (2011) and the work accomplished by Rasmussen et al. (2015). The model describes both the observed circadian and ultradian rhythms in ACTH and cortisol for humans. Existence and uniqueness of the solutions, the existence of an attracting trapping region and positivity were proven. The system was investigated for different constant values of the function $C(t)$ (describing the circadian rhythm), revealing a stable equilibrium of the systems for constant $C(t)$. The model was simulated for eight subject and the parameters of the model was estimated to fit data of ACTH and cortisol. The model was well approximated by a model, where the Michaelis-Menten function in CRH was approximated by a linear term which led to satisfying fits for six of the eight subjects. A visual residual analysis was carried out. The behaviour of the residuals were satisfying. The model was calibrated to data from humans with normal cortisolemic level. In the future, it could be interesting to investigate whether model features a possible biomarker, distinguishing between normal and hyper- or hypocortisolemic levels (associated with depressed humans).

In the last part of the thesis, a model describing the coupling between the two studied subsystems of the immune system was formulated. The proposed mechanisms describing the interactions between the variables in the models were formulated partly by biological reasoning and partly by fitting the model to a mean of human data measured on ten individuals exposed to LPS. The measured data contains information for the concentrations of TNF-α, ACTH and cortisol after exposure of LPS dose 2 ng/kg. The simulations of the calibrated model was compared to a recently proposed model by Malek et al. (2015), which was calibrated to the same data. The coupled model formulated in the thesis fits the data set better than the model proposed by Malek et al. (2015). The model was simulated for different scenarios: injections of different LPS doses, different times of LPS injection, repeated LPS injections and the effect of a LPS injection under the influence of constant LPS infusion. Eventually, different data might help to validate the model and the simulated response to LPS. To fit the

model to the circadian and ultradian rhythms in ACTH and cortisol before a LPS injection, measurements over a longer period priori to the injection could be handy. Data for different doses of LPS injection, could be used to fit the model, to describe the response to different injection doses.

The three models formulated in this thesis are all adequate models of the different systems studied. The models represents simplifications of complex systems. The most important thing, is to capture the main effects and interactions in the systems of interest. The models are formulated by combining biological knowledge, mathematical and statistical modelling, in order to find a suitable level of details, i.e. neither being to simple nor too detailed.

Appendix A

Rat Model of Acute Inflammatory Response

In this appendix, supplements associated with the three models of the acute inflammatory response handled in Chapter 2 are presented.

A.1 Up- and Down-regulating Functions

Up-regulating and down-regulating functions associated with the eight dimensional rat model of the acute inflammatory response proposed by Roy et al. (2009) presented in Section 2.2. Functions of the form $fUP_{ij}(t)$ represent up-regulating effects of mediator j on mediator i while $fDN_{ij}(t)$ represent the down-regulating effects of mediator j on mediator i.

In the equation for N:

$$\begin{aligned} fUP_{NTNF}(t) &= \frac{TNF(t)}{x_{NTNF} + TNF(t)} \\ fUP_{NIL6}(t) &= \frac{IL6(t)}{x_{NIL6} + IL6(t)} \\ fDN_{NCA}(t) &= \frac{x_{NCA}}{x_{NCA} + C_A(t)} \\ fDN_{NIL10}(t) &= \frac{x_{NIL10}}{x_{NIL10} + IL10(t)} \end{aligned}$$

In the equation for $IL6$:

$$\begin{aligned} fUP_{IL6TNF}(t) &= \frac{TNF(t)}{x_{IL6TNF} + TNF(t)} \\ fUP_{IL6IL6}(t) &= \frac{IL6(t)}{x_{IL6IL6} + IL6(t)} \\ fDN_{IL6CA}(t) &= \frac{x_{IL6CA}}{x_{IL6CA} + C_A(t)} \\ fDN_{IL6IL10}(t) &= \frac{x_{IL6IL10}}{x_{IL6IL10} + IL10(t)} \end{aligned}$$

In the equation for TNF:

$$\begin{aligned} fUP_{TNFTNF}(t) &= \frac{TNF(t)}{x_{TNFTNF} + TNF(t)} \\ fDN_{TNFIL6}(t) &= \frac{x_{TNFIL6}}{x_{TNFIL6} + IL6(t)} \\ fDN_{TNFCA}(t) &= \frac{x^6_{TNFCA}}{x^6_{TNFCA} + C_A(t)^6} \\ fDN_{TNFIL10}(t) &= \frac{x_{TNFL10}}{x_{TNFIL10} + IL10(t)} \end{aligned}$$

In the equation for $IL10$:

$$\begin{aligned} fUP_{IL10TNF}(t) &= \frac{TNF(t)}{x_{IL10TNF} + TNF(t)} \\ fUP_{IL10IL6}(t) &= \frac{IL6(t)^4}{x^4_{IL10IL6} + IL6(t)^4} \\ fDN_{IL10d}(t) &= \frac{x_{IL10d}}{x_{IL10d} + IL10(t)} \end{aligned}$$

A.2 Analysis of Rat Model

In the following, the simulation of the eight dimensional model (System (2.1)-(2.2) presented in Section 2.2) is simulated, compared to data and analysed by reconsidering each equation, leading to the reduced six dimensional model (System (2.3) presented in Section 2.3).

Using the initial conditions from Appendix A.3 and parameter values from Appendix A.4, both obtained from the paper by Roy et al., simulations of the model are carried out.

To get a better understanding of the time evolution of the reactions in the system, the model is simulated and plotted in one plot. In Figure A.1 the simulations for P(0) = 3 mg/kg and P(0) = 12 mg/kg are shown respectively. The curves are normed, since the time evolution and not the magnitude of the responses is of interest. The acute inflammation response is initiated by the

introduction of endotoxin, which activates the phagocytic cells. The concentration of the phagocytic cells is the first to increase in the system. The increase up-regulates TNF-α, IL-10, IL-6, tissue damage marker and C_A, respectively. The phagocytic cells and TNF-α are the first concentrations to peak followed by the first peak of IL-10 and the tissue damage marker. While the phagocytic cells, TNF-α, IL-6 and the tissue damage marker decreases, the concentration of IL-10 increases to reach a second peak at the same time as the peak of Y_{IL10} and at last the peak of C_A occurs. At the end of the simulation ($t = 25$) the concentrations of P, TNF, $IL6$, D and N are low, almost negligible, while the concentrations of C_A, $IL10$ and Y_{IL10} are high but decreasing. TNF-α seems to be the fastest component of the system, in the way of the very fast activation and elimination, while the slow acting anti-inflammatory mediators (C_A) have the slowest increase and decrease over time.

The major difference between the two responses seen in Figure A.1, looks like the delay of the peaks and the greater deviation of IL-10 for endotoxin dose 12 mg/kg. An impact on TNF-α is also seen, the peak almost occurs before the peak of the phagocytic cells for $P(0) = 12$ mg/kg and the clearance is even faster. Thus the introduced endotoxin triggers the activation of the phagocytic cells, which up-regulates the inflammatory mediators. The pro-inflammatory cytokines operates first, after which the anti-inflammatory mediators takes over to inhibit the inflammation. The inflammation is inhibited after the threat is eliminated to prevent tissue damage amongst other inflammation driven issues. The immediate effect of the pro-inflammatory cytokines is a remarkable contrast to the implication of the anti-inflammatory mediators, which clearance is slower. This illuminates the issues concerning new pathogenic threats.

The model proposed by Roy et al. (2009) fits the experimental data convincingly. They use the data for endotoxin doses 3 and 12 mg/kg for calibrating the model and obtaining estimates for the parameter values. Afterwards they use data for endotoxin dose 6 mg/kg to validate the model. However, the validation would be stronger, if an endotoxin dose outside the interval [3, 12] or a larger sample size and frequency were used.

The resimulations of the model for the three different doses of endotoxin are shown in Figure A.2-A.4. As seen, the simulations for the three endotoxin dose levels all seem to capture the dynamic of IL-6, TNF-α and IL-10. However there are some limitations of the predictions. As seen in Figure A.2, the best agreement between data and simulation is for dose 3 mg/kg. Only the second data point of IL-6 is not predicted well. The predictions for dose level 6 and 12 mg/kg are poorly compared to the first prediction. In both cases, the peak of IL-6 and TNF-α occurs to early compared to the experimental data, resulting in a deficient description of the first data points for these variables. Furthermore, the behaviour of the decreasing period of IL-10 for dose 6 mg/kg is not

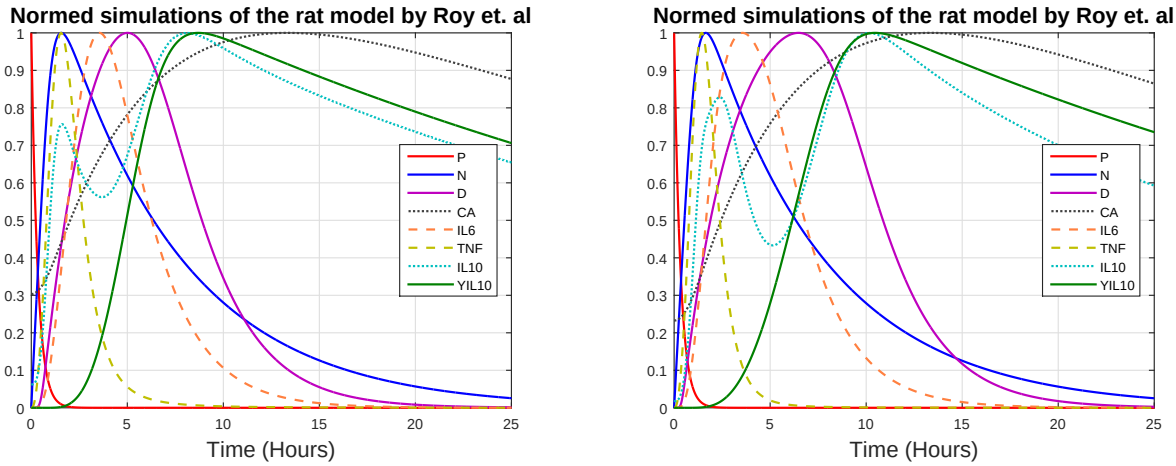

(a) $P(0) = 3$ mg/kg **(b)** $P(0) = 12$ mg/kg

Figure A.1: In (a) and (b) an overview of the normed simulations of the variables in the eight dimensional rat model is shown for endotoxin dose 3 and 12 mg/kg respectively. The figures describe the reaction times of the substances over time. At time $t = 0$, endotoxin is introduced to the system. For both doses, the elimination of endotoxin (P) happens within the first few hours. The presence of P (red solid line) initiates the immune response by activating the phagocytic cells (N, blue solid line) which further up-regulates both the pro-inflammatory cytokines ($IL6$, orange dashed line and TNF, yellow dashed line), tissue damage marker (D, magenta solid line) and the anti-inflammatory mediators ($IL10$, cyan dotted line and C_A, black dotted line). At last the IL-10 promoter is up-regulated (Y_{IL10}, green solid line) causing a second peak of IL-10, before the anti-inflammatory mediators inhibit the system. At time $t = 25$, the concentrations of P, N, D(t), $IL6$ and TNF are vanishing while the concentrations of C_A, $IL10$ and Y_{IL10} are rather high, but descreasing.

completely satisfying. The model fit this data very well, all things considered.

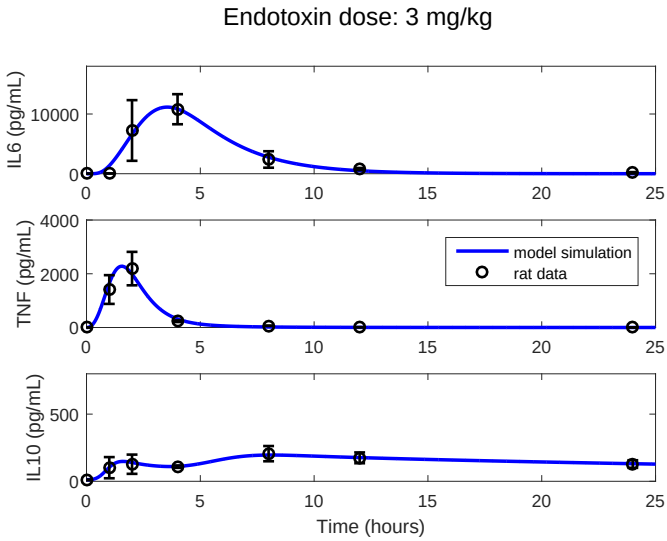

Figure A.2: Comparison of the resimulation of the eight dimensional acute inflammatory respose-model (Model (2.1)-(2.2), solid line) and experimental rat data for injection of an endotoxin dose of 3 mg/kg at time $t = 0$ (circles). The data for endotoxin dose level 3 and 12 mg/kg were used for calibration of the parameter values, while the data for endotoxin dose level 6 mg/kg were used for validation. The simulation of the model agrees very well with the data. The data are a mean of measurements from four rats and the standard deviation at each data point is shown.

The overall performance of the acute inflammatory response-model proposed by Roy et al. (2009) is indeed capturing the dynamics of three of the major inflammatory cytokines IL-6, TNF-α and IL-10. However the model consists of eight differential equations, some more or less complex mathematical terms and 46 parameters. Thus it is of interest to see, whether the model can be simplified to obtain a reduced model system which still captures the dynamics of IL-6, TNF-α and IL-10.

It is desirable to reduce the model, since it is aimed to be a part of a more complicated coupling-model describing the interactions between the acute inflammatory system and the HPA axis. The importance of the variables in the system is evaluated and the number of parameters is reduced. Furthermore, the missing biological aspect is reconsidered for some mechanisms.

The analysis and reductions are described in details in the following, were each of the equations in model are revisited one by one.

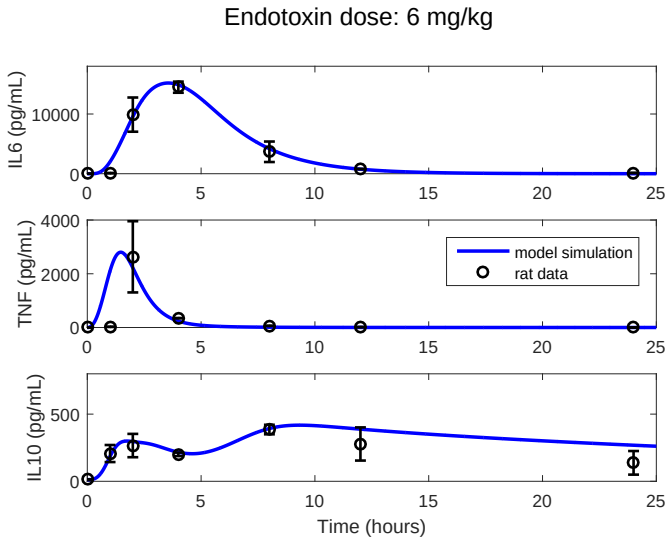

Figure A.3: Comparison of the resimulation of the eight dimensional acute inflammatory respose-model (Model (2.1)-(2.2), solid line) and experimental rat data for injection of an endotoxin dose of 6 mg/kg at time $t = 0$ (circles). The data for endotoxin dose 3 and 12 mg/kg were used for calibration of the parameter values, while the data set for endotoxin dose 6 mg/kg were used for validation. The prediction of the model seems to capture the overall dynamics of the three cytokines, however the agreement between the experimental data and the prediction is unsatisfactory for the decresing period of IL-10 and poor for the increasing period of TNF-α. The data are a mean of measurements from four rats and the standard deviation at each data point is shown.

A.2.1 The Equation for Endotoxin

The first equation in the model system describes the dynamics of the elimination of the induced endotoxin. The endotoxin P decays exponentially with $d_p = 3\ hr^{-1}$, which is consistent with values from literature[29]. A noticeable thing is the non-explicit dependence of the number of phagocytic cells, as it must be reasonable to assume that the concentration of endotoxin is proportional to the number of activated engulfing phagocytic cells. It this way, it makes it impossible for the endotoxin to be eliminated when there is no presence of phagocytic cells.

This feature can be included in the model by modifying the equation for the concentration of endotoxin by:

$$\frac{dP(t)}{dt} = -d_p P(t) N(t). \tag{A.1}$$

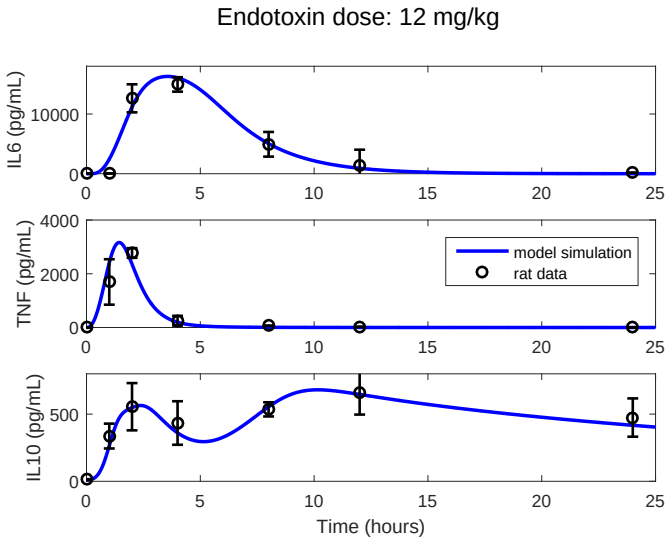

Figure A.4: Comparison of the resimulation of the eight dimensional acute inflammatory respose-model (Model (2.1)-(2.2), solid line) and experimental rat data for injection of an endotoxin dose of 12 mg/kg at time $t = 0$ (circles). The data for endotoxin dose 3 and 12 mg/kg were used for calibration of the parameter values, while the data for endotoxin dose 6 mg/kg were used for validation. The model fits the data very well. The data are a mean of measurements from four rats and the standard deviation at each data point is shown.

This modification ensures that, when no activated phagocytic cells exists, the endotoxin cannot be eliminated. Even though this is not a simplification of the model, the biological rationale supports the induction. Introducing this change, the parameter d_p must be changed to obtain the same results as Roy et al. (2009). The parameter is divided by a characteristic value for N.

The effects of introducing N in the equation for the concentration of endotoxin, can be seen in Appendix A.5. For all dose levels of endotoxin, the curve for P becomes more steep. Additionally, for endotoxin dose level 3 mg/kg , there is a tendency for overestimation. Especially $IL10$ and Y_{IL10} have higher levels than in the original model. For the 6 mg/kg endotoxin dose, the model containing the modification seems to agree with the original model, however it underestimates both $IL10$ and Y_{Il10}. Underestimation of the modified model seems also to be the problem for endotoxin dose 12 mg/kg. At this dose level, the underestimation is clearer and especially the underestimation of $IL10$ and Y_{IL10} are distinctive. The model containing the modification captures the dynamics of the original model well, however it has problems with under- and overestimation of $IL10$ and Y_{IL10} in particular.

A.2.2 The Equation for Phagocytic Cells

As mentioned, the equation for the number of activated phagocytic cells (N) is rather complex. The first term of the equation consists of four Michealis-Menten functions incorporated in yet another Michaelis-Menten function, without any biological rationale. Therefore, it seems reasonable to investigate whether this expression can be simplified, still capturing the dynamics of the system.

A way to accomplish that, is to remove the outer Michaelis-Menten function. Further studies of the system reveal that $IL6$ contributes with a very small up-regulation of N, thus it can be removed from the equations, resulting in an underestimation of $IL10$ and Y_{IL10} which will be taken into account later. At last the influence of the tissue damage marker (D) is insignificant, thus it is removed from the equation.

The simplified N-equation can now be written as:

$$\frac{dN(t)}{dt} = k_N R(t) P(t) - d_N N(t), \tag{A.2}$$

where

$$R(t) = \left(1 + k_{TNF} \frac{TNF(t)}{x_{NTNF} + TNF(t)}\right) \cdot \frac{x_{NCA}}{x_{NCA} + C_A(t)} \cdot \frac{x_{NIL10}}{x_{NIL10} + IL10(t)}. \tag{A.3}$$

In Figure A.5, the changes in the model compared to the original model ((2.1)-(2.2)) are shown for the three different endotoxin dose levels. As seen, the dynamic of the phagocytic cells is maintained, however the peak occurs earlier in time. In addition, the number of phagocytic cells reaches a higher maximum for the endotoxin doses 6 and 12 mg/kg. To obtain these figures, the parameters k_N an d_N were changed to make up for the simplification of the equation for N. The change in the equation also affects the other variables. For endotoxin dose 3 mg/kg, a small decrease in D and C_A is observed together with larger decreases in $IL6$, $IL10$ and Y_{IL10}. For endotoxin dose 6 mg/kg, the change induces a slightly decrease in D and C_A while a decrease in $IL6$, $IL10$ and Y_{IL10} is observed, leaving TNF unchanged. At last the modification causes an increase in $IL6$ and C_A and a greater increase in TNF, $IL10$ and Y_{IL10} for endotoxin dose 12 mg/kg.

A.2.3 The Equation for TNF-α

The first simplification to consider, is the power of one and a half, assigned to N. By increasing the parameter k_{TNF} sufficiently, the power can be reduced

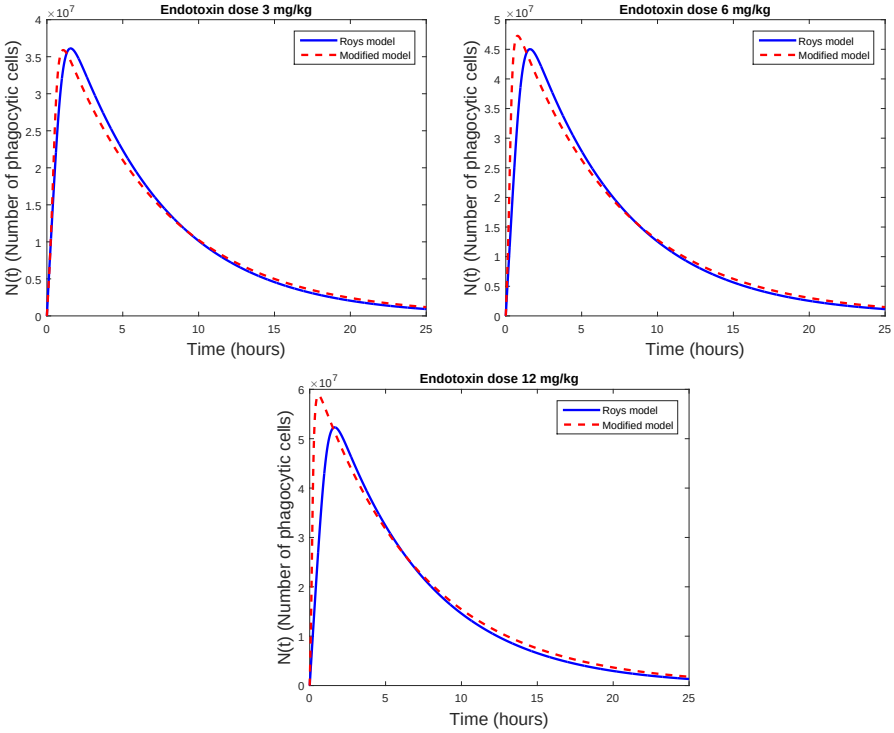

Figure A.5: Simulation of the number of activated phagocytic cells for the model proposed by Roy et al. (2009) (blue solid) and for the model with modified equation of P (Eq. (A.1)) and simplified equation for N (Eq. (A.2)). The modified model captures the overall dynamic, but for endotoxin dose level 6 and 12 mg/kg (in (b) and (c) respectively) the peak occurs remarkably earlier and reaches a higher maximum value.

to one, without reversing the dynamics of the system. By removing one of the terms in the equation at a time, the impact of the separate variable can be investigated. By first removing the auto-up-regulating term it is clear, that it does not contribute to the behaviour of the system. The same goes for the term including $IL10$, while the term including $IL6$ only contributes with a very small up-regulation of TNF. Hence these terms are removed from the model. Left is the sixth order Hill function in C_A. By studying the behaviour of the system, it is found that a power of four is adequate to maintain the dynamics of TNF-α, when some of the constants are adjusted.

However, introducing these changes in the equation lead to a too early peak of TNF-α compared to the experimental data. Thus the auto-up-regulation of TNF-α is reintroduced in the equation, but with different parameter values.

This induces the needed delay of the concentration peak. These changes result in the following simplified equation for TNF-α:

$$\begin{aligned}\frac{dTNF(t)}{dt} =& N(t) \cdot \frac{x_{TNFCA}^4}{x_{TNFCA}^4 + C_A(t)^4} \cdot \left(k_{TNF} + k_{TNFTNF} \cdot \frac{TNF(t)}{x_{TNFTNF} + TNF(t)}\right) \\ & - d_{TNF} \cdot TNF(t).\end{aligned} \tag{A.4}$$

In Figure A.6, a comparison of the original model proposed by Roy et al. (2009)

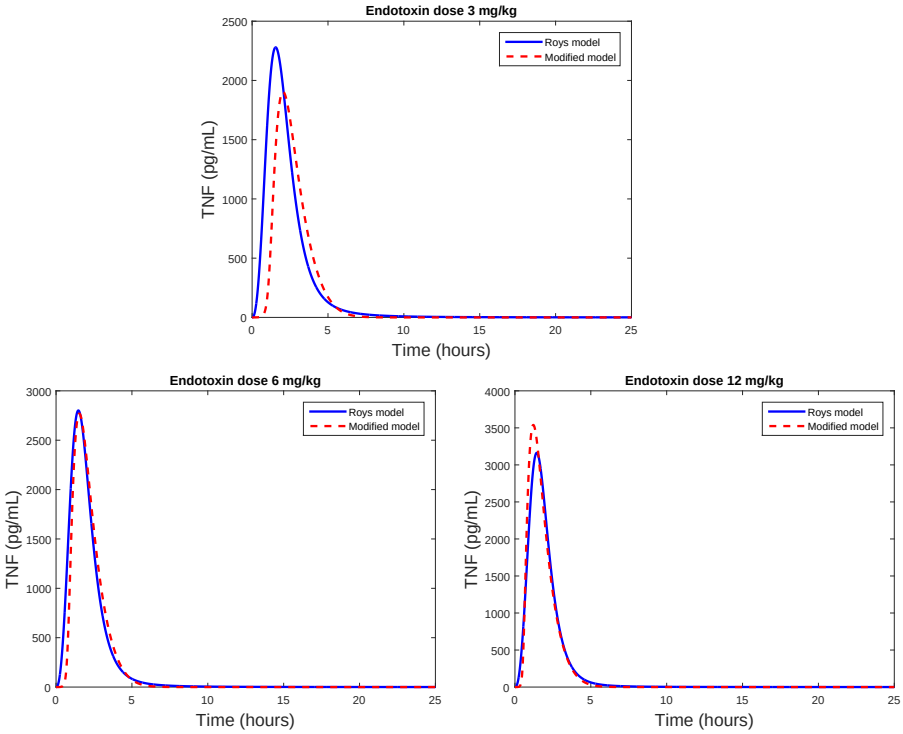

Figure A.6: Comparison of the new implemented equation of TNF-α (Eq. (A.4), dashed red line) and the original model proposed by [29] (Model (2.1)-(2.2), solid blue line). The comparison of the concentraion of TNF-α, shows that the big difference between the models results in a smaller and later response for endotoxin dose 3 mg/kg, a higher response for endotoxin dose 12 mg/kg and somewhat the same response, slightly delayed for endotoxin dose 6 mg/kg when compared to the original model. To obtain this result, some parameters were changed and the modifications introduced in Appendix A.2.1, A.2.2 and A.2.3 were implemented.

and the modified model with the changes in the equations of P, N and TNF is shown.

The modified model mimics the original model, however the peak of TNF occurs later and gives a smaller response for endotoxin dose 3 mg/kg and a higher

response for endotoxin dose 12 mg/kg. For endotoxin dose 6 mg/kg the responses are very alike, only with a slightly delay in the peak of the modified model. The changes in the equation also induce changes in the response for the other variables, however, this will be addressed later.

A.2.4 The Equation for Interleukin-6

Removing the inhibiting term in C_A in the equation of $IL6$, induces a very small change in magnitude of the response of $IL6$, but none of the other variables. Hence it is removed from the equation.
Looking at the auto-up-regulating term of $IL6$, it can be linearised by $\frac{IL6}{x_{IL6IL6}+IL6}$ $\approx \frac{IL6}{x_{IL6IL6}}$ for IL6 $\ll$ x_{IL6IL6} which is the case here. The parameter x_{IL6IL6} is chosen to be $1.987 \cdot 10^5$ pg/mL by Roy et al., while the concentration of $IL6$ does not exceed approximately $1.5 \cdot 10^4$ pg/mL. From a biological perspective almost all reactions have a saturation point, but in this model, the concentration of IL6 is not close to this value.

Furthermore, no change in the model outcome is observed, by changing the fourth order Hill function in N to a fourth order dependence, when adjusting some parameters. These changes can be summarised in the modified equation:

$$\begin{aligned}\frac{dIL6(t)}{dt} =& N(t)^4 \cdot \left(k_{IL6} + k_{IL6TNF}\frac{TNF(t)}{x_{IL6TNF}+TNF(t)} + k_{IL6IL6}IL6(t)\right) \\ & \cdot \frac{x_{IL6IL10}}{x_{IL6IL10}+IL10(t)} - d_{IL6}IL6(t).\end{aligned} \tag{A.5}$$

To obtain sufficiently good results, the equation for $IL10$ is multiplied by a factor. Even though the change actually improves the model prediction of IL-6, the dynamics of IL-10 is lost compared to the original model, since the second peak of IL-10 is negligible for endotoxin dose 12 mg/kg and vanishes for endotoxin dose 3 and 6 mg/kg. In Figure A.7, the induced changes in the concentrations of $IL6$ and $IL10$ are shown. In (a)-(c), the improved result of $IL6$ is seen. The red dashed line represents the new model, with the modification of the $IL6$-equation and the green dotted line represents the old modified model (with modifications of the equations of P, N and TNF). It is clear, that the change makes the modified model mimics the original model (blue solid line) better. Still the new model seems to underestimate for endotoxin dose 3 mg/kg and overestimate the concentration of $IL6$ for endotoxin dose 12 mg/kg slightly. However, the change also induces some change in the dynamics of $IL10$, causing the second peak of $IL10$ vanishing for endotoxin dose level 3 and 6 mg/kg (see (d)-(e)).

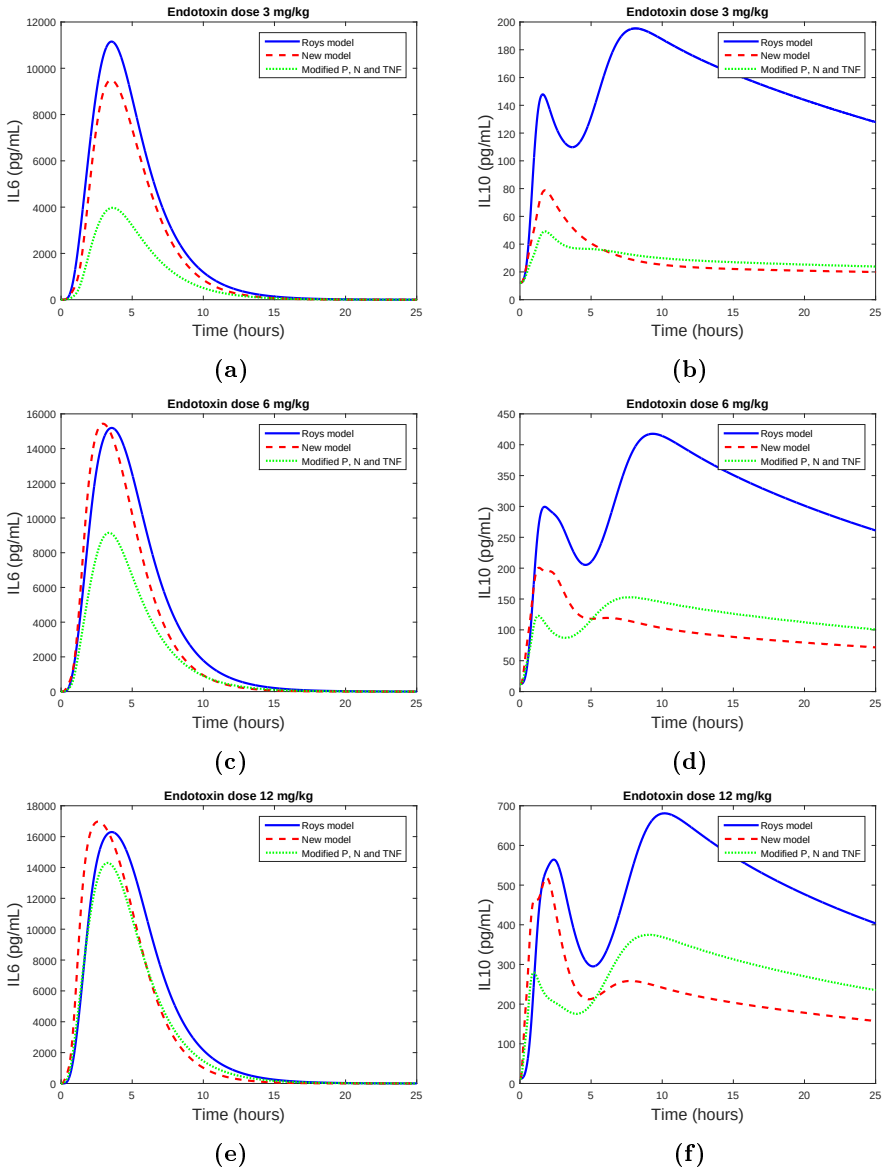

Figure A.7: Results of inducing the change in the equation for Interleukin-6 (Eq. (A.5)). The modification to the $IL6$-equation (dashed red line) is compared to the original model proposed by Roy et al. (2009) (Model (2.1)-(2.2), solid blue line) and the model including the modifications introduced in Appendix A.2.1, A.2.2 and A.2.3 (green dotted line). As seen in (a), (c) and (e), the modification improves the result for $IL6$ to mimic the original model, however the dynamic of $IL10$ is changed from two peaks to only one for endotoxin doses 3 and 6 mg/kg (see (b), (d) and (f)).

A.2.5 The Equation for Interleukin-10

There is no perceptible contribution from TNF in the equation for $IL10$, therefore it is removed from the equation. Furthermore, the main contribution to the second peak in the $IL10$-response is from Y_{IL10}, but is barely seen in the modified equation. In an attempt to recreate the second peak and to eliminate the dependence of Y_{IL10}, the term including Y_{IL10} is replaced by a sixth order Hill function in C_A. From a biological perspective, this seems like a reasonable introduction, since glycocorticoids (cortisol, which is represented by C_A) promote the production of $IL10$ [4,32]. Furthermore the variable Y_{IL10} only appears as a link between D and $IL10$, but since the dependence of D is removed from the system by removing it from the equation of N (see Section A.2.2), the presences of Y_{IL10} is redundant. Replacing the linear term in Y_{IL10} by a sixth order Hill-function in C_A containing two parameters is a complication of the $IL10$-equation, however, it implies that the equation for Y_{IL10} can be removed from the system, resulting in a simplification of the system of equations. For data fitting purposes, the order of six is chosen for the Hill function in C_A, which is a relatively high order, but ensures that the model prediction fits the data.

The changes constitute an elimination of two parameters, but introduces two new parameters (k_{IL10CA} and x_{IL10CA}):

$$\begin{aligned}\frac{dIL10}{dt} =& \frac{N^3}{x_{IL10}^3 + N^3}\left(k_{IL10} + k_{IL10IL6}\frac{IL6^4}{x_{IL10IL6}^4 + IL6^4}\right) \\ &+ k_{IL10CA}\frac{C_A^6}{x_{IL10CA}^6 + CA^6} - d_{IL10}\frac{x_{IL10d}}{x_{IL10d} + IL10}IL10 + s_{IL10}.\end{aligned} \tag{A.6}$$

Further simplification of the equation has been examined, however the best result comparing to the data was found with this expression.

The results for the dynamics of $IL10$ by introducing this change in the equation can be seen in Figure A.8. For the endotoxin dose 3 mg/kg, the new proposed model mimics the original model better for the first peak and includes perhaps an overestimation at the second peak. The modified model reproduces the response of $IL10$ very well compared to the model proposed by Roy et al. (2009) for the endotoxin dose 6 mg/kg, while it overestimates especially the first peak for endotoxin of dose 12 mg/kg. The extensive difference between the new model and the model proposed by Roy et al. (2009) seems to be the shape of the second peak, which now is created by different sources.

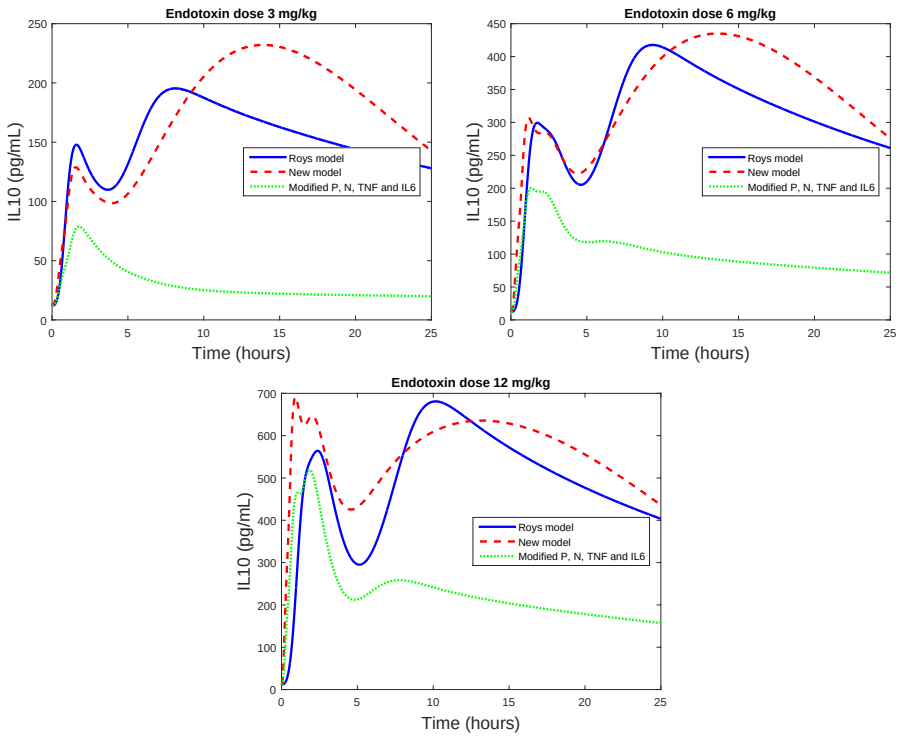

Figure A.8: $IL10$ simulation for the three endotoxin doses 3, 6 and 12 mg/kg. The blue solid line represents the original model proposed by Roy et al. (2009), the green dotted line represents the model with modification of the equations for P, N, TNF and $IL6$ while the red dashed line represents the modified model with also a modification of the $IL10$-equation presented in Appendix A.2.5. The modification recreates the second peak of $IL10$ as observed in data.

A.2.6 The Equations for C_A, D and Y_{IL10}

The equation for the slow acting anti-inflammatory mediators (C_A) is not simplified, since it appears fairly simple.

From the simplification and modifications of the model, it is now seen, that the tissue damage marker (D) and the tissue driven IL-10 promoter (Y_{IL10}) is not to be found in any of the other equations. Thereby the two variables can be eliminated from the model. Possibly, the tissue damage marker can be incorporated in the model if needed. From a biological perspective, it is reasonable to assume, that the acute inflammatory response perceives damaged tissue in a similar way as endotoxin, meaning that these are regarded as something in the body, which should be eliminated. In this way, the tissue damage can be

included in the model, if needed.

By revisiting the equations one by one, the eight dimensional model model proposed by Roy et al. (2009) is reduced to a six dimensional model. The model is reduced by two variables and 16 parameters. The model is presented and compared to the eight dimensional model in section 2.3. In the same section, the model is further simplified to a five dimensional model.

A.3 Initial Conditions

Initial conditions ($t = 0$) used for the simulations of Model (2.1)-(2.2) presented in Appendix A.2, obtained from Roy et al. (2009).

$$\begin{aligned}
P(0) &= 3, \quad 6 \quad \text{or} \quad 12, \\
N(0) &= 0, \\
D(0) &= 0, \\
C_A(0) &= \frac{s_{CA}}{d_{CA}}, \\
IL6(0) &= 0, \\
TNF(0) &= 0, \\
IL10(0) &= \frac{s_{IL10} \cdot x_{IL10d}}{d_{IL10} \cdot x_{IL10d} - s_{IL10}}, \\
Y_{IL10} &= 0,
\end{aligned}$$

The initial condition for P depends on the assumed dose level of endotoxin given to the rat. Unlike the other variables, the anti-inflammatory mediators C_A and $IL10$ starts at different levels than zero. The difference is an attempt, to model the hypothesis, that the system is slightly anti-inflammatory under basal conditions[29]. The initial condition for Y_{IL10} was not described in Roy et al. (2009) and therefore it was chosen accordingly to Frank (2010).

A.4 Parameter Values

Reproduction of the parameter values used for the simulations of the eight dimensional rat model of the acute inflammatory response proposed by Roy et al. (2009) (Model (2.1)-(2.2)) is shown in the following table. The simulations can be found in Appendix A.2.

Table A.1: Table of parameter values for Model (2.1)-(2.2), the eight dimensional model proposed by Roy et al. (2009).

No.	Parameter	Value	Unit	No.	Parameter	Value	Unit
1	d_p	3	hr^{-1}	24	$x_{IL6IL10}$	1.1818	$\frac{pg}{mL}$
2	k_N	$5.5786{\cdot}10^{7}$	hr^{-1}	25	k_{IL6IL6}	122.92	–
3	x_N	14.177	$N-unit$	26	x_{IL6IL6}	$1.987{\cdot}10^{5}$	$\frac{pg}{mL}$
4	d_N	0.1599	hr^{-1}	27	x_{IL6CA}	4.2352	$\frac{pg}{mL}$
5	k_{NP}	41.267	$\frac{N-unit\cdot kg}{mg}$	28	k_{TNF}	$3.9{\cdot}10^{-8}$	$\frac{pg}{mL\cdot N-unit^{1.5}}$
6	k_{ND}	0.013259	$\frac{N-unit}{D-unit}$	29	d_{TNF}	2.035	hr^{-1}
7	x_{NTNF}	1693.9509	$\frac{pg}{mL}$	30	$x_{TNFIL10}$	$2.2198{\cdot}10^{7}$	$\frac{pg}{mL}$
8	x_{NIL6}	58080.742	$\frac{pg}{mL}$	31	x_{TNFCA}	0.19342	$\frac{pg}{mL}$
9	x_{NCA}	0.07212	$\frac{pg}{mL}$	32	k_{TNFTNF}	$1.0{\cdot}10^{-10}$	–
10	x_{NIL10}	147.68	$\frac{pg}{mL}$	33	x_{TNFTNF}	$9.2969{\cdot}10^{6}$	$\frac{pg}{mL}$
11	k_{NTNF}	12.94907	–	34	x_{TNFIL6}	55610	$\frac{pg}{mL}$
12	k_{NIL6}	2.71246	–	35	$k_{IL10TNF}$	$2.9951{\cdot}10^{-5}$	–
13	k_D	2.5247	$\frac{D-unit}{hr}$	36	$x_{IL10TNF}$	$1.1964{\cdot}10^{6}$	$\frac{pg}{mL}$
14	d_D	0.37871	hr^{-1}	37	$k_{IL10IL6}$	4.1829	–
15	x_D	$1.8996{\cdot}10^{7}$	$N-unit$	38	$x_{IL10IL6}$	26851	$\frac{pg}{mL}$
16	k_{CA}	$.154625{\cdot}10^{-8}$	$\frac{pg}{mL\cdot hr\cdot N-unit}$	39	k_{IL10}	$1.3374{\cdot}10^{5}$	$\frac{pg}{mL\cdot hr}$
17	d_{CA}	$.31777{\cdot}10^{-1}$	hr^{-1}	40	d_{IL10}	98.932	hr^{-1}
18	s_{CA}	0.004	$\frac{pg}{mL\cdot hr}$	41	x_{IL10}	$8.0506{\cdot}10^{7}$	$N-unit$
19	k_{IL6TNF}	4.4651	–	42	s_{IL10}	1187.2	$\frac{pg}{mL\cdot hr}$
20	x_{IL6TNF}	1211.3	$\frac{pg}{mL}$	43	x_{IL10d}	791.27	$\frac{pg}{mL}$
21	k_{IL6}	$9.0425{\cdot}10^{7}$	$\frac{pg}{mL\cdot hr}$	44	k_{IL102}	$1.3964{\cdot}10^{7}$	$\frac{YIL10-unit}{hr}$
22	d_{IL6}	0.43605	hr^{-1}	45	d_{IL102}	0.0224	hr^{-1}
23	x_{IL6}	$1.7856{\cdot}10^{8}$	$N-unit$	46	x_{IL102}	37.454	$D-unit$

A.5 Effects of Modifying The Equation for P

In Appendix A.2.1 the equation for P is modified such that the decrease in the concentration of the endotoxin is proportional to the number of activated phagocytic cells (see Equation A.1). To obtain somewhat the same results as Roy et al. (2009), the parameter d_p is divided by a characteristic value of N changing the parameter from $d_p = 3\ hr^{-1}$ to $d_p = 1.35 \cdot 10^{-7}\ (hr \cdot N\text{-units})^{-1}$. The effects of changing the equation can be seen in Figure A.9-A.11, see Appendix A.2.1 for further discussion.

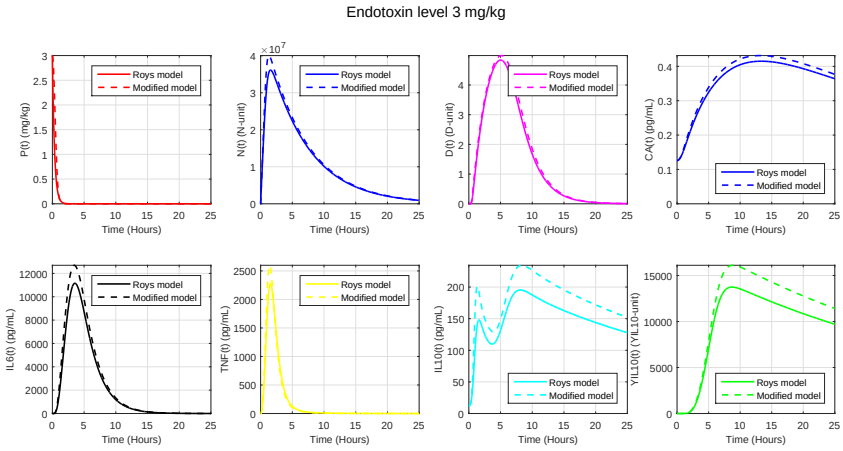

Figure A.9: The effects of introducing N (the activated phagocytic cells) in the equation for P (The concentration of endotoxin). Solid lines represent the model proposed by Roy et al. (2009) (Model 2.1-(2.2)), while the dashed lines represent the model containing the modification from Equation A.1. The model overstimates several of the concentrations, especially $IL10$, for endotoxin dose level 3 mg/kg.

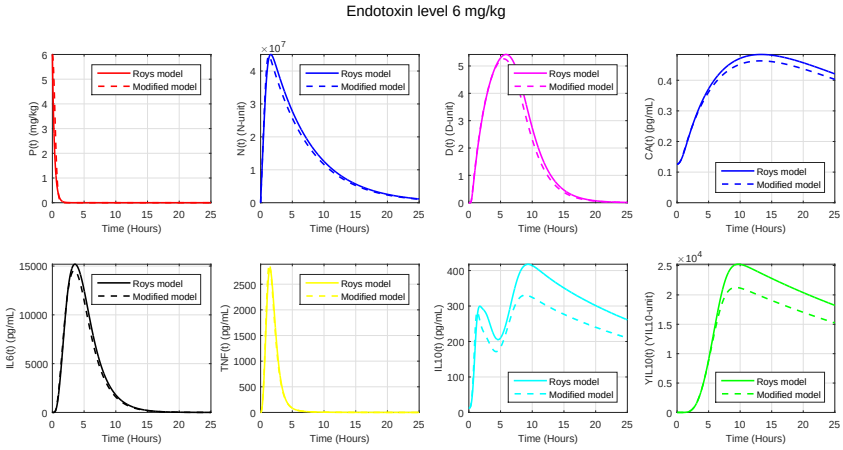

Figure A.10: The effects of introducing N (the activated phagocytic cells) in the equation for P (The concentration of endotoxin). Solid lines represent the model proposed by Roy et al. (2009) (Model 2.1-(2.2)), while the dashed lines represent the model containing the modification from Equation A.1. The model seems to capture the dynamics very well, however it understimates $IL10$ and Y_{IL10}, for endotoxin dose level 6 mg/kg.

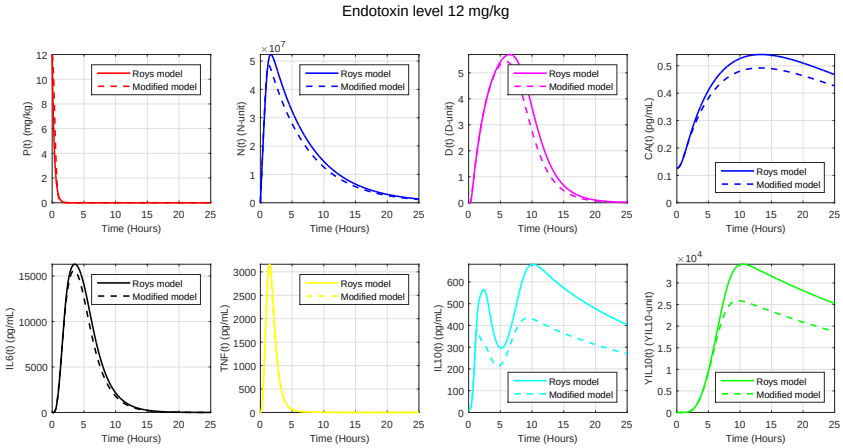

Figure A.11: The effects of introducing N (the activated phagocytic cells) in the equation for P (The concentration of endotoxin). Solid lines represent the model proposed by Roy et al. (2009) (Model 2.1), while the dashed lines represent the model containing the modification from Equation A.1. The model underestimates several of concentrations reflected in the decreases. Especially $IL10$ is underestimated, for endotoxin dose level 12 mg/kg.

A.6 Parameter Values for the 5- and 6-Dimensional Model

The parameter values used for the simulations of the six dimensional rat model of the acute inflammatory response presented in Section 2.3 is shown in the following table.

Table A.2: Table of parameter values for Model (2.3), the six dimensional model presented in Section 2.3.

No.	Parameter	Value	Unit	No.	Parameter	Value	Unit
1	d_p	$1.35{\cdot}10^{-7}$	$(hr \cdot \text{N-unit})^{-1}$	16	k_{IL6IL6}	122.92	$hr^{-1} \cdot \text{N-unit}^{-4}$
2	k_N	$4.9956{\cdot}10^{7}$	$\frac{\text{N-unit}\cdot kg}{hr\cdot mg}$	17	k_{TNF}	$4.2962{\cdot}10^{-7}$	$\frac{pg}{hr\cdot mL\cdot\text{N-unit}}$
3	d_N	0.1439	hr^{-1}	18	d_{TNF}	2.442	hr^{-1}
4	x_{NTNF}	1693.9509	$\frac{pg}{mL}$	19	x_{TNFCA}	0.1382	$\frac{pg}{mL}$
5	x_{NCA}	0.07212	$\frac{pg}{mL}$	20	k_{TNFTNF}	$1.2{\cdot}10^{-3}$	$\frac{pg}{hr\cdot mL\cdot\text{N-unit}}$
6	x_{NIL10}	147.68	$\frac{pg}{mL}$	21	x_{TNFTNF}	929.69	$\frac{pg}{mL}$
7	k_{NTNF}	12.94907	–	22	$k_{IL10IL6}$	$1.1188{\cdot}10^{6}$	$\frac{pg}{hr\cdot mL}$
8	k_{CA}	$.154625{\cdot}10^{-8}$	$\frac{pg}{hr\cdot mL\cdot N-unit}$	23	$x_{IL10IL6}$	26851	$\frac{pg}{mL}$
9	d_{CA}	$.31777{\cdot}10^{-1}$	hr^{-1}	24	k_{IL10}	$2.67480{\cdot}10^{5}$	$\frac{pg}{mL\cdot hr}$
10	s_{CA}	0.004	$\frac{pg}{mL\cdot hr}$	25	k_{IL10CA}	$4.3875{\cdot}10^{4}$	$\frac{pg}{hr\cdot mL}$
11	k_{IL6TNF}	$1.7850{\cdot}10^{-23}$	$\frac{pg}{hr\cdot mL\cdot\text{N-unit}^4}$	26	x_{IL10CA}	0.38	$\frac{pg}{mL}$
12	x_{IL6TNF}	$4.8452{\cdot}10^{4}$	$\frac{pg}{mL}$	27	d_{IL10}	98.932	hr^{-1}
13	k_{IL6}	$3.9976{\cdot}10^{-25}$	$\frac{pg}{hr\cdot mL\cdot\text{N-unit}^4}$	28	x_{IL10}	$8.0506{\cdot}10^{7}$	N-unit
14	d_{IL6}	0.5102	hr^{-1}	29	x_{IL10d}	791.27	$\frac{pg}{mL}$
15	$x_{IL6IL10}$	1.1818	$\frac{pg}{mL}$	30	s_{IL10}	1187.2	$\frac{pg}{hr\cdot mL}$

Appendix B

Model of HPA Axis

In this appendix, supplements associated with the model of the HPA axis handled in Chapter 3 are presented.

B.1 Parameter Values for The HPA Model

The parameter values used for the simulations of the HPA axis model presented in Section 3.2 are shown in the following table.

Table B.1: Table of parameter values for Model (3.1)-(3.2), the HPA axis model presented in Section 3.2.

No.	Parameter	Value	Unit
1	a_0	0.001	$\frac{pg/mL}{min}$
2	a_1	$4.1040 \cdot 10^{12}$	$\frac{pg/mL}{min}$
3	a_2	$1.7558 \cdot 10^{9}$	$\left(\frac{dL}{\mu g}\right)^2$
4	μ	600	$\frac{pg}{mL}$
5	a_3	$2.3688 \cdot 10^{4}$	min^{-1}
6	a_4	$1.7778 \cdot 10^{5}$	$\frac{dL}{\mu g}$
7	a_5	$7.8779 \cdot 10^{-4}$	$\frac{\mu g/dL}{min \cdot (pg/mL)^2}$
8	ω_1	0.039	min^{-1}
9	ω_2	0.01	min^{-1}
10	ω_3	0.04	min^{-1}

Table B.2: Table of parameter values for Model (3.1)-(3.2), used for the function creating the circadian rhythm in the HPA axis model presented in Section 3.2.

No.	Parameter	Value	Unit
1	δ	0	min
2	α	300	min
3	k	5	–
4	β	950	min
5	l	6	–
6	ϵ	0.01	–

B.2 Existence and Uniqueness of the Solution to the HPA Model

To prove existence and uniqueness in Section 3.2.2 of the solution to the System (3.3), the right-hand-side must be Lipschitz continuous[20].

In the following, it is shown that $f(u,t)$ is Lipschitz continuous in u over any domain

$$\mathcal{D} = \{(u,t)| \parallel u - u_0 \parallel \leq \eta, t_0 \leq t \leq t_1\},$$

with $\eta > 0$ and $t_1 > t_0$, i.e. there exists a constant $\mathcal{L} \geq 0$ such that

$$\parallel f(u,t) - f(u^*,t) \parallel \leq \mathcal{L} \parallel u - u^* \parallel$$

for all (u,t), $(u^*,t) \in \mathcal{D}$.

The Lipschitz continuity is shown using the L^1-norm, since the equivalence of finite-dimensional norms ensures that if $f(u,t)$ is Lipschitz continuous in one norm, it holds for any other norm (only the Lipschitz constant $\mathcal{L}$ may depend on the chosen norm)[20].

Considering the L^1-norm, it is seen that

$$\parallel u - u^* \parallel_1 = |CRH(t) - CRH^*(t)| + |ACTH(t) - ACTH^*(t)| + |Cortisol(t) - Cortisol^*(t)|$$

and

$$\parallel f(u,t) - f(u^*,t) \parallel_1 = |f_1(u,t) - f_1(u^*,t)| + |f_2(u,t) - f_2(u^*,t)| + |f_3(u,t) - f_3(u^*,t)|.$$

Looking at the terms one by one, it can be shown, that $\parallel f(u,t) - f(u^*,t) \parallel_1$ is bounded by $\mathcal{L} = \mathcal{L}_1 + \mathcal{L}_2 + \mathcal{L}_3 = a_1 + (2a_2 + a_3a_4 + 2a_5)(\eta + \parallel u_0 \parallel) + a_3 + \omega_1 + \omega_2 + \omega_3$. The following calculations show how to find $\mathcal{L}_1$, $\mathcal{L}_2$ and $\mathcal{L}_3$ (assuming

that all parameter values are positive) :

$$
\begin{aligned}
|f_1(u,t) - f_1(u^*,t)| &= \Big| a_0 + C(t)\frac{a_1}{1+a_2 Cortisol^2}\frac{CRH}{\mu + CRH} - \omega_1 CRH \qquad \dots \\
&\qquad - \left(a_0 + C(t)\frac{a_1}{1+a_2 (Cortisol^*)^2}\frac{CRH^*}{\mu + CRH^*} - \omega_1 CRH^* \right) \Big| \\
&\le \left| a_1 \left(\frac{1}{1+a_2 Cortisol^2}\frac{CRH}{\mu + CRH} - \frac{1}{1+a_2 (Cortisol^*)^2}\frac{CRH^*}{\mu + CRH^*} \right) - \omega_1 (CRH - CRH^*) \right| \\
&\le \left| a_1 \frac{1}{1+a_2 Cortisol^2} \left(\frac{CRH}{\mu + CRH} - \frac{CRH^*}{\mu + CRH^*} \right) \right| \qquad \dots \\
&\qquad + \left| \frac{CRH^*}{\mu + CRH^*} \left(\frac{1}{1+a_2 Cortisol^2} - \frac{1}{1+a_2 (Cortisol^*)^2} \right) \right| \qquad \dots \\
&\qquad + \left| \omega_1 (CRH - CRH^*) \right| \\
&\le a_1 \left| CRH - CRH^* \right| + \left| \frac{a_2 (Cortisol^2 - (Cortisol^*)^2)}{(1+a_2 (Cortisol^*)^2)(1+a_2 Cortisol^2)} \right| + \omega_1 \left| CRH - CRH^* \right| \\
&\le (a_1 + 2 \cdot (\eta + \parallel u_0 \parallel) \cdot a_2 + \omega_1) \parallel u - u^* \parallel \\
&\equiv \mathcal{L}_1 \parallel u - u^* \parallel .
\end{aligned}
$$

The last inequality holds since

$$
\begin{aligned}
\left| \frac{a_2 (Cortisol^2 - (Cortisol^*)^2)}{(1+a_2 (Cortisol^*)^2)(1+a_2 Cortisol^2)} \right| &\le |a_2 (Cortisol^2 - (Cortisol^*)^2)| \\
&\le a_2 |Cortisol^* - Cortisol||Cortisol^* + Cortisol| \\
&\le a_2 \cdot \parallel u - u^* \parallel \cdot (\parallel u \parallel + \parallel u^* \parallel) \\
&\le 2 \cdot a_2 (\eta + \parallel u_0 \parallel) \parallel u - u^* \parallel .
\end{aligned}
$$

Considering the second term

$$
\begin{aligned}
|f_2(u,t) - f_2(u^*,t)| &= \left| \frac{a_3 CRH}{1+a_4 Cortsiol} - \omega_2 ACTH - \left(\frac{a_3 CRH^*}{1+a_4 Cortisol^*} - \omega_2 ACTH^* \right) \right| \\
&= \left| a_3 CRH \left(\frac{1}{1+a_4 Cortisol} - \frac{1}{1+a_4 Cortisol^*} \right) + \frac{a_3 (CRH - CRH^*)}{1+a_4 Cortisol^*} - \omega_2 (ACTH - ACTH^*) \right| \\
&\le a_3 a_4 \left| CRH (Cortisol - Cortisol^*) \right| + a_3 \left| CRH - CRH^* \right| + \omega_2 \left| ACTH - ACTH^* \right| \\
&\le (a_3 (a_4 (\eta + \parallel u_0 \parallel) + 1) + \omega_2) \parallel u - u^* \parallel \\
&\equiv \mathcal{L}_2 \parallel u - u^* \parallel
\end{aligned}
$$

and finally, the third term is bounded by

$$
\begin{aligned}
|f_3(u,t) - f_3(u^*,t)| &= \left| a_5 ACTH^2 - \omega_3 Cortisol - \left(a_5 (ACTH^*)^2 - \omega_3 Cortisol^* \right) \right| \\
&\le a_5 |ACTH - ACTH^*||ACTH + ACTH^*| + \omega_3 |Cortisol - Cortisol^*| \\
&\le (2 a_5 (\eta + \parallel u_0 \parallel) + \omega_3) \parallel u - u^* \parallel \\
&\equiv \mathcal{L}_3 \parallel u - u^* \parallel .
\end{aligned}
$$

Hence, $\parallel f(u,t) - f(u^*,t) \parallel$ is bounded by $\mathcal{L} = \mathcal{L}_1 + \mathcal{L}_2 + \mathcal{L}_3$ which means that $f(u,t)$ is Lipschitz continuous in u over $\mathcal{D}$.

The Lipschitz continuity of $f(u,t)$ over $\mathcal{D}$ implies that there exists an unique solution to the System (3.3) at least up to a time $t_2 = \min(t_1, t_0 + \eta/S)$ where $S = \max_{(u,t)\in\mathcal{D}} \parallel f(u,t) \parallel$, following from the *existence and uniqueness theorem* [20].

B.3 Influence of Parameters in The HPA Model

The influence of the parameters in the HPA Model ((3.1)-(3.2)) considered in Section 3.2, is shown in following figures. The parameters are changed one at a time to examine the change in the output of the model.

The parameters are first increased by 50% and then decreased by 50% and the model simulations are then compared to the simulation for the original value of the parameter. The green dashed line represents the simulation with the parameter decreased by 50 %, the red dashed line represents the simulation with the parameter increased by 50 % while the solid blue line represents the simulation with the original parameter value. By manually changing the parameters in this way, it is easier to get an interpretation of the influence on the system. This can also be used to obtain good and reliable initial guesses for parameter estimation.

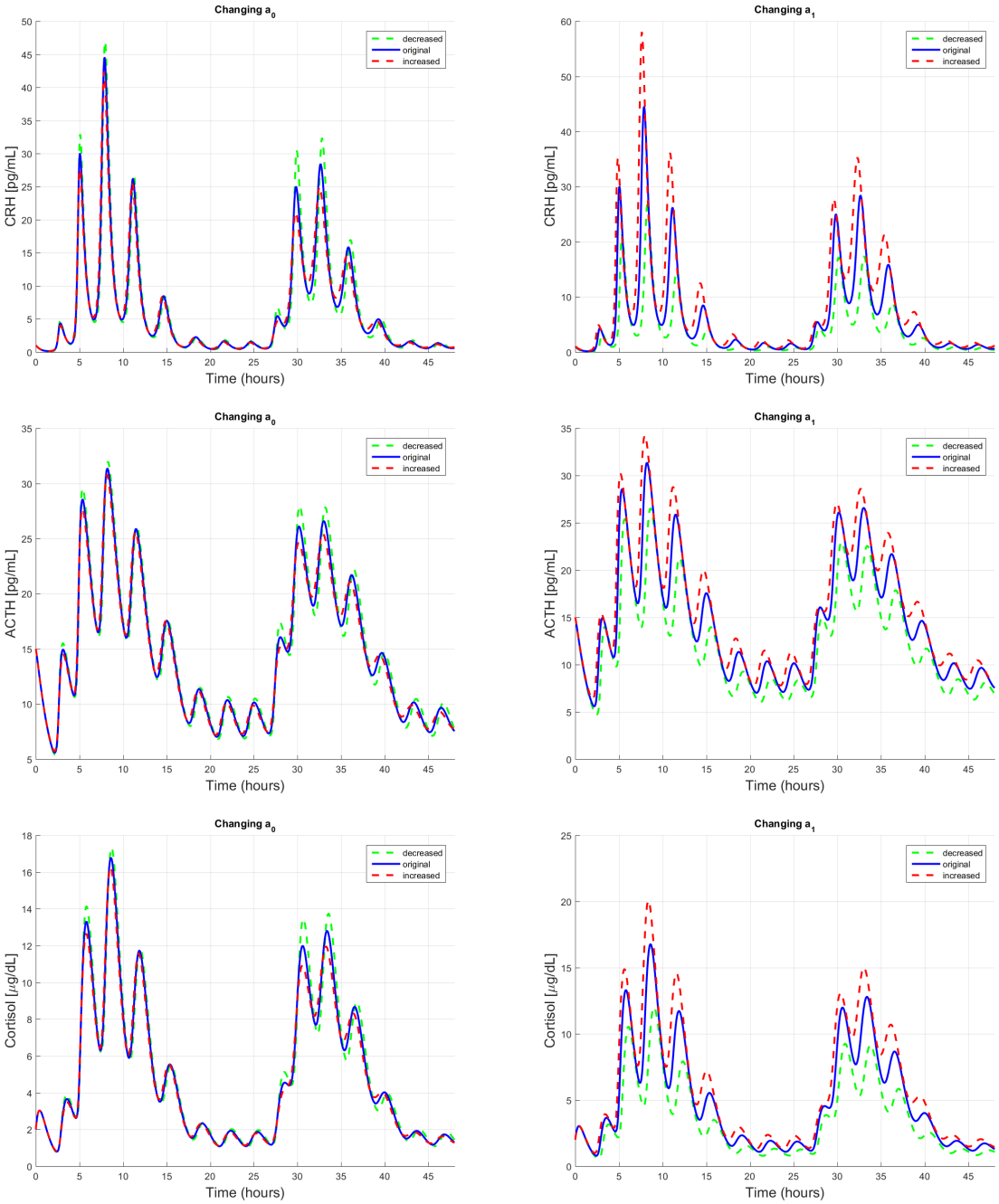

Figure B.1: Influence of the parameters in the HPA axis model ((3.1)-(3.2)).

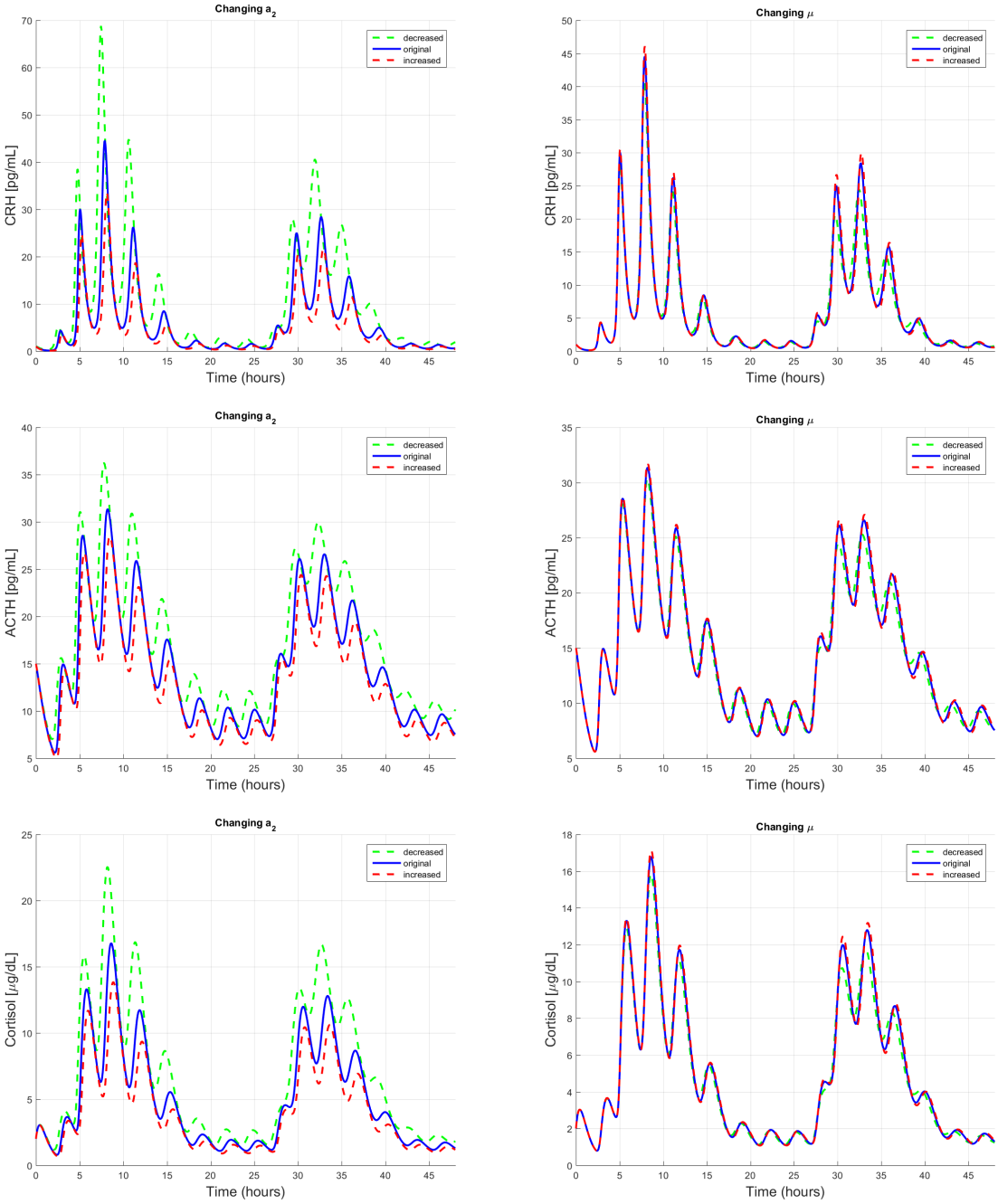

Figure B.2: Influence of the parameters in the HPA axis model ((3.1)-(3.2)).

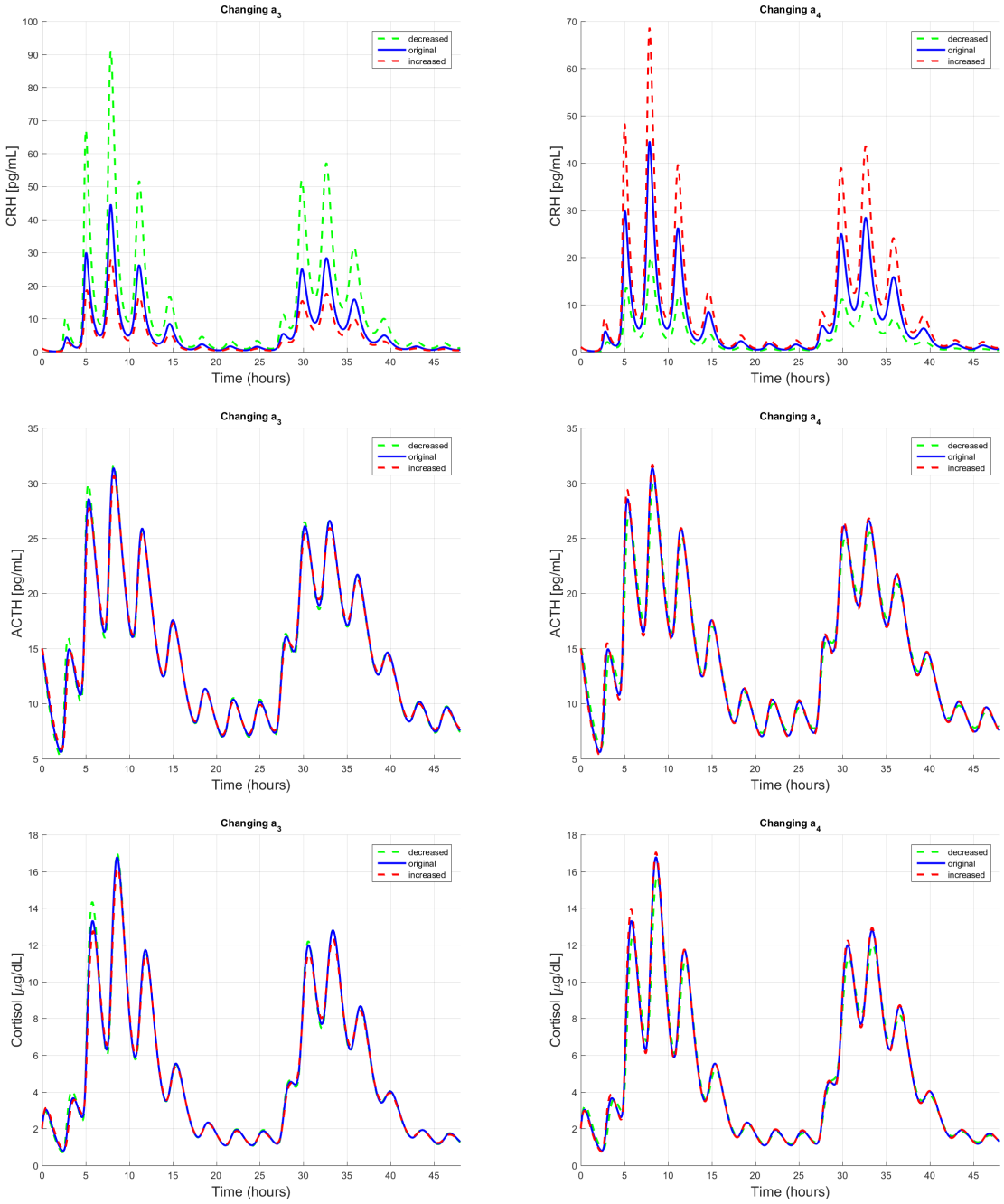

Figure B.3: Influence of the parameters in the HPA axis model ((3.1)-(3.2)).

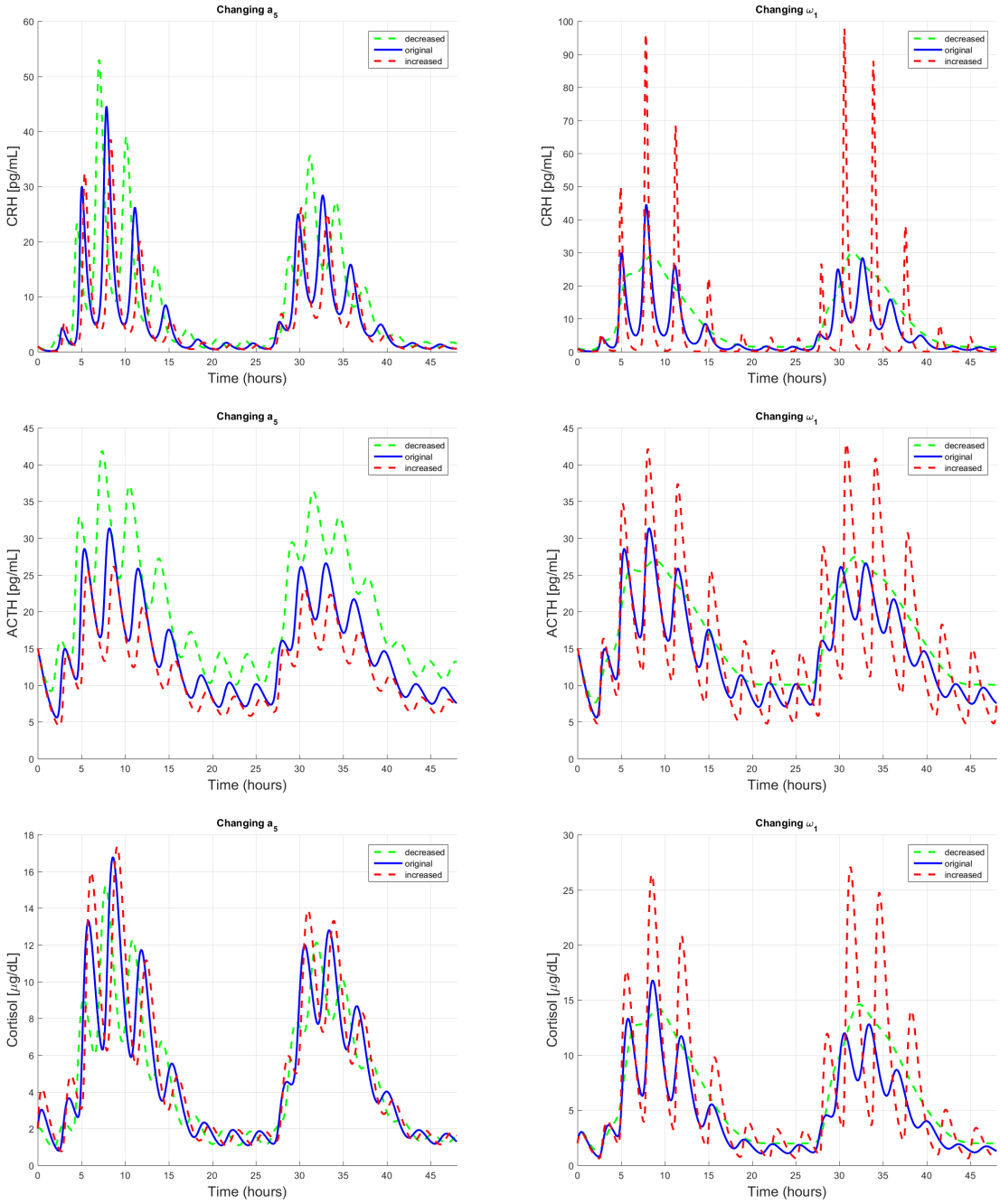

Figure B.4: Influence of the parameters in the HPA axis model ((3.1)-(3.2)).

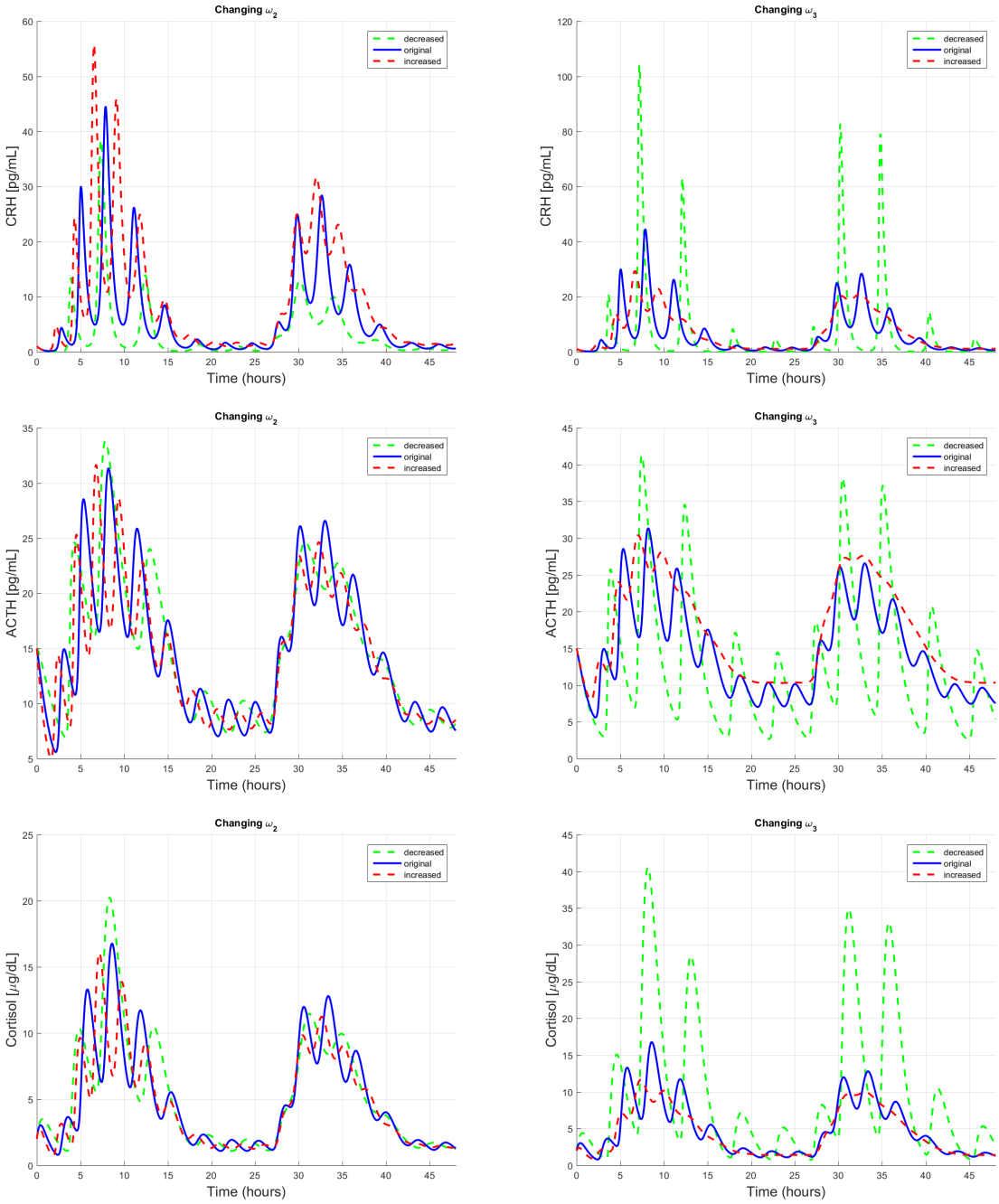

Figure B.5: Influence of the parameters in the HPA axis model ((3.1)-(3.2)).

B.4 Parameter Values for The HPA Model

The parameter values used for the simulations of the reduced HPA axis model ((3.4)-(3.5)) presented in Section 3.2.4 are shown in the following table.

Table B.3: Table of parameter values for the reduced HPA axis model ((3.4)-(3.5)), presented in Section 3.2.4.

No.	Parameter	Value	Unit
1	a_0	0.001	$\frac{pg/mL}{min}$
2	a_1	$6.8400 \cdot 10^9$	$\frac{pg/mL}{min}$
3	a_2	$1.7558 \cdot 10^9$	$\left(\frac{dL}{\mu g}\right)^2$
4	a_3	$2.3688 \cdot 10^4$	min^{-1}
5	a_4	$1.7778 \cdot 10^5$	$\frac{dL}{\mu g}$
6	a_5	$7.8779 \cdot 10^{-4}$	$\frac{\mu g/dL}{min \cdot (pg/mL)^2}$
7	ω_1	0.036	min^{-1}
8	ω_2	0.01	min^{-1}
9	ω_3	0.04	min^{-1}

Table B.4: Table of parameter values for Model (3.4)-(3.5), used for function creating the circadian rhythm in the HPA axis model presented in Section 3.2.4.

No.	Parameter	Value	Unit
1	δ	0	min
2	α	300	min
3	k	5	–
4	β	950	min
5	l	6	–
6	ϵ	0.01	–

Appendix C

The Coupled Model

In this appendix, supplements associated with the coupled model considered in Chapter 4 are presented.

C.1 Non-dimensionalisation

The sub-systems of the acute inflammatory system and the HPA-axis are partially non-dimensionalised in the meaning of removing all units of the systems except the time unit. Furthermore, the time unit of the HPA-model is changed from minutes to hours. This is accomplished, to explore the structure of the models and the effects of different model approaches of coupling mechanisms. Non-dimensionalisation of a system means, that a suitable substitution of the variables of the system, gives rise to a possible simplification of the system, while the units of the system changes from SI-units.

The variables of the acute inflammatory response model presented in Section 2.3.2, are scaled by the characteristic values

$$P = p \cdot \widetilde{P},\ N = n \cdot \widetilde{N},\ TNF = tnf \cdot \widetilde{TNF},\ C_A = ca \cdot \widetilde{C}_A \text{ and } IL10 = il10 \cdot \widetilde{IL10}, \tag{C.1}$$

which gives the system

$$\begin{aligned}
\frac{d\widetilde{P}}{dt} &= -\widetilde{d}_p\widetilde{P}\cdot\widetilde{N}\\
\frac{d\widetilde{N}}{dt} &= \widetilde{k}_N\left(\left(1+\frac{k_{NTNF}\widetilde{TNF}}{\widetilde{x}_{NTNF}+\widetilde{TNF}}\right)\frac{\widetilde{x}_{NCA}}{\widetilde{x}_{NCA}+\widetilde{C}_A}\cdot\frac{\widetilde{x}_{NIL10}}{\widetilde{x}_{NIL10}+\widetilde{IL10}}\right)\cdot\widetilde{P}-d_N\widetilde{N}\\
\frac{d\widetilde{C}_A}{dt} &= \widetilde{k}_{CA}\cdot\widetilde{N}-d_{CA}\widetilde{C}_A+\widetilde{s}_{CA}\\
\frac{d\widetilde{TNF}}{dt} &= \widetilde{N}\cdot\frac{\widetilde{x}^4_{TNFCA}}{\widetilde{x}^4_{TNFCA}+\widetilde{C}^4_A}\left(\widetilde{k}_{TNF}+\frac{\widetilde{k}_{TNFTNF}\widetilde{TNF}}{\widetilde{x}_{TNFTNF}+\widetilde{TNF}}\right)-d_{TNF}\widetilde{TNF}\\
\frac{d\widetilde{IL10}}{dt} &= \widetilde{k}_{IL10}\frac{\widetilde{N}^3}{\widetilde{x}^3_{IL10}+\widetilde{N}^3}-d_{IL10}\frac{\widetilde{x}_{IL10d}}{\widetilde{x}_{IL10d}+\widetilde{IL10}}\widetilde{IL10}+\frac{\widetilde{k}_{IL10CA}\widetilde{C}^6_A}{\widetilde{x}^6_{IL10CA}+\widetilde{C}^6_A}+\widetilde{s}_{IL10},
\end{aligned}\tag{C.2}$$

where

$$\begin{aligned}
&\widetilde{d}_p = d_p\cdot n,\\
&\widetilde{k}_N=\frac{k_N\cdot p}{n},\quad \widetilde{x}_{NTNF}=\frac{x_{TNF}}{tnf},\quad \widetilde{x}_{NCA}=\frac{x_{NCA}}{ca},\quad \widetilde{x}_{NIL10}=\frac{x_{NIL10}}{il10},\\
&\widetilde{k}_{CA}=\frac{k_{CA}\cdot n}{ca},\quad \widetilde{s}_{CA}=\frac{s_{CA}}{ca},\\
&\widetilde{x}_{TNFCA}=\frac{x_{TNFCA}}{ca},\quad \widetilde{k}_{TNF}=\frac{k_{TNF}\cdot n}{tnf},\quad \widetilde{k}_{TNFTNF}=\frac{k_{TNFTNF}\cdot n}{tnf},\\
&\widetilde{x}_{TNFTNF}=\frac{x_{TNFTNF}}{tnf},\\
&\widetilde{k}_{IL10}=\frac{k_{IL10}}{il10},\quad \widetilde{x}_{IL10}=\frac{x_{IL10}}{n},\quad \widetilde{x}_{IL10d}=\frac{x_{IL10d}}{il10},\quad \widetilde{k}_{IL10CA}=\frac{k_{IL10CA}}{il10},\\
&\widetilde{x}_{IL10CA}=\frac{x_{IL10CA}}{ca},\quad \widetilde{s}_{IL10}=\frac{s_{IL10}}{il10}
\end{aligned}$$

noticing that the four elimination rates d_N, d_{CA}, d_{TNF} and d_{IL10} together with k_{NTNF} are the only parameters not affected by the scaling.

Choosing

$$n=\frac{1}{d_p},\quad p=\frac{n}{k_n}=\frac{1}{k_n\cdot d_p},\quad ca=s_{CA},\quad tnf=x_{TNFTNF}\quad\text{and}\quad il10=s_{IL10},\tag{C.3}$$

five parameters of the system are eliminated.

Similar, the HPA system can be non-dimensionalised by scaling the variables by

$$CRH=crh\cdot\widetilde{CRH},\quad ACTH=acth\cdot\widetilde{ACTH},\quad Cortisol=cort\cdot\widetilde{Cortisol}.\tag{C.4}$$

Furthermore, the time scale can be changed from minutes to hours by defining $\widetilde{t}=\tau t$, such that the time scales in the two models are equal. This results in the following equations

$$\begin{aligned}
\frac{d\widetilde{CRH}}{d\widetilde{t}} &= C(\widetilde{t})\frac{\widetilde{a}_1\widetilde{CRH}}{1+\widetilde{a}_2\widetilde{Cortisol}^2}-\widetilde{\omega}_1\widetilde{CRH}\\
\frac{d\widetilde{ACTH}}{d\widetilde{t}} &= \frac{\widetilde{a}_3\widetilde{CRH}}{1+\widetilde{a}_4\widetilde{Cortisol}}-\widetilde{\omega}_2\widetilde{ACTH}\\
\frac{d\widetilde{Cortisol}}{d\widetilde{t}} &= \widetilde{a}_5\widetilde{ACTH}^2-\widetilde{\omega}_3\widetilde{Cortisol},
\end{aligned}\tag{C.5}$$

where

$$\widetilde{a}_1 = a_1 \cdot \tau, \quad \widetilde{a}_2 = a_2 \cdot cort^2, \quad \widetilde{a}_3 = a_3 \cdot \tau \cdot crh/acth, \quad \widetilde{a}_4 = a_4 \cdot cort, \quad \widetilde{a}_5 = a_5 \cdot \tau \cdot acth^2/cort$$
$$\widetilde{\omega}_1 = \tau \cdot \omega_1, \quad \widetilde{\omega}_2 = \tau \cdot \omega_2, \quad \widetilde{\omega}_3 = \tau \cdot \omega_3.$$

By choosing $\tau = 60$, the time scales is changed from minutes to hours, furthermore choosing

$$cort = a_4^{-1}, \quad acth = \sqrt{cort/(a_5 \cdot \tau)} \quad \text{and} \quad crh = acth/(a_3 \cdot \tau) \tag{C.6}$$

eliminates three parameters of the system and it is possible to eliminate one more by choosing τ as the inverse of one of the elimination rates or a_1, however, since it is of interest to keep the time unit in hours, this is not done.

The two non-dimensionalised models were used to investigate the effects of including different interaction mechanisms between the systems and forms the basis of the mathematical descriptions of the interplay.

C.2 Attracting Trapping Region for the Coupled Model

In this section, existence and uniqueness of the solution to the extended coupled system ((4.1)-(4.2)) presented in Section 4.1 is proved. This result is used when finding the trapping region of the extended model in the next section.

The model is extended by including a Michaelis-Menten function in CRH instead of the linear approximation the equation for CRH (similar to Chapter 3).

Consider the System (4.1)-(4.2) on the form

$$\begin{aligned} \frac{du(t)}{dt} &= f(u,t) \\ u(t_0) &= u_0, \end{aligned} \tag{C.7}$$

where $u(t) = [P(t), N(t), TGF(t), TNF(t), IL10(t)CRH(t), ACTH(t), Cortsiol(t)]'$, u_0 denotes the initial condition and $f(u,t)$ is a vector containing the right-hand-side of the system. It follows that $f(u,t)$ is Lipschitz continuous in u over any domain

$$\mathcal{D} = \{(u,t) | \parallel u - u_0 \parallel \leq a, t_0 \leq t \leq t_1\},$$

with $a > 0$ and $t_1 > t_0$, i.e. there exists a constant $\mathcal{L} \geq 0$ such that

$$\parallel f(u,t) - f(u^*,t) \parallel \leq \mathcal{L} \parallel u - u^* \parallel$$

for all (u,t), $(u^*,t) \in \mathcal{D}$, if the first derivatives of $f(u,t)$ are bounded over the domain $\mathcal{D}$[14].

Since the first derivatives of $f(u,t)$ are bounded over $\mathcal{D}$, it follows from the *Existence and Uniqueness Theorem* that there exists a unique solution to Equation (C.7) for all finite time intervals $[t_0, t_2]$. t_2 can be calculated as $t_2 = \min(t_1, t_0 + \eta/S)$ where $S = \max_{(u,t)\in\mathcal{D}} \parallel f(u,t) \parallel$.[20]

C.2.1 Trapping Region

Existence and uniqueness of the solutions to the coupled model ((4.1)-(4.2)) is now used to prove the existence of an attracting trapping region T_R for the system.

Assume that all parameter values are positive and the initial conditions are non-negative. It follows that for any $u(t_0) \in (\mathbb{R}^+ \cup \{0\})^8 \backslash T_R$ then $u(t) \in T_R$ for $t > t_1$, for some $t_1 > t_0$ where $T_R = [0, M_P] \times [0, M_N] \times [0, M_{TGF}] \times [0, M_{TNF}] \times$

$[0, M_{IL10}] \times [0, M_{CRH}] \times [0, M_{ACTH}] \times [0, M_{Cortisol}]$.

In a similar way, as in the sections 2.3.3 and 3.2.3, the positivity of the system can be realised. This constitute the lower bounds of T_R. The upper bounds are found to be:

$$\begin{aligned}
M_P &\equiv P(t_0) \\
M_N &\equiv \frac{k_N(1+k_{NTNF})M_P}{d_N} \\
M_{TGF} &\equiv \frac{k_{TGF}M_N + q_1}{d_{TGF}} \\
M_{IL10} &\equiv \frac{(k_{IL10N} + k_{IL10TGF} + s_{IL10})x_{IL10d}}{x_{IL10d}d_{IL10} - (k_{IL10N} + k_{IL10TGF} + s_{IL10})} \\
M_{CRH} &\equiv \frac{a_0 + a_1 + q_3 M_{TNF}}{\omega_1} \\
M_{ACTH} &\equiv \frac{a_3 M_{CRH} + q_4}{\omega_2} \\
M_{Cortisol} &\equiv \frac{a_5 M_{ACTH}^2}{\omega_3}
\end{aligned}$$

for $x_{IL10d}d_{IL10} > (k_{IL10N} + k_{IL10TGF} + s_{IL10})$.

Thus there exists an attracting trapping region T_R, where solutions starting outside T_R is attracted into the region and solutions inside can not leave the region.

C.3 Parameter Values for the Coupled Model

The parameter values used for the simulations of the coupled model ((4.1)-(4.2)) presented in Section 4.1 and the biological interpretation are shown in the following table.

No.	*Parameter*	*Value*	*Unit*	*Biological Interpretation*
1	d_p	$1.35 \cdot 10^{-7}$	$(hr \cdot \text{N-unit})^{-1}$	The elimination rate of P in the presences of N
2	k_N	$4.9956 \cdot 10^7$	$\frac{\text{N-unit} \cdot kg}{hr \cdot pg}$	The strength of the stimulation of N in the presents of P and the absence of TNF, TGF and $IL10$

3	k_{NTNF}	12.94907	–	Accounts for part of the activation rate of N by TNF (together with k_N) in the presence of P and the absence of TGF and $IL10$
4	x_{NTNF}	1693.9509	$\frac{pg}{mL}$	The half-saturation constant of TNF in the up-regulating function in the equation for N
5	x_{NTGF}	0.07212	$\frac{pg}{mL}$	The half-saturation constant of TGF in the down-regulating function in the equation for N
6	x_{NIL10}	147.68	$\frac{pg}{mL}$	The half-saturation constant of $IL10$ in the down-regulating function in the equation for N
7	d_N	0.1439	hr^{-1}	The elimination rate of N
8	k_{TGF}	$.154625 \cdot 10^{-8}$	$\frac{mL}{pg \cdot \text{N-unit} \cdot hr}$	The strength of the stimulation of TGF by N
9	d_{TGF}	.031777	hr^{-1}	The elimination rate of TGF
10	q_1	0.5	$\frac{mL}{pg \cdot hr}$	The saturation level for the stimulation of TGF by $Cortisol$
11	q_2	500	$\frac{\mu g}{dL}$	The half-saturation constant of $Cortisol$ in the up-regulating function in the equation for TGF

12	k_{TNFN}	$550 \cdot 10^4$	N-unit	The half-saturation constant of N in the up-regulating function in the equation for TNF
13	x_{TNFTGF}	0.1589	$\frac{pg}{mL}$	The half-saturation constant of TGF in the down-regulating function in the equation for TNF
14	k_{TNF}	25.5194	$\frac{pg}{mL \cdot hr}$	The minimum saturation level (for $TNF = 0$) for the stimulation of TNF in the presence of N and the absence of TGF
15	k_{TNFTNF}	$3.5514 \cdot 10^4$	$\frac{pg}{mL \cdot hr}$	Additional saturation level (for large TNF) for the stimulation of TNF in the presence of N and the absence of TGF
16	x_{TNFTNF}	$1.5495 \cdot 10^3$	$\frac{pg}{mL}$	The half-saturation constant of TNF in the auto-up-regulating function in the equation for TNF
17	d_{TNF}	0.0307	$\frac{mL}{pg \cdot hr}$	The elimination rate of TNF per TNF
18	k_{IL10N}	267480	$\frac{pg}{mL \cdot hr}$	Saturation level for N-dependent $IL10$ stimulation
19	x_{IL10N}	$8.0506 \cdot 10^7$	N-unit	The half-saturation constant of N in the up-regulating function in the equation for $IL10$

20	d_{IL10}	98.932	hr^{-1}	The elimination rate of $IL10$ for small concentrations
21	x_{IL10d}	791.27	$\frac{pg}{mL}$	The half-saturation constant of $IL10$ in the auto-down-regulating function
22	$k_{IL10TGF}$	43875	$\frac{pg}{mL \cdot hr}$	The strength of the stimulation of $IL10$ by TGF
23	$x_{IL10TGF}$	0.38	$\frac{pg}{mL}$	The half-saturation constant of TGF in the up-regulating function in the equation for $IL10$
24	s_{IL10}	1187.2	$\frac{pg}{mL \cdot hr}$	The basis level of $IL10$ in the absence of N and TGF
25	a_0	0.001	$\frac{pg/mL}{min}$	The basis level of CRH stimulation
26	a_1	$6.8400 \cdot 10^9$	$\frac{pg/mL}{min}$	The strength of the auto-up-regulation of CRH in the absence of $Cortisol$ under influence of the 'circadian clock'
27	a_2	$1.7558 \cdot 10^9$	$\left(\frac{dL}{\mu g}\right)^2$	The strength of the inhibition of CRH by $Cortisol$
28	ω_1	0.032	min^{-1}	The elimination rate of CRH
29	q_3	0.0667	min^{-1}	The strength of the stimulation of CRH by TNF
30	a_3	$2.3688 \cdot 10^4$	min^{-1}	The strength of the stimulation of $ACTH$ by CRH in the absence of $Cortisol$

31	a_4	$1.7778 \cdot 10^5$	$\frac{dL}{\mu g}$	The strength of the inhibition of $ACTH$ by $Cortisol$
32	ω_2	0.016	min^{-1}	The elimination rate of $ACTH$
33	q_4	112	$\frac{pg}{mL \cdot min}$	The saturation level for TNF-dependent stimulation of $ACTH$
34	q_5	80	$\frac{pg}{mL}$	The half-saturation constant of TNF in the up-regulating function in the equation for $ACTH$
35	a_5	$5.0746 \cdot 10^{-4}$	$\frac{\mu g/dL}{min \cdot (pg/mL)^2}$	The strength of the stimulation of $Cortisol$ by $ACTH$ per $ACTH$ in the absence of TGF
36	q_6	12	$\frac{pg}{mL}$	The strength of the inhibition of $Cortisol$ by TGF
37	ω_3	0.0266	min^{-1}	The elimination rate of $Cortisol$
38	α	300	min	The half-saturation constant of the increasing Hill function in $C(t)$
39	k	5	–	The steepness of the increasing Hill function in $C(t)$ at time $t = \alpha$
40	β	950	min	The half-saturation constant of the decreasing Hill function in $C(t)$
41	l	6	–	The steepness of the decreasing Hill function in $C(t)$ at time $t = \beta$

42	ϵ	0.01	–	The basis contribution of the circadian clock function $C(t)$
43	δ	76, 37	min	The time shifting of the circadian clock

Table C.1: Table of the biological interpretation and the values of the parameters in the coupled model ((4.1)-(4.2)) presented in Section 4.1.

Bibliography

[1] Albrecht, U. (2012). Timing to perfection: The biology of central and peripheral circadian clock. *Neuron*, 74(2):246–260.

[2] Andersen, M., Vinther, F., and Ottesen, J. (2013). Mathematical modeling of the hypothalamic-pituitary-adrenal gland (hpa) axis, including hippocampal mechanisms. *Mathematical Bioscience*, 246(1):122–138.

[3] Baker, M., Denman-Johnson, S., Brook, B. S., Gaywood, I., and Owen, M. R. (2013). Mathematical modelling of cytokine-mediated inflammation in rheumatoid arthritis. *Mathematical Medicine and Biology*, 30(4):311–337.

[4] Beishuizen, A. and Thijs, L. G. (2003). Revies: Endotoxin and the hypothalamo-pituitary-adrenal (hpa) axis. *Innate Immunity*, 9(1):3–24.

[5] Carroll, B. J., Cassidy, F., Naftolowitz, D., Tatham, N. E., Wilson, W. H., Iranmanesh, A., Liu, P. Y., and Veldhuis, J. D. (2007). Pathophysiology of hypercortisolism in depression. *Acta Psychiatrica Scandinavia*, 115(Suppl 433):90–103.

[6] Chow, C. C., Clermont, G., Kumar, R., Lagoa, C., Tawadrous, Z., Gallo, D., Betten, B., Bartels, J., Constantine, G., Fink, M. P., Billiar, T. R., and Vodovotz, Y. (2005). The acute inflammatory response in diverse shock states. *SHOCK*, 24(1):74–84.

[7] Christensen, O. (2009). *Differentialligninger og uendelige rækker*. Institut for Matematik, DTU.

[8] Clodi, M., Vila, G., Geyeregger, R., Riedl, M., Stulnig, T. M., Struck, J., Luger, T. A., and Luger, A. (2008). Oxytocin alleviates the neuroendocrine and cytokine response to bacterial endotoxin in healthy men. *Am. J. Physiol. Endocrinol. Metab.*, 295:686–691.

[9] Cobelli, C. and Carson, E. (2008). *Introduction to modelling in physiology and medicine*. Academic Press.

[10] Conrad, M., Hubold, C., Fischer, B., and Peters, A. (2009). Modeling the hypothalamus-pituitary-adrenal system: homeostasis by interacting positive and negtive feedback. *J. Biol. Phys.*, 35:149–162.

[11] Foster, S. J., McCormick, L. M., Ntolosi, B. A., and Campbell, D. (1993). Production of tnf alpha by lps-stimulated murine, rat and human blood and its pharmacological modulation. *Agents and Actions*, 02(38):77–79.

[12] Frank, D. O. (2010). *Derivation and parameter estimation of a reduced mathematical model of acute inflammatory response to endotoxin challenge*. PhD thesis, North Carolina State University.

[13] Gupta, S., Aslakson, E., Gurbaxani, B. M., and Vernon, S. D. (2007). Inclusion of the glucocorticoid receptor in a hypothalamic pituitary adrenal axis model reveals bistability. *Theoretical Biology and Medical Modelling*, 4(8).

[14] Hansen, V. L. (1999). *Fundamental Concepts in Modern Analysis*. World Scientific Publishing Co. Pte. Ltd.

[15] Hosseinichimeh, N., Rahmandad, H., and Wittenborn, A. K. (2015). Modeling the hypothalamus-pituitary-adrena axis: A review and extension. (in press).

[16] Jelić, S., Željko Čupić, and Kolar-Anić, L. (2005). Mathematical modeling of the hypothalamic-pituitary-adrenal system activity. *Math. Biosci.*, 197:173–187.

[17] John, C. D. and Buckingham, J. C. (2003). Cytokines: regulation of the hypothalamo-pituitary-adrenocortical axis. *Current Opinion in Pharmacology*, 3(1):78–84.

[18] Kemna, E., Pickkers, P., Nemeth, E., van der Hoeven, H., and Swinkelsl, D. (2005). Time-course analysis of hepcidin, serum iron, and plasma cytokine levels in humans injected with lps. *Blood*, 106(5).

[19] Khan, F. A. and Kahn, M. F. (2010). Inflammation and acute phase respose. *International Journal of Applied Biology and Pharmaceutical Technology*, 1(2):312–321.

[20] LeVeque, R. J. (2007). *Finite Difference Methods for Ordinary and Partial Differential Equations: Steady-State and Time-Dependent Problems*. SIAM.

[21] Liakos, P., Lenz, D., Bernhardt, R., Feige, J.-J., and Defaye, G. (2003). Transforming growth factor β1 inhibits aldosterone and cortisol production in the human adrenocortical cell line nci-h295r through inhibition of cyp11b1 and cyp11b2 expression. *Journal of Endocrinology*, 176:69–82.

[22] Lightman, S. L., Wiles, C. C., Atkinson, H. C., Henley, D. E., Russell, G. M., Leendertz, J. A., McKenna, M. A., Spiga, F., Wood, S. A., and Conway-Campell, B. L. (2008). The significance of glucocorticoid pulsatility. *European Journal of Pharmacology*, 583(1-2):255–262.

[23] Malek, H., Ebadzadeh, M. M., Safabakhsh, R., Razavi, A., and Zaringhalam, J. (2015). Dynamics of the hpa axis and inflammatory cytokines: Insights from mathematical modeling. *Computers in Biology and Medicine*, 67:1–12.

[24] Montgomery, D. C. (2013). *Design and Analysis of Experiments*. John Wiley & Sons, 8 edition.

[25] Ottesen, J. T. (2011). Patient specific modelling in diagnosing depression. *IFAC Workshop Series*.

[26] Rankin, J., Walker, J. J., Windle, R., Lightman, S. L., and Terry, J. R. (2012). Characterizing dynamic interactions between ultradian glucocorticoid rhythmicity and acute stress using the phase response curve. *PLoS one*, 7(2).

[27] Rasmussen, A., Fogh, A., Niebuhr, A., Böttiger, E., Furbo, S., and Larsen, S. (2015). Matematisk modellering: En simulering af hpa-aksen.

[28] Reynolds, A., Rubin, J., Clermont, G., Day, J., Vodovotz, Y., and Ermentrout, G. B. (2006). A reduced mathematical model of the acute inflammatory response: I. derivation of model and analysis of anti-inflammation. *Journal of Theoretical Biology*, 242(1):220–236.

[29] Roy, A., Daun, S., Clermont, G., Rubin, J., Vodovotz, Y., Lagoa, C., and Parker, R. S. (2009). A mathematical model of acute inflammatory response to endotoxin challenge. (Preprint).

[30] Silverman, M. N., Pearce, B. D., Biron, C. A., and Miller, A. H. (2005). Immune modulation of the hypothalamic-pituitary-adrenal (hpa) axis during viral infection. *Viral Immunol.*, 18(1):41–78.

[31] Sriram, K., Rodriguez-Fernandez, M., and III, F. J. D. (2012). Modeling cortisol dynamics in the neuro-endocrine axis distinguishes normal, depression, and post-traumatic stress disorder (ptsd) in humans. *PLoS Comput. Biol.*, 8(2).

[32] Sternberg, E. M. (2006). Neural regulation of innate immunity: a coordinated nonspecific host response to pathogens. *Nature Reviews Immunology*, 6:318–328.

[33] Tracey, K. J. (2002). The inflammatory reflex. *Nature*, 420:853–859.

[34] van der Poll, T., Coyle, S. M., Barbosa, K., Braxton, C. C., and Lowry, S. F. (1996). Epinephrine inhibits tumor necrosis factor-a and potentiates interleukin 10 production during human endotoxemia. *J. Clin. Invest.*, 97(3):713–719.